

MICROCOPY RESOLUTION TEST CHART  
NATIONAL BUREAU OF STANDARDS-1963-A

**DTIC FILE COPY**

**Naval Ocean Research and Development Activity**

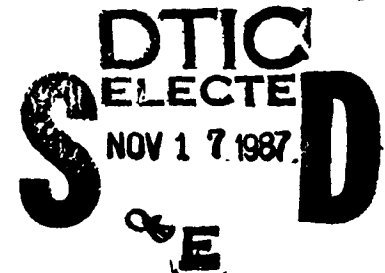
August 1987

Report 211



## **Rapid Underway Sediment Classification by Electrical Methods**

AD-A187 477



**Philip J. Valent**  
Seafloor Geoscience Division  
Ocean Science Directorate

**Edward C. Mozley**  
Mapping, Charting, and Geodesy Division  
Ocean Science Directorate

**Robert F. Corwin**  
Consulting Geotechnical Engineer  
El Cerrito, California

87 11 03 18

## Foreword

---

Proper support of Mine Warfare, Mine Countermeasures, Amphibious Warfare, Special Warfare, and Antisubmarine Warfare requires techniques and equipment to characterize the surface and near-surface sea-floor sediments in real-time from vessels while underway.

The Naval Ocean Research and Development Activity (NORDA) is investigating and developing acoustic, electric resistivity, (DC) and electromagnetic (EM) technologies for application to the real-time, underway sediment classification task. This report shows that DC and EM technologies have potential practical application in the underway sediment classification task; work continues in clarifying the limits of application of this technology in the Navy mission execution.



**A. C. Esau, Captain, USN**  
**Commanding Officer, NORDA**

# Executive summary

The initial results of a technical feasibility study for using direct current (DC) electric resistivity, electromagnetic (EM), and induced polarization (IP) methods to classify surficial sea-floor sediments are reported herein. Analytical work performed in this study and a review of related work show that both the DC and EM resistivity techniques can provide electrical resistivity measurements of sufficient resolution to classify sediments according to type (mud, clay, silt, sand, gravel, etc.). Both DC and EM antennas must be close to the sea-floor surface (within 10 m) so that surficial sediment resistivities can be sufficiently resolved to permit sediment classification. To resolve the resistivity of a 1-m-thick surficial sea-floor sediment layer, the DC antennas must be deployed less than 1 m above the sea floor. Both DC and EM methods can adequately resolve the resistivity of a 6-m-thick surficial layer at a standoff distance of 10 m. Noise tests with an inverted Schlumberger array towed in the water column and on the sea floor show noise levels to be within acceptable limits. The level of development of the IP method for clay mineral detection is reported; this method shows considerable promise as a contributor to a remote underway sediment classification system.

Accession For	
NTIS GRA&I	<input checked="" type="checkbox"/>
DTIC TAB	<input checked="" type="checkbox"/>
Unannounced	<input type="checkbox"/>
Justification	
By _____	
Distribution/	
Availability Codes	
Dist	Avail and/or Special
A-1	



# Acknowledgments

---

This work was initiated in October 1985 as the Sediment Classification Task under the Shallow Water Oceanography Support Project in the 6.2 Oceanographic Block. The task is now part of the Mapping, Charting, and Geodesy Task (under direction of Mr. Kuno Smits, NORDA) in the Oceanographic Support Block (PE62435N) managed by Dr. Gerald B. Morris, NORDA, and sponsored by the Office of Naval Technology under the direction of Mr. G. Spaulding and Mr. R. Feden, ONT 22/228.

# Contents

---

<b>Introduction</b>	1
Purpose	1
Background	1
Approach	2
<b>Electric resistivity of seafloor materials</b>	2
The phenomena	2
Formation factor	2
Typical values of formation factor	2
<b>Direct current resistivity methods</b>	4
The technique	4
Optimum array geometries	4
Equipment	5
Current transmitter	5
Transmitting electrodes	6
Receiving electrodes	6
Connecting cables	6
Instrumentation	6
Data reduction and interpretation	6
<b>Signal and noise levels for marine DC array</b>	7
<b>Analytical studies of DC array performance</b>	11
Description	11
Results	11
Discussion	13
<b>Electromagnetic methods</b>	13
The technique	13
Array geometries	16
Straight Wire System	16
Loop-Loop Systems	17
<b>Development of predictive techniques</b>	17
<b>Analytical studies of EM array performance</b>	18
Description	18
Results	18
Discussion	24
Possible design	24
<b>Induced polarization (IP) methods</b>	24

<b>Summary and conclusions</b>	26
<b>Recommendations</b>	27
<b>References</b>	27
<b>Appendix A. Calculated resistivity resolutions for DC Schlumberger array</b>	31
<b>Appendix B. Analytical Model for transverse electric (TE) and transverse magnetic (TM) fields</b>	51
<b>Appendix C. Sketches of seven cases examined in EM analytical studies</b>	55

# Rapid underway sediment classification by electrical methods

---

## Introduction

### Purpose

This report presents the results of work conducted during fiscal year 1986 in the evaluation of direct current (DC) and electromagnetic (EM) technologies for use in the geoaoustic/geotechnical characterization of sea-floor sediments.

### Background

The Navy requires more rapid techniques and equipment to characterize the surface and near-surface sea-floor sediments to properly support Antisubmarine Warfare (ASW), Mine Warfare (MIW), Mine Countermeasures (MCM), and Amphibious Forces. Present techniques for this sediment characterization include measurement of properties on sediment cores either on a ship or in the laboratory, in situ measurement of sediment properties using instrumented free-fall penetrometers and instrumented probes from bottom-resting platforms, and calculation of properties through inversion of geophysical reflection and refraction data.

The first two methods are labor intensive and/or expensive and, more importantly, both corers and in situ penetrometers/probes gather data only at the specific location sampled, allowing deviations between sample locations to pass undetected. The third method samples nearly continuous along a trackline, but the data measured are generally usable only to the Antisubmarine Warfare community; even then, resolution in the surficial sediments is less than desired. Techniques/equipment that can be applied from an underway vessel are highly desirable or mandatory to meet Navy requirements. The need for an underway system leads to the selection of remote sensing systems, using acoustic, DC resistivity and/or EM induction sensing technologies, with the aid of possible ground-truthing using penetrometers or sediment cores.

An acoustic sediment classification system has been developed and is being improved and adapted to specialized applications by the Naval Ocean Research and Development Activity (NORDA) for various

sponsors. An evaluation of the accuracy of sediment type and properties predicted by the acoustic system over sea-floor sediments ranging from soft muds to dense sands (Lambert, 1987) indicates the acoustic system does properly classify surficial continental shelf sediments about 90% of the time, when ground truth data are available to constrain the sediment type and property predictions. With the addition of a second, remote sensing technology, i.e., one or both of the electrical technologies, it appears possible to improve the accuracy of the remote classifications to provide correct predictions 95-98% of the time, with a reduction in the number of ground truth data required. In addition, the electrical techniques are capable of performing sediment classifications where the acoustic methods cannot perform adequately: (1) in classifying a sediment of low impedance (soft mud) beneath a layer of higher acoustic impedance (sand), (2) in properly classifying gassy sediments, (3) in classifying sediments below the subseafloor design classification depth of the present acoustic system of 6 m in soft clays and 1 m in sands, and (4) in measuring the sediment thickness over rock of low permeability.

Expendable geotechnical penetrometer systems are available for obtaining ground-truth data from a vessel underway (Beard, 1984), and a more-economical, shallow-water, recoverable penetrometer system can be assembled from existing hardware and technology (Valent, 1986). Thus the ground-truthing portion of the remote underway system is available.

Thus, the electrical techniques are the only elements of the rapid sea-floor sediment classification system not near-operational at this time. Direct current resistivity and electromagnetic techniques are highly developed for terrestrial use for locating and delineating bodies of certain mineral deposits and deposits of water bearing gravels and sands. In the oceans, DC resistivity techniques have been used on the continental shelf in the Arctic to measure the unfrozen sediment thickness over permafrost and to measure the thickness of the permafrost (Corwin, 1983). Electromagnetic techniques employed from aircraft-towed sensors in a bird have been used for the measurement of sea ice thick-

ness and water depth in the near shore, and may prove capable of classifying sediments in shallow ocean depths (i.e., in the near shore) (Won and Smits, 1985). The concept of mounting the EM source and receiver in a towfish permits the classifier hardware to be flown closer to the sea-floor sediment being scrutinized, and thereby improves the reliability of the EM system sediment classification and its resolution of sediment layers. The viability of such a system was first proposed by Hulbert et al. (1982).

## Approach

The technical feasibility of using DC and EM techniques for classifying sea-floor material has been initiated through the use of analytical techniques. The FY86 effort was a quick-look evaluation of the influence of stand-off distance between the array and the sea floor; the capability to discriminate between sediment types; and the probable geometries, sizes, and power requirements of the arrays. Work on the DC technology area was subcontracted to Harding-Lawson Associates, Novato, California, (Dr. Robert F. Corwin). Dr. Corwin delivered a collection of measured in situ sediment electrical resistivities, the results of a computer study of the performance of a DC array used in the sediment classification mode, and the results obtained from field measurements of signal-to-noise ratio in a full-scale DC array towed in San Francisco Bay (Corwin, 1986). In-house studies have first developed and validated a computer algorithm to predict the performance of an EM system with both source and receiver towed in the seawater column. This algorithm has been exercised to produce some preliminary results of EM system performance reported herein. This report presents the results of these FY86 efforts, starting with a brief discussion of electrical resistivity in sediments, followed by a description of the DC and EM techniques, and finally the performance results provided by the computer analyses.

## Electrical resistivity of sea-floor materials

### The phenomena

Electrical conduction in most indurated sediments and rocks and in most cohesionless sediments is essentially electrolytic via the material pore fluid, because most mineral grains are insulators. The seawater pore fluid of marine rocks and sediments provides the ideal medium for the conduction of an electrical current, with the resistivity of the formation inversely related to the effective porosity and the degree of saturation. The effective porosity is a function of the measured porosity, i.e., the ratio of the volume of voids to the total volume, and of the grain size and shape, and

pore size and shape. When sediments and rocks contain a measurable portion of clay minerals and/or metallic sulfides and magnetite, the sediment matrix materials do take part in the electrical conduction process. With clay minerals, conduction takes place in the cation double layer surrounding the actual mineral particle.

The resistivities of terrestrial geologic materials cover a very wide range, from less than  $1\Omega\text{m}$  to greater than  $10^8\Omega\text{m}$  (Griffiths and King, 1965; Keller and Frischknecht, 1966). The resistivities of sea-floor sediments are much lower, ranging from  $0.3\Omega\text{m}$  to  $26\Omega\text{m}$  (data referenced by Corwin, 1986), primarily because of the highly conductive seawater pore fluid.

## Formation Factor

Because the resistivity of a geological formation is largely dependent on the resistivity of the pore fluid, the discussion of formation resistivities is simplified by use of the formation factor ( $F$ ), defined as (Archie, 1942):

$$F = \rho_f / \rho_w, \quad (1)$$

where  $\rho_f$  = resistivity of the bulk formation, and  $\rho_w$  = resistivity of the pore water. For terrestrial, consolidated, relatively low-porosity rock,  $F$  is related to porosity ( $n$ ) by the empirical formula known as Archie's law:

$$F = an^{-m}, \quad (2)$$

where  $a$ ,  $m$  are constants with values close to 1 and 2, respectively (Keller and Frischknecht, 1966).

The results of thousands of measurements verify the direct relationship between  $n$  and  $F$  for terrestrial rocks of low clay content. However, because clay minerals readily conduct an electric current in their surface double layer, the measured electrical resistances ( $\rho_f$ ) and formation factors ( $F$ ) for clay-rich rocks and sediments may be significantly lower than predicted by Archie's law for a given porosity.

## Typical values of formation factor

Because the salinity of seawater is greater than that of most terrestrial sediment pore water, the absolute resistivity and formation factors of marine sediments and rocks are generally considerably lower than that of the same materials on land. Measured values of  $F$  for sea-floor sediments range from less than 1 for near-mudline arctic sediments with elevated salt concentration in the pore water to about 15 for some coarse sands and gravels (Table 1). Formation factors greater than 7 or 8 generally indicate rock or bonded permafrost rather than unfrozen sedimentary material.

There is no unique relationship, applicable world-wide, between resistivity and sea-floor sediment properties. On a world-wide basis, measured resistivities for clay may overlap those for silts, silts may overlap sands, and sands may overlap gravels. However, within a survey area, the relationship between electrical resistivity and sediment type is usually much better

Table 1. Summary of selected sea-floor resistivity studies (from Corwin, 1986).

No.	Reference	Location	Water Depth Range (m)	Depth Below Sea Floor (m)	Sediment Type	Pore or Sea Water Resistivity Range ( $\Omega\text{m}$ )	Sea Water Resistivity Range ( $\Omega\text{m}$ )	Formation Factor (F) Range	Relation between F & Porosity ( $\phi$ , %)	Comment
1	Schlumberger et al. (1934)	Algiers Harbor	5-38	1.5-21	"Mud"	0.2	0.74	3.70	-	Sea-floor DC
2	Boyce (1967)	Bering Sea	122-3914	0.05-3.08	Clay-silt-sand	0.16-0.20	0.29-0.71	1.59-3.00	$F=5.31-0.044\phi$ ; $F=1.30\phi-1.45$	Core sample measurements at 25°C
3	Kernabon et al. (1969)	Adriatic Sea	3600	0-7.5	Clay, sand	0.22	0.31-0.77	1.4-3.5	$\phi=5.9F+40.0F^2-105F+171$	Probe and core measurements
4	Hutt and Berg (1968)	Off Oregon coast	2560	0-3.7	Clay, silt	0.33	0.46-0.83	1.4-2.5	-	Core sample measurements
5	Beyer (1971)*	Laboratory tests	-	-	Quartz sand Dolomite sand	0.2-0.6	variable	3.56-3.81 3.01-3.79	$F=\phi^{-1.26}$ $F=\phi^{-1.15}$	Variety of grain sizes tested
6	Corwin and Conli (1973a)	Gulf of California	6-12	0-3	Carbonate sand	0.22	0.79-1.19	3.6-5.4	$F=0.074\phi+8.09$	Sea-floor DC
7	Barnes et al. (1973)	Santa Cruz Harbor, California	10-27	0-3	Sand, rock	-	-	2-6	-	Surface-towed DC
8	Corwin (1965)	Beaufort Sea, Alaska	2-4	0-40	Sand, silt Bonded sand, silt	0.51-0.81	1.3-1.9 150-200	1.91-3.51 195-430	-	Sea-floor DC
9	Corwin (1983)	Beaufort Sea, Alaska	2.6-14	0-40	Clay, silt, sand	0.35-0.42	1.26-27.4 30-188 (bonded)	3.0-7.7 84-530 (bonded)	-	Surface and sea-floor DC
10	Bischoff (1978)	Mediterranean Sea	varied	0-2	Fine sand	0.16-0.20	0.42-1.15	2.2-6.0	-	Probes, sea-floor DC
		North Sea (off Scotland)	varied	0-3	Coarse sand Clay, silt clay	0.17-0.19	1.20-2.50 0.6-2.3	6.3-13.1 4.4-12.6	-	
11	Bennett et al. (1983)	Strait of Florida	18-21	0-6	Carbonate sand	0.20	0.7-2.5	3.5-12.5	$F=\phi^{-2.0}$	Sediment probe
12	Francis (1977)	Atlantic Ocean off Cornwall, England	24-40	several m	Rock	0.24-0.25	1-13	5-50	-	Surface-towed DC
13	Beckmann and Demiray (1976)	Adriatic Sea	varied	0.05	varied	-	0.4-1.4	1-6	$F=0.62\phi^{-2.15}$	Towed sea-floor logger
14	Bogostovsky and Oghy (1974)	USSR, varied	-	-	varied	varied	1-9	-	-	Sea-floor and surface DC

\*Unpublished report

constrained, and sediment type can be predicted from the measured resistivity.

Generally, a difference of one unit in formation factor indicates a significant difference in sediment properties. Thus, for example, in a given survey area where a silty sediment has a formation factor of 2, a change to 3 in the measured formation factor would indicate significantly larger grain size, decreased porosity, or increased degree of consolidation.

## Direct current resistivity methods

### The technique

In the DC method for measuring the electrical resistivity of the sea-floor materials, a current is injected into the sediments or into the seawater by means of two electrodes, and the potential difference between a second pair of electrodes placed in line between the first pair is measured (Fig. 1a and b). From the magnitude of the ratio of potential difference to applied current and a knowledge of the electrode separation, a quantity known as the apparent resistivity can be calculated. If the sea-floor material is homogeneous, then this measured resistivity is the same as the true ground resistivity, but in general it is a weighted average of the resistivities of the various strata through which the current passes.

For marine application, the inverted Schlumberger array (Fig. 1c) provides the best combination of layer resolution, signal-to-noise ratio, and convenience of operation. In terrestrial applications, the current (receiver) electrodes are installed at the center of the array, the potential electrode spacing is expanded, and

measurements are made at each new position to develop the curve of apparent resistivity versus electrode separation. In marine applications, it is more convenient to deploy the electrodes in a single string or eel behind a towing vessel, with the string towed in the water column or dragged slowly along the sea floor. The marine system uses an inverted Schlumberger configuration with the current-transmitting electrodes A and B deployed at the center of the array (Fig. 2a) and the voltage-receiving electrodes  $M_1, M_2, \dots, M_n$  and  $N_1, N_2, \dots, N_n$  placed at logarithmically increasing spacings from the center of the array. This multiplicity of receiving electrodes allows all the voltage readings to be obtained simultaneously from a single current pulse, all at virtually the same instant in time, so that quality data can be gathered from a vessel underway.

### Optimum array geometries

Values of the current and potential electrode spacings,  $AB$  and  $MN$ , are selected to provide both adequate resolution of relatively thin layers close to the sea floor and adequate depth of investigation below the sea floor. The maximum subseafloor depth of investigation of a DC resistivity measurement is a complex function of the resistivity structure and the separation of the outer electrodes (Roy and Elliot, 1981). In general, with the electrodes at the sea-floor surface, the effective depth of investigation is about one-sixth to one-fourth of the maximum potential electrode separation ( $MN$ ). Thus, for the array depicted in Figure 2a, with a maximum  $MN$  of 63.2 m and array deployed on the sea floor, apparent resistivities and structure will be resolved to a subseafloor depth of about 10 to 15 m.

The minimum potential electrode spacing is selected to resolve the minimum desired thicknesses close to the sea floor. Again, for the array of Figure 2a, the minimum potential electrode separation ( $AB$ ) of 2.0 m will allow resolution of the parameters of a layer of about 0.3 m thickness at the sea floor.

Accurate interpretation of data from a Schlumberger array requires that the current electrode spacing ( $AB$ ) be very small as compared to the potential electrode spacing ( $MN$ ). A practical minimum spacing is about one-fourth of the potential electrode spacing, or

$$(AB)_{\text{recommended}} = (1/4) (MN). \quad (3)$$

While optimally the current electrode spacing ( $AB$ ) must be small to permit resolution of thin layers, the spacing must be large to develop an adequate received voltage signal at the outermost potential electrodes. For a given transmitted current level ( $I$ ) at the current electrodes, larger current electrode spacing ( $AB$ ) yields larger potential difference (voltage) at the receiving electrodes. The received voltage or signal at the potential electrodes varies as the inverse of the square of the distance between the electrodes ( $MN$ )<sup>2</sup>, so that the

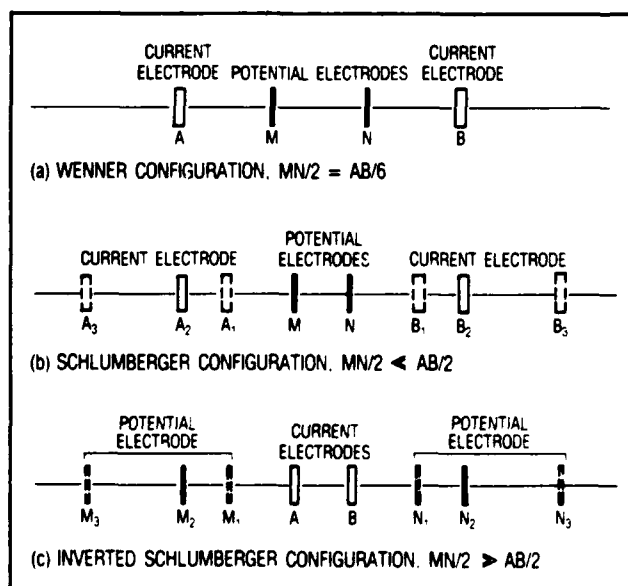


Figure 1. Example arrangements of electrodes for DC method.

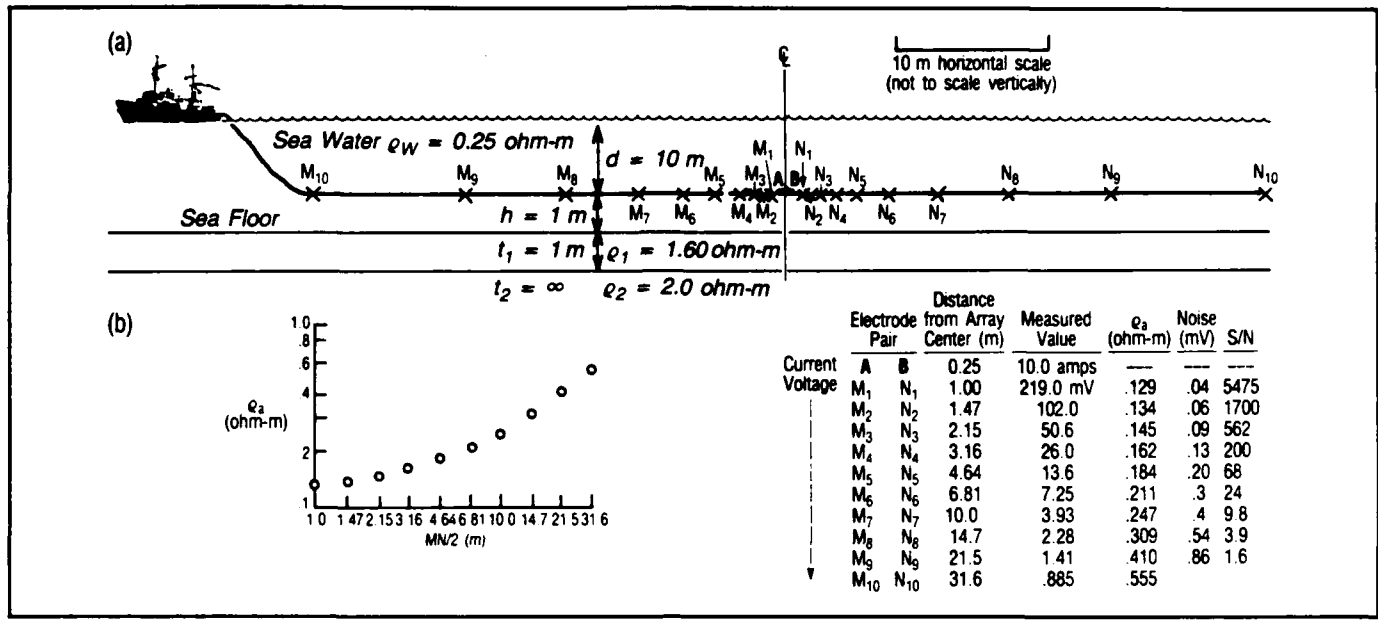


Figure 2. (a) Schematic of towed marine Schlumberger array for direct current resistivity profiling, and (b) a typical plot of apparent resistivity data versus receiver electrode spacing.

signals at large voltage electrode spacings are much smaller than those at the inner electrodes. If, to obtain the required penetration, the outer potential electrode spacing ( $MN$ ) must be made very large and the received signal is then unacceptably small, then a second set of current electrodes at a larger spacing ( $AB$ ) can be used. Appropriate sequential switching circuitry then would be used to ensure that readings are taken from the appropriate potential electrode pairs ( $MN$ ) when transmitting from various current electrode pairs ( $AB$ ).

Thus, selection of the current electrode spacing ( $AB$ ) and the minimum and maximum potential electrode spacings ( $MN$ ) must be balanced among requirements for maximum depth of investigation, desired resolution, available transmitter current levels, and acceptable signal-to-noise ratios at the larger current electrode spacings ( $MN$ ).

### Equipment

The major components of a marine DC resistivity measurement system include a current transmitter, transmitting and receiving electrodes, cables connecting the electrodes to the transmitter and receiver, and instrumentation to measure and record the transmitted current and received voltages.

#### Current transmitter

Because the DC voltage across the receiving electrodes exhibits a certain amount of drift (discussed below), current is transmitted in the form of a square wave with a frequency of about 0.1 to 1 Hz. By

measuring the peak-to-peak voltage across the receiving electrodes and dividing by two, the effect of any DC offset is automatically removed and the true signal voltage amplitude can be determined.

The current transmitter system consists of a power supply, a switching system, and equipment to measure and record the transmitted current. To provide usable signals for a practical array, the transmitted current must be of the order of several amperes (A) or more and have very low noise level. Transmission of currents of this magnitude into seawater requires a power supply of several hundred volts. A 3.5-kW, gasoline-powered, motor-generator and a control system that steps up, rectifies, and filters the AC output of the generator, providing a continuously variable output of 0 to 800 VDC at up to 10 A has been used for this task. Larger systems using the same concept could easily be constructed.

Switching frequencies of about 0.1 to 1 Hz allows transient switching effects to die out before the voltage measurements are made. Higher frequencies may allow more rapid data acquisition, but transient and inductive and capacitive effects may impair data accuracy.

Switching the current electrode polarity can be accomplished manually or electronically. Manual switching offers high reliability and continuous operator control over the duty cycle, but is not practical for extended survey lines and for operating frequencies greater than about 1 Hz. Electronic switching frees the operator for other tasks, but requires sophisticated high-power circuitry.

## Transmitting electrodes

Current transmitting (*AB*) electrodes for marine DC measurements can be fabricated as wire wrapped around the outside of the electrode streamer cable (discussed below). A length of about 10 cm wrapped around a cable of 1- to 2-cm diameter gives an effective contact resistance of a few tens of ohms. Thus a source voltage of about 250 VDC will drive a current of about 5 to 10 A through such an electrode. We have found both copper and Monel wire to be satisfactory electrode materials, with minimal metal loss even after many days of operation at 10-A levels.

## Receiving electrodes

The voltage-receiving (*MN*) electrodes must permit measuring voltage differences of a few tenths of a millivolt (mV) with minimal intrinsic noise and drift. Although bare metallic electrodes of noble metals, such as gold or platinum, are used for such measurements in the laboratory, their noise and drift levels increase to unacceptable levels during field use. Nonpolarizing silver-silver chloride ( $\text{Ag-AgCl}$ ) electrodes perform well for marine measurements (Corwin and Conti, 1973). These electrodes consist of a chloridized silver wire immersed in a conductive gel contained in a plastic housing. Contact between the seawater and the gel is through a porous ceramic junction. Thus the wire electrode element is isolated from direct contact with the seawater, with a corresponding reduction in noise generated by water turbulence and water temperature and salinity variations. Intrinsic noise levels for such electrodes deployed stationary on the sea floor are of the order of a few microvolts ( $\mu\text{V}$ ), and long-term drift is less than a few millivolts per day.

Electrodes of this type are available commercially (they are used as reference electrodes for pH and other electrochemical measurements), or can be fabricated to meet special requirements.

## Connecting cables

For a marine DC resistivity system all the transmitting and receiving electrodes are fabricated into a single multiconductor electrode streamer cable. Components of this streamer include transmitter and receiver cables, connectors, electrodes, a strength member, an outer jacket, and (in some cases) floats or other buoyancy control means.

The gauge of the transmitter cables depends on the maximum transmitted current. Eighteen-gauge cable is adequate for current levels of about 10 A. Because the receiver cables carry virtually no current, they can be of very light gauge. As mentioned, current electrodes are wrapped around the outer cable jacket, and voltage electrodes are spliced to the outside of the jacket.

Integrity of cable and connector insulation is crucial to data quality. Leakage of current to the seawater at

locations other than the current electrodes can result in erroneous voltage readings; contact between seawater and the metallic conductors leading to the voltage electrodes will generate spurious voltages, noise, and drift. Thus great care must be taken to ensure that all connections are watertight and that no leaks exist in the cable insulation.

To protect the individual cables from damage, they are enclosed in an outer jacket. Jackets of polyurethane material are used for seismic cables and have proven sufficiently rugged for bottom-towed operations in which the cable is dragged across the sea floor. A central strength member of Kevlar or similar rope is used to relieve the mechanical towing stress on the electrical cables.

Surface-towed cables are fabricated with a buoyant outer jacket, and bottom-towed cables are made negatively buoyant. A streamer cable to be towed within the water column would be neutrally buoyant, with towing depth controlled by a V-fin or similar device.

## Instrumentation

Instrumentation consists of electronic devices to measure, record, and store the transmitted current and received voltage values. The on-board instrumentation also may perform initial data reduction and interpretation.

The simplest system for acquiring marine DC data consists of a multichannel strip chart recorder with appropriate preamplifiers for the individual current and voltage channels. Such a system is relatively inexpensive and reliable, and allows the interpreter to directly observe data quality. However, because a full data set is acquired with each current pulse every few seconds of operation, a great deal of time is required to later manually read and record the current and voltage levels for each transmitted current pulse.

A computer-controlled multichannel digital data acquisition system can be used to greatly reduce data reduction and interpretation time. In such a system, each current and voltage pulse is automatically digitized and stored on tape or floppy disks for later reduction and interpretation. This type of system would be considerably more complex and expensive than the strip chart recorder described above, but would greatly reduce data interpretation time. Further time savings could be effected by feeding necessary supplementary information such as vessel position and water depth and resistivity directly into the data acquisition system.

## Data reduction and interpretation

A marine DC resistivity data set consists of the peak-to-peak amplitudes of sequential positive and negative current pulses and the peak-to-peak amplitudes of the associated voltage pulses across electrode pairs  $M_1N_1$ ,  $M_2N_2$ , ...,  $M_nN_n$ . For each pulse, the

peak-to-peak amplitude is divided by two to give the true zero-to-peak amplitude without the effects of any DC offsets. For each MN electrode pair, the apparent resistivity for the Schlumberger array is calculated from:

$$\rho_a = \pi (V/I) [(MN/2)^2 - (AB/2)^2] / 2(AB/2) \quad (4)$$

where  $\rho_a$  = apparent resistivity ( $\Omega\text{m}$ ),

$V$  = voltage at potential electrodes (mV),

$I$  = current at transmitting electrodes (mA),

$MN/2$  = one-half of potential electrode spacing (m), and

$AB/2$  = one-half of current electrode spacing (m)

For manual interpretation, the apparent resistivity data are presented on double logarithmic plots of apparent resistivity ( $\rho_a$ ) versus electrode spacing ( $MN/2$ ) (Fig. 2b) (Griffiths and King, 1965). By convention, the electrode spacing parameter is taken to be one-half the potential electrode spacing ( $MN/2$ ). The logarithmic spacing of electrodes yields uniformly spaced data points on the electrode spacing axis (Fig. 2b).

Manual interpretation of apparent resistivity data to obtain layer thicknesses and resistivities involves comparing the measured resistivity curve with a set of theoretical curves, superimposing or overlaying the field curve on a similarly shaped group of theoretical curves until a fit is obtained. For the terrestrial environment, complete solutions of layer thicknesses and resistivities for structures of up to three layers are readily achievable from published curves for the Schlumberger array (Griffiths and King, 1965), and computer programs are available to generate resistivity curve sets for structures with an arbitrary number of layers.

Computerized data inversion programs are now available to automatically determine the best-fit layer parameters for a given data set. With sophisticated programming and relatively consistent layered structure, the complete data analysis and structure evaluation can be done by computer. To date, when applying these procedures for geotechnical purposes, the number of layers and their approximate thicknesses and resistivities have been estimated first by an experienced interpreter from an examination of the apparent resistivity curve. These first estimates are then used as input to a computer inversion program to iteratively refine the estimates of the layer parameters.

Data taken at the sea surface can be interpreted using one of a number of published or commercially available inversion programs written for onshore DC resistivity data interpretation. For an electrode array deployed within the water column or on the sea floor, Harding Lawson Associates has written a forward modeling program (SUBSOND) and an inversion program

(SUBVERT) based on DC resistivity surface modeling and inversion programs (SOND and INVERT) written at the University of California, Berkeley, modified using expressions for buried electrodes given by Alfano (1962). SUBVERT will handle a sea-floor structure of up to three layers (two layers overlying an infinitely deep basement). The program can be run on a mainframe computer or on an IBM-PC or equivalent. Inversion of one data set requires a few seconds or less on a mainframe computer or a few minutes on an IBM-PC-AT. For production use, this program could be upgraded to handle more layers and reduce running time.

Because acquisition of a data set requires only a few seconds but the inversion process for the data set requires a few minutes, interpreted data cannot be displayed as rapidly as they are acquired. However, data quality can be monitored by observation of the apparent resistivity values, which can be calculated and displayed immediately using Equation 4. After data acquisition has been completed, the interpreter can decide how many and which data sets are to be interpreted. This decision is based on the desired density of data coverage. For example, for a boat speed of 5 knots and a transmitter frequency of 1 Hz, a full data set is acquired for each meter of survey line. For a desired lateral resolution of 10 m, only every tenth data set would have to be interpreted.

The accuracy of the inversion process can be greatly improved if one or more of the layer parameters is known in advance. For marine measurements, it is easy to independently determine the water depth and resistivity at each station. Fixing these parameters in the input to the inversion program allows improved resolution of the desired subseafloor layer parameters. Thus continuous measurement of seawater depth and resistivity should be carried out as part of any marine resistivity survey.

## Signal and noise levels for marine DC array

As part of the feasibility assessment of using DC resistivity techniques for classifying marine sediments in situ, measurements were conducted in San Francisco Bay in water depths of 3-4 m with a towed Schlumberger array to directly measure noise levels.

The resolution of sea-floor layering attainable by DC resistivity measurements depends on distinguishing among apparent resistivity curves for various layered structures. This ability is a function of data signal-to-noise (S/N) levels. That is, if error bars on individual  $\rho_a$  field readings are large relative to the separation between apparent resistivity curves that represent different layered structures, then the interpreter or computer algorithm will not be able to distinguish which

of the layered structures represents the true geology. Therefore, expected signal and noise levels for actual field measurements must be determined before geologic resolution capabilities of marine DC resistivity systems can be determined.

Noise levels depend on electrode properties and operating conditions. As discussed above, intrinsic noise levels for stationary Ag-AgCl electrodes separated by a few meters and immersed in calm seawater are a few microvolts. Thus under these conditions signal levels greater than about 0.1 mV will give S/N ratios of 100 or more, permitting resolutions of  $\rho_a$  values better than 1%.

Noise levels generated by continuous-towed operations will depend on sea state, wave activity, bottom conditions, towing speed, currents, and seawater temperature and salinity variations (Corwin and Conti, 1972; Corwin, 1976). Measurements conducted in San Francisco Bay were used to establish preliminary S/N levels for use in this study. A streamer cable with current electrode separation ( $AB/2$ ) of 0.25 m and voltage electrode separations ( $MN/2$ ) of 1, 20, and 100 m was towed at varying speeds on the surface, within the water column, and along the floor of the bay (Fig. 3). Note that for construction purposes the 100-m  $MN$  electrode pair is offset from the center of the array. Thus the noise levels on this electrode pair will be representative, but signal levels will be 12.7 times greater than those for a concentric array with the same  $MN$  spacing.

Water depth in the test area was about 3-4 m, and measured water parameters are given in Table 2. Wave height varied from about 30 to 60 cm throughout the test period. Currents of up to several knots velocity were encountered along the test profile.

The array was operated in the following modes: (1) towed at the sea surface at speeds of about 4-5 knots and 7-8 knots; (2) towed at about 2-m water depth at the same speeds; (3) deployed stationary on the sea floor; and (4) towed along the sea floor at about 4 knots. In each mode, noise levels across each of the three  $MN$  pairs were measured with no current transmitted to allow maximum receiver sensitivity. Current in the form of 5- or 10-A square wave pulses then was transmitted across the  $AB$  electrodes to allow determination of S/N levels.

The intrinsic noise level of a pair of Ag-AgCl electrodes with  $MN/2$  of 1 m and resting stationary on the sea floor was found to be of the order of 0.02 mV (Fig. 4d). As  $MN/2$  increases to 20 m, the corresponding noise level increased to about 0.6 mV peak-to-peak (Fig. 5b); and stationary noise levels at 100-m  $MN/2$  were about 2 mV peak-to-peak (Fig. 6d). Thus the stationary noise level is roughly proportional to electrode separation  $MN/2$ .

When towed along the surface at about 5 knots, noise levels were about 0.04 mV for  $MN/2$  of 1 m, about 0.8

Table 2. Water parameters for DC array noise tests, San Francisco Bay.

Depth (m)	Temperature (°C)	Salinity (ppt)	Resistivity ( $\Omega$ m)
0.5	20.0	19.0	0.36
2.0	19.5	20.5	0.33
3.5	19.0	14.5	0.48

mV for  $MN/2$  of 20 m, and about 2 mV for  $MN/2$  of 100 m (Fig. 4a, 5a, and 6b). Thus noise increases only slightly with the array in motion. Increasing towing speed to about 8 knots appeared to increase the frequency, but not the amplitude, of the noise level. Arrays towed along the sea floor showed noise levels very similar to those for surface-towed arrays.

Current waveforms for the surface-towed array (Fig. 7) show that current amplitude is resolvable within about 1-3% from the chart recorder records. For a potential electrode spacing ( $MN/2$ ) of 1 m and applied current ( $I$ ) of 5 A, the received signal level was about 175 mV (Fig. 4c), which when combined with noise levels of 0.04 mV gives an S/N ratio of about 5000 and a corresponding resolution of better than 1% for  $\rho_a$ . For  $MN/2 = 20$  m (Fig. 5d), a transmitted current of 10 A gives a signal level of about 2.5 mV and a corresponding S/N ratio of about 4 in the presence of a large (0.6 mV) noise pulse and about 8 for more typical noise levels of about 0.3 mV peak-to-peak. Increasing current levels to at least 20 A (as would be done for an operational array) would give S/N ratios of about 8 to 16, with corresponding  $\rho_a$  resolution of about 6 to 12%.

These results for 20-m  $MN/2$  are useful, as this spacing would be the maximum electrode spacing for a sea-floor towed array with a subseafloor depth of investigation of about 6 m. Resolution of the noisiest  $\rho_a$  value for this array, then, would be no worse than about 12%, and resolution would improve rapidly as  $MN/2$

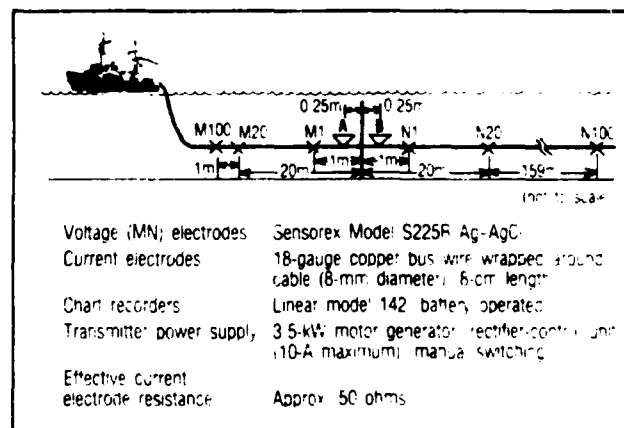


Figure 3. Configuration of test cable for NORDA marine direct current resistivity study.

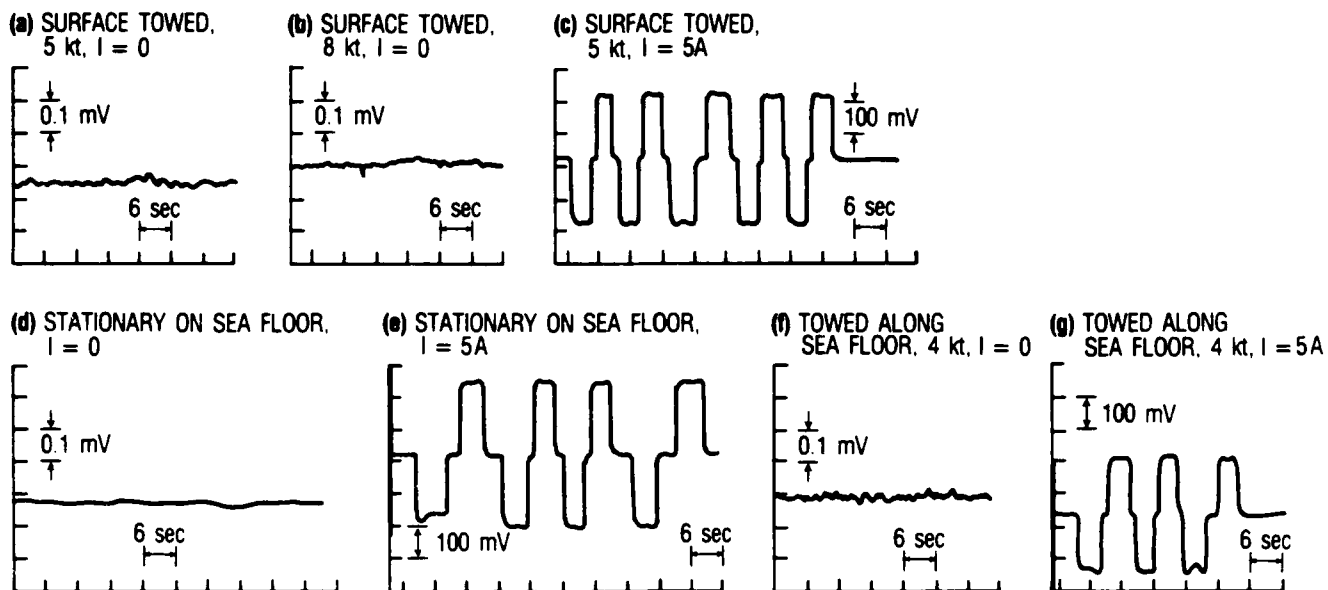


Figure 4. Results of noise tests in San Francisco Bay,  $MN/2 = 1$  m, NORDA marine direct current resistivity study.

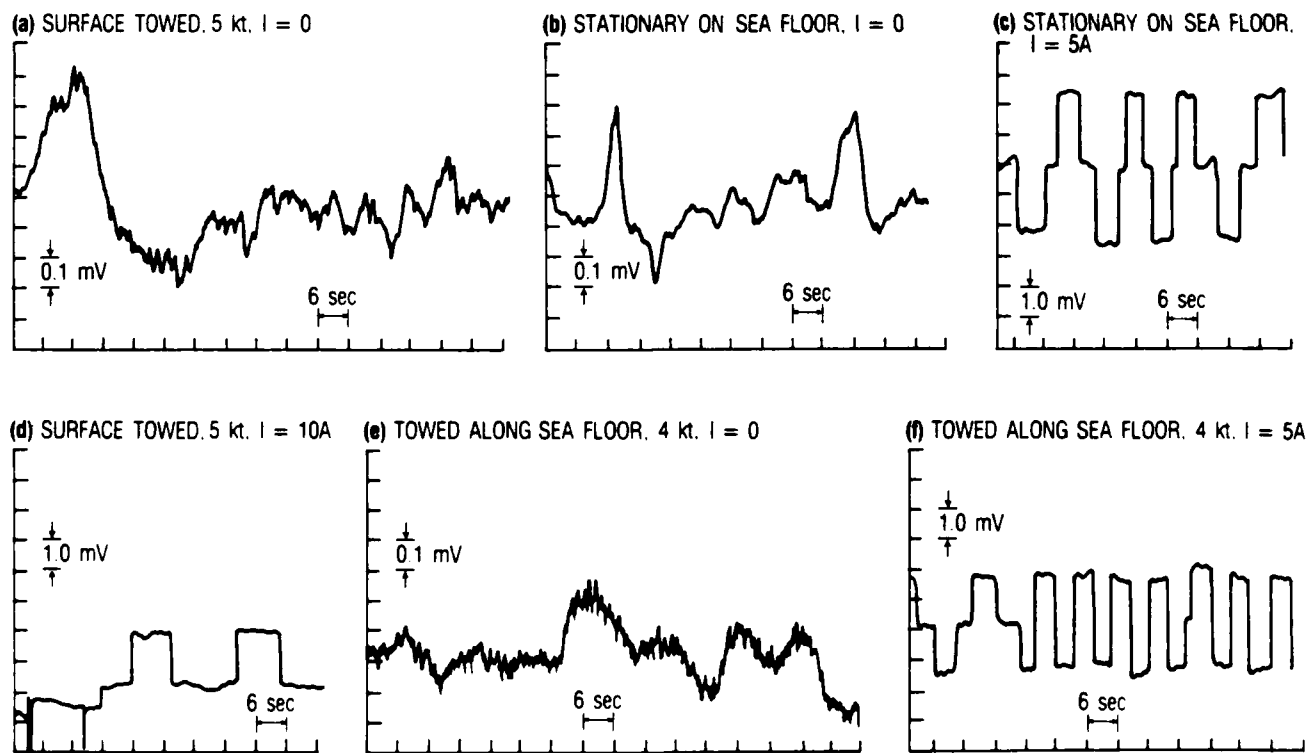
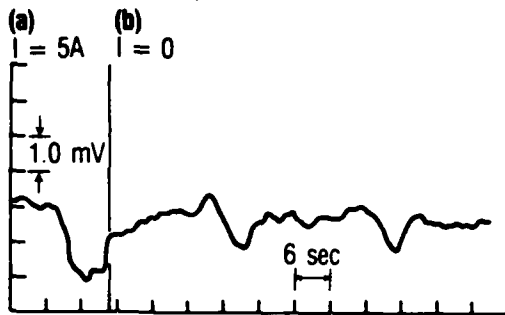
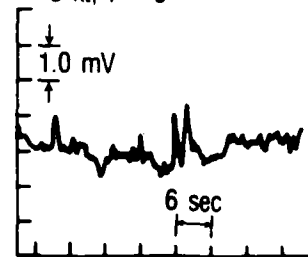


Figure 5. Results of noise tests in San Francisco Bay,  $MN/2 = 20$  m, NORDA marine direct current resistivity study.

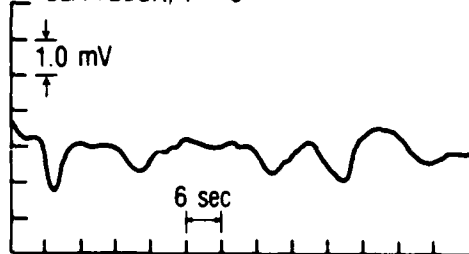
SURFACE TOWED, 5 kt



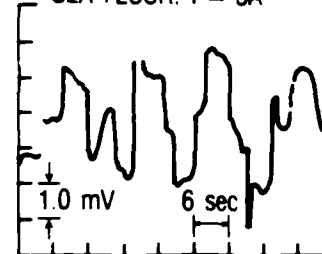
(c) SURFACE TOWED,  
8 kt,  $I = 0$



(d) STATIONARY ON  
SEA FLOOR,  $I = 0$



(e) STATIONARY ON  
SEA FLOOR,  $I = 5A$



(f) TOWED ALONG SEA FLOOR,  
4 kt,  $I = 0$

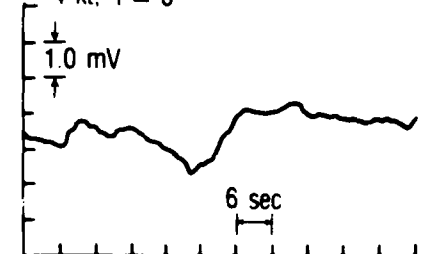
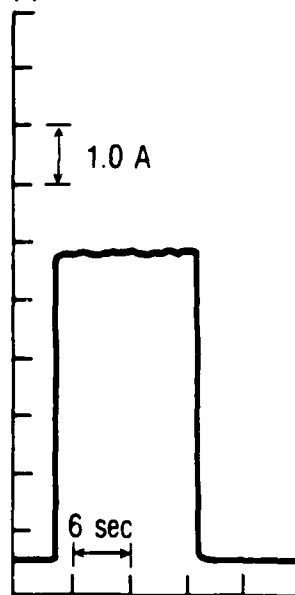


Figure 6. Results of noise tests in San Francisco Bay,  $MN/2 = 100$  m, NORDA marine direct current resistivity study.

(a) SURFACE TOWED, 5 kt



(b) SURFACE TOWED, 8 kt

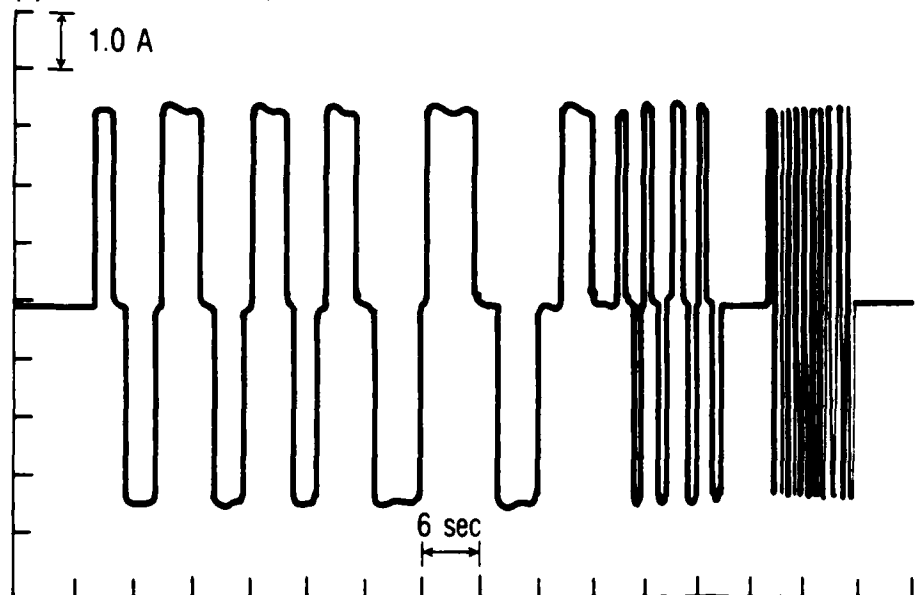


Figure 7. Transmitted current in noise tests in San Francisco Bay,  $AB/2 = 0.25$  m, NORDA marine direct current resistivity study.

decreases, signal levels increase, and noise levels decrease. Thus a practical array with maximum  $MN/2$  of about 20 m dragged along the sea floor should give acceptable resolution of subseafloor layer parameters to depths of 6 m.

Although the received signal is detectable for the 100-m  $MN/2$  pair, its amplitude of about 1 mV is poorly resolved (Fig. 6a). As mentioned previously, a practical array with  $MN/2$  values greater than about 20 m would use a second pair of current transmitting electrodes with considerably greater separation  $AB/2$  to provide a larger signal and acceptable  $\rho_a$  resolution for large receiving electrode separations.

In this brief study, no attempt was made to analyze the sources of electrode noise (which probably include wave and current activity, changes in seawater properties, and motion of the connecting cables through the earth's magnetic field). Better understanding of these sources could produce methods to reduce this noise and thus improve S/N ratios without the necessity for larger transmitter currents.

## Analytical studies of DC array performance

### Description

A series of computer modeling studies were conducted using the program SUBSOND to obtain a preliminary idea of the resolution of sea-floor sediment properties provided by the marine DC resistivity method. The sea floor was modeled as a two-layer system: a surficial sediment layer over a more resistive layer of infinite depth. In this study, the resolution of the resistivity of the upper layer was the parameter of major interest, the thickness of the upper layer was of secondary interest, and resistivity of the underlying strata was considered the least important.

The nomenclature and range of parameters used in these preliminary parameter studies are illustrated in Figure 8 and are listed as follows:

- $d$  = water depth (10, 100, and 1000 m used),
- $h$  = height of the electrode array off the sea floor (0, 1, 10, 30, and 100 m above the sea floor all used),
- $t_1$  = thickness of the upper layer of the sea floor (1, 6, 60 m used),
- $t_2$  = thickness of the second layer (infinite),
- $\rho_w$  = resistivity of the overlying water (assumed 0.25  $\Omega$ m),
- $\rho_1$  = resistivity of the upper layer of sea floor (0.4, 0.8, 1.6  $\Omega$ m used), and
- $\rho_2$  = resistivity of the second sea-floor layer (2.0  $\Omega$ m used).

The maximum potential electrode half-separation ( $MN/2$ ) used for all cases was 316 m. Table 3

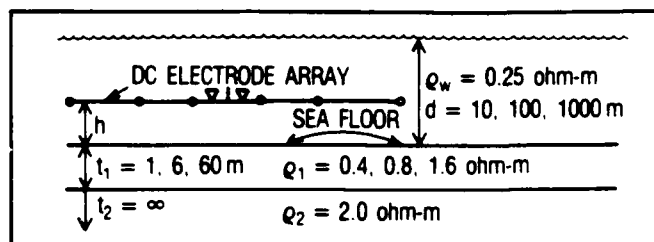


Figure 8. Nomenclature used in describing case geometries for analytical studies, marine DC resistivity study.

summarizes parameters selected for each of the cases examined.

The ability to differentiate between a given pair of resistivity curves depends on the S/N ratio of the individual data points defining the curves. The S/N ratio will vary depending on operating conditions, transmitted current amplitude, and voltage receiver electrode separation (or half-spacing,  $MN/2$ ). Thus no single S/N ratio can be assumed for the entire range of a given resistivity curve, nor can the S/N ratio be assumed to be the same for different environments. Because this study is only a preliminary effort, the S/N ratio was assumed to be a constant-15-for all receiver electrode spacings, or, said differently, a resolution level of  $\pm 7\%$  has been assumed for all receiver electrode spacings. Quite conveniently, the line width on the computer plots generated for this study just happened to also represent a resolution of about 7%; thus, when two computer-generated curves are visually distinguishable, then field-measured data should also be resolvable to the accuracies required. (For example, Figure A-1 of Appendix A presents the computer-generated performance prediction for Case 1 (see Table 3), showing that Layer 1 resistivities are resolvable for the 1-m-thick layer only for receiver electrode half-spacing ( $MN/2$ ) less than 3 m.

S/N ratios will be considerably greater than 15 for most of the inner potential electrodes ( $MN$ ) under most operating conditions; therefore, computer-generated curves that were not visually distinguishable at small receiver spacings ( $MN/2$ ) often may be resolvable from field data. Therefore, using 15 for the value of the S/N ratio over the entire calculated curve is a conservative assumption.

## Results

The computer-generated plots of apparent resistivity ( $\rho_a$ ) versus receiver electrode half-spacing ( $MN/2$ ) for each of these cases listed in Table 3 are reproduced in Appendix A (from Corwin, 1986). The essential contents of the Appendix A figures are summarized in Table 4, where the electrode spacing ( $MN/2$ ) required to resolve the resistivity of the sediment layer 1 ( $\rho_1$ ) is

Table 3. Layer parameters for model studies (resolution of sea-floor resistivity).

Case	$d$ (m)	$h$ (m)	$t_1$ (m)	$\rho_1$ ( $\Omega\text{m}$ )			$\rho_2$ ( $\Omega\text{m}$ )
				Curve 1	Curve 2	Curve 3	
1	10	0	1	0.4	0.8	1.6	2.0
2	10	0	6	0.4	0.8	1.6	2.0
3	10	0	60	0.4	0.8	1.6	2.0
4	10	1	1	0.4	0.8	1.6	2.0
5	10	1	6	0.4	0.8	1.6	2.0
6	10	1	60	0.4	0.8	1.6	2.0
7	10	10	1	0.4	0.8	1.6	2.0
8	10	10	6	0.4	0.8	1.6	2.0
9	10	10	60	0.4	0.8	1.6	2.0
10	100	0	1	0.4	0.8	1.6	2.0
11	100	0	6	0.4	0.8	1.6	2.0
12	100	0	60	0.4	0.8	1.6	2.0
13	100	1	1	0.4	0.8	1.6	2.0
14	100	1	6	0.4	0.8	1.6	2.0
15	100	1	60	0.4	0.8	1.6	2.0
16	100	30	1	0.4	0.8	1.6	2.0
17	100	30	6	0.4	0.8	1.6	2.0
18	100	30	60	0.4	0.8	1.6	2.0
19	100	100	1	0.4	0.8	1.6	2.0
20	100	100	6	0.4	0.8	1.6	2.0
21	100	100	60	0.4	0.8	1.6	2.0
22	1000	0	1	0.4	0.8	1.6	2.0
23	1000	0	6	0.4	0.8	1.6	2.0
24	1000	0	60	0.4	0.8	1.6	2.0
25	1000	1	1	0.4	0.8	1.6	2.0
26	1000	1	6	0.4	0.8	1.6	2.0
27	1000	1	60	0.4	0.8	1.6	2.0
28	1000	30	1	0.4	0.8	1.6	2.0
29	1000	30	6	0.4	0.8	1.6	2.0
30	1000	30	60	0.4	0.8	1.6	2.0
31	1000	100	1	0.4	0.8	1.6	2.0
32	1000	100	6	0.4	0.8	1.6	2.0
33	1000	100	60	0.4	0.8	1.6	2.0

listed for each case. The data of Table 4 is rearranged in Table 5, first in terms of the thickness of the surficial sediment layer, second in terms of the height of the array above the sea floor, and third in terms of the water depth (to the sea floor).

Table 5 shows that the resistivity of a 1-m-thick surficial sediment layer can be resolved as being 0.4, 0.8, or 1.6  $\Omega\text{m}$  only when the array is laying on the sea floor and only for receiver electrode half-spacings ( $MN/2$ ) of 3 m or less. Even when the array is towed as close as 1 m above the sea floor, the resolution of the apparent resistivity ( $\rho_a$ ) for the surficial 1-m layer is not adequate to permit individual sediment classification for that 1-m layer.

When the thickness of the surficial sediment layer is 6 m, then sufficient resolution can be achieved to classify

the sediments of that layer by towing the array up to 10 m above the sea floor. When towed at 10 m above the sea floor, the half-spacing of one or more pairs of receiving electrodes must be at least 12 m, requiring an array length of at least 24 m, in order to adequately resolve the apparent resistivity ( $\rho_a$ ) and to permit calculation of the layer 1 resistivity ( $\rho_1$ ).

For a surficial sediment layer 60 m thick, classification is possible with an array towed anywhere from on the sea floor to 30 m above it. However, as the position of the array is raised above the sea floor, the spacing of receiver electrodes required to achieve the required resolution for sediment classification also increases. For an array 30 m above the sea floor the required electrode half-spacing varies with the water depth ( $d$ ): for  $d$  of 100 m,  $MN/2$  must be at least 35 m.

Table 4. Electrode spacings (MN/2) required in order to resolve  $\rho_1$ .

Case	$d$ (m)	$h$ (m)	$t_1$ (m)	MN/2 Required (m)
1	10	0	1	$\leq 3$
2	10	0	6	$\leq 140$
3	10	0	60	1 through 316
4	10	1	1	None
5	10	1	6	2 through 130
6	10	1	60	1 through 316
7	10	10	1	None
8	10	10	6	12 through 130
9	10	10	60	8 through 316
10	100	0	1	1 through 3
11	100	0	6	1 through 15
12	100	0	60	1 through 316
13	100	1	1	None
14	100	1	6	1 through 22
15	100	1	60	1 through 316
16	100	30	1	None
17	100	30	6	None
18	100	30	60	35 through 316
19	100	100	1	None
20	100	100	6	None
21	100	100	60	110 through 316
22	1000	0	1	1 through 30
23	1000	0	6	1 through 15
24	1000	0	60	1 through 150
25	1000	1	1	None
26	1000	1	6	1 through 20
27	1000	1	60	1 through 150
28	1000	30	1	None
29	1000	30	6	None
30	1000	30	60	60 through 200
31	1000	100	1	None
32	1000	100	6	None
33	1000	100	60	None

and for  $d$  of 1000 m, MN/2 must be 60 m. It is significant to note that an array towed 100 m above the sea floor achieves sufficient resolution to distinguish resistivities ( $\rho_1$ ) for a 60-m-thick surficial layer when the water depth is 100 m, but does not have the required resolution in 1000-m water depth.

## Discussion

The formation factors used for these cases (1.6, 3.2, and 6.4) (resistivities of 0.4, 0.8, and 1.6  $\Omega$ m) typically would represent, respectively, a poorly consolidated, fine-grained sediment (e.g., clay or fine silt); a moderately consolidated, medium-grained material (e.g., fine sand or silty sand); and coarse-grained, well-compacted material (e.g., gravel or compacted sand). Thus the resolvability of the three curves on each

figure of Appendix A is indicative of our ability to distinguish between the most common sea-floor materials.

Comparison between cases with  $t_1$  values of 1, 6, and 60 m indicates that it is increasingly easy to resolve the resistivity of the upper layer as its thickness increases. For all of the cases, in any water depth, an array on or just above the sea floor can resolve the resistivity of a 1-m-thick upper layer. An array at the sea surface in 10 m of water cannot resolve the resistivity of a 1-m-thick layer (Fig. A-7, Table 5), but can resolve the resistivity of a 6- or 60-m-thick upper layer (Figs. A-8 and A-9, Table 5).

For 100 m or 1000 m water depth, an array 30 m above the sea floor or at the surface cannot resolve the the resistivity of a 1- or 6-m-thick upper layer but can resolve that of a 60-m-thick layer. Thus for any water depth the array must be towed at or close to the sea floor to resolve the resistivity of layers that are thin relative to the water depth. As the thickness of a given layer becomes larger relative to water depth, its resistivity becomes easier to determine, and the array can be towed at a greater height off the sea floor.

## Electromagnetic methods

### The technique

The EM method proposed for measuring the electrical resistivity of surficial sea-floor sediments is one of a family of geoelectrical prospecting techniques that utilize a controlled time-varying current to generate a source field. These primary fields induce currents within the surrounding media. The amplitude and phase of these secondary fields reflect the variation in physical parameters that occurs in the vicinity of the current source. This type of exploration method will be referred to as the EM technique. The EM methods described herein use a current source, which varies over a band of frequencies from 10 to 10,000 Hz.

In implementing the method, a magnetic field is generated by driving a time-varying electric current through a loop of wire or through a straight wire grounded at both ends. When any conductive materials, such as seawater and sea-floor sediments, are present, induced eddy currents will flow in closed paths or loops normal to the direction of magnetic field. These eddy currents, in turn, generate secondary magnetic fields. Thus, at any point in space, the total magnetic field may be thought of as consisting of two parts: (1) a primary or normal field due to the source current and (2) a secondary or disturbing field due to eddy currents induced in conductors (Keller and Frischknecht, 1966).

The functioning of an EM/induction system may be compared with that of a transformer having three windings, with one of the windings being shorted to simulate the effect of a conductive body (see Fig. 9). A

Table 5. Resolvability of  $\rho_1$ .

$t_1$ (m)	$h$ (m)	$d$ (m)	Case	$\rho_1$ Resolvable?
1	0	10	1	Yes $MN/2 \leq 3$
1	0	100	10	Yes $MN/2 \leq 3$
1	0	1000	11	Yes $MN/2 \leq 3$
1	1	10	4	No
1	1	100	13	No
1	1	1000	25	No
1	10	10	7	No
1	30	100	16	No
1	30	1000	28	No
1	100	100	19	No
1	100	1000	31	No
6	0	10	2	Yes $MN/2 \leq 140$
6	0	100	11	Yes $1 \leq MN/2 \leq 15$
6	0	1000	23	Yes $1 \leq MN/2 \leq 15$
6	1	10	5	Yes $2 \leq MN/2 \leq 130$
6	1	100	14	Yes $1 \leq MN/2 \leq 22$
6	1	1000	26	Yes $1 \leq MN/2 \leq 20$
6	10	10	8	Yes $12 \leq MN/2 \leq 130$
6	30	100	17	No
6	30	1000	29	No
6	100	100	20	No
6	100	1000	32	No
60	0	10	3	Yes $1 \leq MN/2 \leq 316$
60	0	100	12	Yes $1 \leq MN/2 \leq 316$
60	0	1000	24	Yes $1 \leq MN/2 \leq 150$
60	1	10	6	Yes $1 \leq MN/2 \leq 316$
60	1	100	15	Yes $1 \leq MN/2 \leq 316$
60	1	1000	27	Yes $1 \leq MN/2 \leq 150$
60	10	10	9	Yes $8 \leq MN/2 \leq 316$
60	30	100	18	Yes $35 \leq MN/2 \leq 316$
60	30	1000	30	Yes $60 \leq MN/2 \leq 200$
60	100	100	21	Yes $110 \leq MN/2 \leq 316$
60	100	10000	33	No

Table 6. Parameters of the seven cases examined in the EM analytical studies.

Case	$d$ (m)	$h$ (m)	$t_1$ (m)	$\rho_1$ ( $\Omega m$ )	$\rho_2$ ( $\Omega m$ )
1A	$\infty$	10	$\infty$	2.50	---
1B	$\infty$	10	$\infty$	1.25	---
1C	$\infty$	10	$\infty$	0.60	---
2A	$\infty$	10	6	1.25	2.5
2B	$\infty$	10	6	0.60	2.5
3A	$\infty$	11	$\infty$	2.50	---
3B	$\infty$	9	$\infty$	2.50	---
4A	15	10	$\infty$	2.50	---
5A	20	10	$\infty$	2.50	---
5B	20	10	$\infty$	1.25	---
5C	20	10	$\infty$	0.60	---
6A	$\infty$	$\infty-10$	-	---	---
7A	$\infty$	20	$\infty$	2.50	---
7B	$\infty$	30	$\infty$	2.50	---

solid conductive body (such as the seawater column or the sediments beneath) behaves in a similar way to the shorted turn, except that the distribution of eddy currents depends not only on frequency but also on the shape, size (thickness  $t$  for horizontal layers), and electrical resistivity ( $\rho_a$ ) of the body. At low applied frequencies eddy currents flow deep within the conductor. At high frequencies, the skin effect restricts current flow to a region near the surface of the body.

EM fields depend on the magnetic permeability of earth materials, as well as on the electrical conductivity. Ordinarily the range of effects that can be attributed to variations in magnetic permeability is small compared to the range of effects caused by variations in electrical conductivity. However, nearby, highly magnetic rocks may distort this normal situation, altering the usual relationship between primary and secondary fields. These perturbations are normally small in a marine environment, but a variable permeability may be incorporated into the interpretation procedure when required.

The marine environment offers several advantages to the use of EM techniques that are not enjoyed on land. The highly conductive seawater provides a low impedance contact for the transmitter antenna with no more hardware involved than a bare wire in the water. Because of the low impedance, a very large transmitter

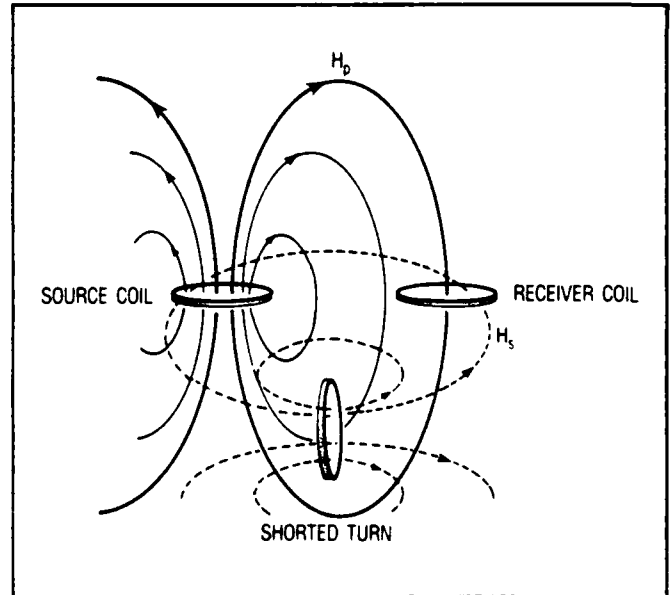


Figure 9. Transformer analogy of an induction system, a primary magnetic field  $H_p$  is generated by an oscillatory current flowing in the source-coil. This field generates current in a shorted turn, representing a conductive earth. This current generates a secondary magnetic field,  $H_s$ . Both fields are measured by the voltage induced in a receiver coil. (From Keller and Frischknecht, 1966)

current of 300 A may be obtained from a moderately powerful supply (Constable et al., 1986). Dipole-type antennas may be towed through the water without interrupting the electrical contact. For a receiving antenna towed near the sea floor, much of the ionospheric noise is removed in the thickness of overlying water, which makes the resolution of very small signals possible. Last, since the seawater is more conductive than the sea-floor materials, at the frequencies of operation (10 Hz to 1 kHz) much of the signal propagates through the sea-floor materials (the region of interest) and not through the seawater column. In very shallow water where the antennas cannot be positioned a large distance from the air-sea interface, some of the EM signal does take an atmospheric path, but this path is unimportant when the water depth is more than one skin depth (25 m at 100 Hz) (Constable et al., 1986).

The major limitation on the use of underwater electromagnetic systems arises as a result of the high attenuation of electromagnetic fields as they propagate through the seawater and the highly conductive surficial sediments. This attenuation is usually presented in terms of a skin depth:

$$\delta = \sqrt{\frac{2}{\omega\mu\sigma}} \quad (5)$$

where

$$\omega = 2\pi f$$

$f$  = signal frequency (Hz),

$\mu$  = magnetic permeability (Henry/m), and

$\sigma$  = electrical conductivity (Siemens/m),  $\sigma = 1/\rho$

As an example, a unit amplitude 100-Hz signal, without considering geometric spreading, would be attenuated as it propagates through the seawater ( $\sigma_{\omega} = 4 \text{ S/m}$ ) to  $e^{-1}$  of its original amplitude in propagating approximately 25 m. (See Fig. 10). Thus, the high attenuation of signal will require that EM systems used for sea-floor description and sediment classification be deployed as close as possible to the sea floor.

## Array geometries

### Straight-wire system

Constable et al. (1986) describe a straight-wire dipole system with grounded ends intended for use in determining geologic structure in marine areas where seismic reflection techniques perform poorly. The dipole-dipole system developed consists of a 30-m transmitting dipole towed in contact with the sea floor, injecting 300 A into the seawater at frequencies of 10 Hz to 1 kHz (Figs. 11a and b). Power is transmitted down the towing cable at 1 kV to limit losses due to cable resistance (Fig. 11b). A transformer near the sea floor converts the power to low voltage, high current.

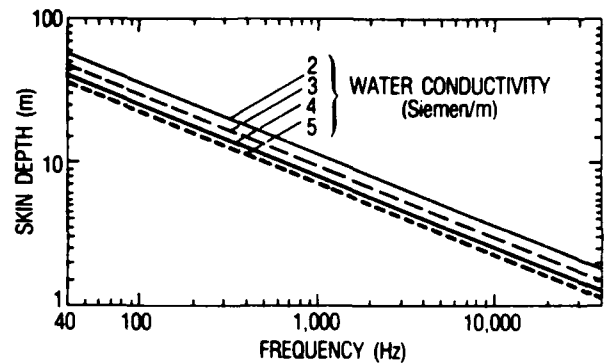


Figure 10. Skin depth of electromagnetic signal as a function of signal frequency and water conductivity (conductivity is the reciprocal of resistivity).

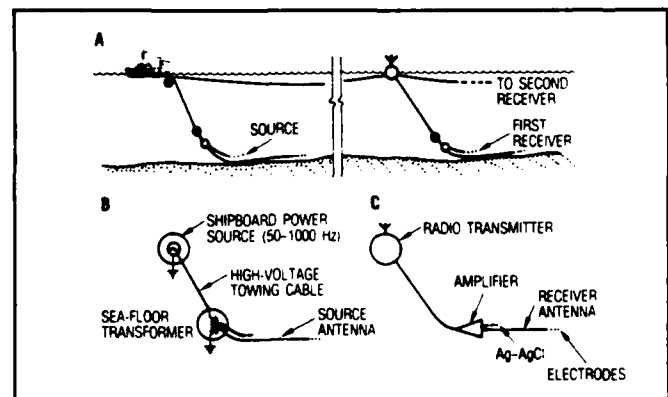


Figure 11. Towed EM system. "A" shows the geometry of an in-line towing system. Black discs represent acoustic transponders used for navigation. "B" and "C" show schematics of the transmitter and receiver, respectively. (After Constable et al., 1986)

Dipole receivers with Ag-AgCl electrodes are (1) towed in tandem with the transmitter from the same ship, (2) towed at a distance from a second ship, or (3) deployed as stationary receivers on the sea floor. Data are collected on magnetic tape and/or transmitted by radio to the transmitter ship (Fig. 11c). Positions of the dipole arrays are established by means of acoustic transponders fitted to the transmitter, the receiver, and the ship (Fig. 11).

The dipole-dipole system includes special receivers that are capable of measuring very small signals and that take advantage of the low input impedance offered by the seawater (Webb et al., 1985). At the highest frequencies, the receiver electrode system has intrinsic noise levels as low as the thermal agitation noise of the  $3 \Omega$  electrode grounding resistance ( $4 \times 10^{-20} \text{ V}^2/\text{Hz}$  above 30 Hz). At frequencies below 1 Hz, electrode noise increases roughly proportional to the inverse of frequency. Receiver noise in the towed array is

dominated by 60-Hz powerline noise and ionospheric noise. Towing of the receivers at 2 knots does result in an increase in noise at frequencies above 60 Hz, but the increase is not overpowering. At frequencies below 60 Hz, towing increases noise from 10 to 100 times due to movement of the receiver antenna (Constable et al., 1986).

### Loop-Loop Systems

Loop-Loop electromagnetic systems are available commercially for search and localization for objects that are either lost on or are shallowly buried in the sea floor. These search systems are designed to detect small electrical-conducting (metal) masses, and their hardware design is likely not optimal for the delineation of horizontal boundaries of sediment layers and measurement of electrical resistivities of those layers.

Airborne electromagnetic (AEM) loop-loop systems have been used to measure sea ice thickness and water depth to the sea floor, and to measure resistivities of surficial sea-floor materials. The AEM work at NORDA has used a commercially available Dighem III frequency-domain system (described by Fraser, 1978, 1979, and 1981) without significant modification. The Dighem III AEM system uses two horizontal-coplanar coil pairs separated by 8 m and operating at 385 Hz and 7200 Hz. The transmitter-sensor (coil pair) was mounted in a bird and towed by a helicopter at the end of a 30-m cable, with the sensor maintained between 40 and 50 m above the sea surface. The resultant AEM field data from track lines in the Cape Cod Bay yield reasonable predictions of sea-floor sediment conductivity up to one skin depth of the source frequency: for the

employed frequencies of 385 Hz and 7200 Hz and for the given water electrical resistivity of  $0.25 \Omega\text{m}$ , the skin depths are 12.8 m and 2.9 m, respectively (Won and Smits, 1985).

In the design of a loop-loop system, the separation between the source loop and the receiver loop must be somewhat more than five times the diameter of either loop in order to facilitate the analysis and permit both loops to be treated as dipoles (Wait, 1954). Four ways are commonly used in which the transmitting and receiving loops are oriented with respect to each other for determining the thickness and resistivity of layered material: horizontal coplanar, vertical coplanar, vertical coaxial, and perpendicular (Fig. 12) (Keller and Frischknecht, 1966).

## Development of predictive techniques

Solutions for the vertical sounding problem using EM techniques in layered terrestrial materials have been developed, and computer-generated solutions are available. In addition, a number of inversion techniques have been developed for the interpretation of data acquired on the surface of a layered earth (Fullagar and Oldenburg 1984; Glenn et al., 1973).

As part of the first-year effort on this project, software has been developed to provide accurate simulations of the EM response for various antennas in a conducting media. The theoretical model used is based on the work of Kong (1972) and Tang (1979). This mathematical approach provides the closed-form solution of Maxwell's equations for arbitrary dipole sources in an  $n$ -layered anisotropic media. The solution is decomposed into two modes, Transverse Electrical (TE) and Transverse Magnetic (TM). These model equations provide a set of integral equations, which have been solved using an adaptive numerical integration package developed by Chave (1983). A portion of the model equations developed and validated as part of this effort are presented in Appendix B.

Software for a VAX 11-780 was developed from the EM model equations of Appendix B and was successfully subjected to a number of internal checks. In addition, the results of the NORDA software have checked well with the published results of Coggen and Morrison (1970) for the vertical magnetic dipole case and those of Weaver (1967) for electric dipoles buried in a simple two-layer model. The model analyses done for this study were calculated on the VAX 11-780, and double-precision accuracy was used for all numerical manipulations. The integrations were calculated using an absolute error criteria of  $10^{-12}$ .

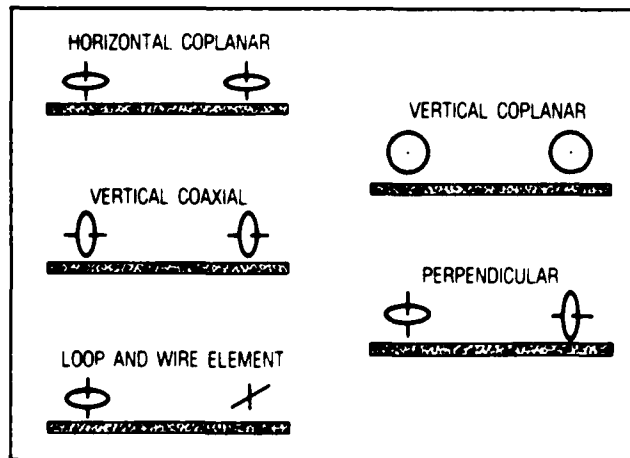


Figure 12. Coil configurations for two-loop soundings. (From Keller and Frischknecht, 1966)

# Analytical studies of EM array performance

## Description

Using the software described above, electric and magnetic fields were calculated for seven basic cases. These simulations provided a starting point for determining the relative ability of various source types to detect expected variations in sea-floor sediment resistivities. The effects of variations in source antenna-receiver antenna roll and pitch also have been examined. The effects of the air-water interface on resistivities measured are considered, and the interaction between the secondary fields generated by both the water and sediment surfaces will be discussed.

The seven cases examined were designed to answer several questions concerning antenna deployment, system characteristics, and data reduction requirements. A set of sketches describing the various case geometries is provided in Appendix C. In the cases considered, the transmitter and receiver antennas were assumed attached to a rigid boom with a separation center-to-center of 10 m. This separation of 10 m was dictated by the assumption of a practical diameter of 1 m for the transmitter. A ratio of antenna separation-to-transmitter diameter of 10 or more is assumed necessary to obtain valid results for the analytical models developed (Appendix B), because these models are derived assuming that the transmitter is an idealized dipole source.

Electric field values for this EM case study are in units of volts per meter (V/m) with a source moment of unity. Magnetic field values are for unit moment sources and are in units of Ampere-turns per meter (A-turns/m). The magnetic permeabilities ( $\mu$ ) of all media were assumed to be  $4\pi \times 10^{-7}$  Henrys per meter (H/m), and the magnetic field values presented may be converted to magnetic induction units by using

$$1 \text{ Ampere-turn/meter} = 1.2566 \times 10^3 \text{ nT } (\gamma).$$

The electric and magnetic field values are composed of contributions from Primary and Secondary fields in the form of Real (In Phase) and Imaginary (Quadrature) Components. The model data are presented in the next section; these electric and magnetic field values are plotted on a linear scale versus an induction number on a log scale:

$$\text{Induction number} = (\omega\mu\sigma)^{1/2}r, \quad (6)$$

where

$$\omega = 2\pi f,$$

$f$  = frequency (Hz), range examined from 10 to 10,000 Hz,

$\mu$  = magnetic permeability (H/m), set at  $4\pi \times 10^{-7}$  H/m,

$\sigma$  = electrical conductivity (S/m), set at 4 S/m, where  $\sigma = 1/\rho$ ,

$\rho$  = electrical resistivity ( $\Omega\text{m}$ ), set at 0.25  $\Omega\text{m}$ , and

$r$  = distance between centers of transmitter and receiver (m), set at 10 m.

The technical feasibility of the underwater EM sediment classification concept will largely depend on the noise level present in the measurement environment. For purposes of this preliminary study of EM performance, noise level criteria have been developed from two sources of field data. First, the electric field noise data presented earlier (Corwin, 1986), believed valid for frequencies below 1 Hz, are expected to represent an upper limit for the noise level, with electric fields at higher frequencies characterized by lower noise levels due to increased propagation attenuation with frequency. Corwin observed noise levels of 2 to 5  $\mu\text{V}$  per meter for his DC resistivity Schlumberger array; thus, for the EM study an electric field noise level of 5  $\mu\text{V/m}$  has been assumed. The magnetic field noise level was selected based on data from an experiment conducted by Giannini and Thayer (1982). Giannini and Thayer towed a horizontal electric dipole source at depths below the sea surface of 20 to 96 m at a speed of 3 m/sec, and measured magnetic fields over depths below the surface from 46 to 109 m. In the frequency range of 1 to 10 Hz, the noise level was determined to be about 0.002 nT, which is equivalent to a magnetic field level of  $1.5 \times 10^{-6}$  A-turn/m. Based on these data, a magnetic field noise level of  $2 \times 10^{-6}$  A-turn/m was used in this study.

## Results

### System 10 m above sea floor, deep water

Figures 13a and b present EM system performance results for an antenna system positioned as shown in Figure C-1 (of Appendix C) with a transmitter moment of 100 A-turn-m<sup>2</sup>. The antenna system is shown operating 10 m above the sea floor in very deep water over three sediment types with resistivities of 0.62, 1.25 and 2.5  $\Omega\text{m}$  (i.e., Formation Factors of 2.5, 5, and 10). Calculations have been performed for horizontal and vertical dipole sources. The use of a horizontal dipole source provides both Transverse Electric (TE) and Transverse Magnetic (TM) coupling into the sediments and theoretically provides more information on sediment resistivities than the other source types. The vertical total magnetic field generated by a horizontal magnetic dipole is shown in Figures 13a and b, with real or in-phase response in Figure 13a and the imaginary or quadrature components given in Figure 13b. The real and imaginary responses have units of A-turn/m and are plotted on an arithmetic scale on the ordinate or vertical axis of the figures. These responses are plotted

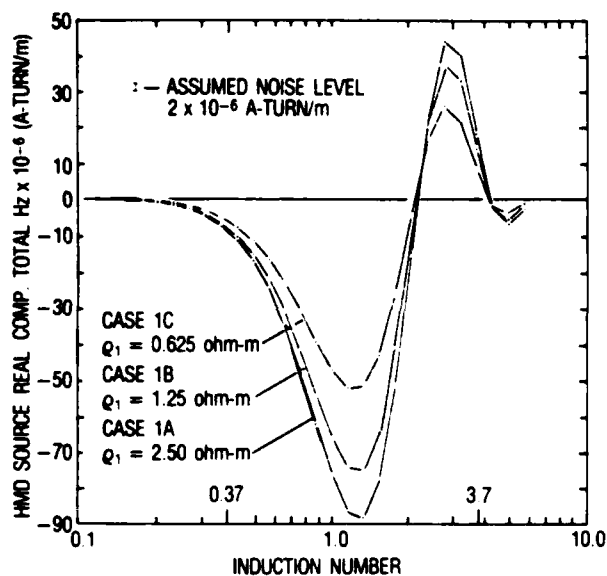


Figure 13(a). Resolution of sediment types, array 10 m above sea floor, overlain by a very thick layer of water; real component of vertical magnetic field (Hz), generated by horizontal magnetic dipole (HMD).

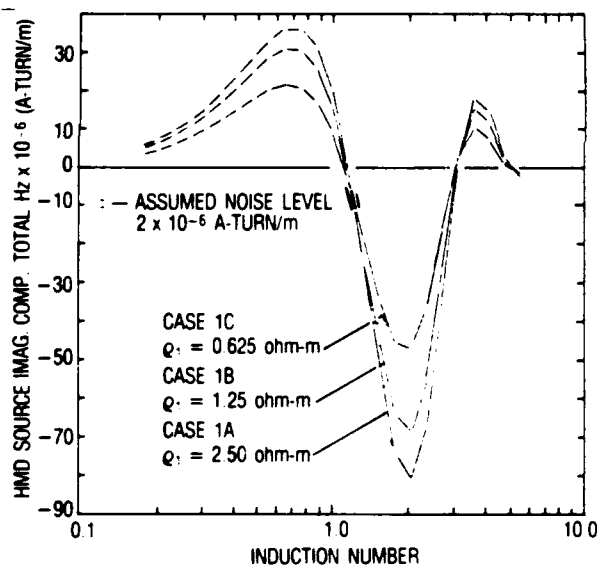


Figure 13(b). Resolution of sediment types, array 10 m above sea floor, overlain by a thick layer of water, imaginary component of Hz generated by HMD.

against corresponding values of induction number (see Equation 6) on a logarithmic scale, where the induction number is a function of frequency which varies from 10 to 10,000 Hz.

Given expected equipment performance, variations on the order  $2 \times 10^{-7}$  A-turn/m in magnetic field should be developed by a source of unit moment, i.e., a source

of 1 A-turn- $m^2$ . Therefore, if a source magnetic moment of 100 A-turn- $m^2$  were to be used, then the amplitude of the magnetic field generated should be  $2 \times 10^{-5}$  A-turn/m. Given the assumed noise level of the magnetic field of  $2 \times 10^{-6}$  A-turn/m, the resulting ratio of S/N level would be about 10. Magnetic moments of 500 A-turns- $m^2$  are reasonably easy to obtain, thus developing an adequate S/N level should not be a problem.

Figures 13 through 19 present calculated magnetic fields at the sensor antenna for a source magnetic moment of 100 A-turn- $m^2$ . On several of these figures, the magnitude of the assumed magnetic noise level,  $2 \times 10^{-6}$  A-turn/m, is also indicated for comparison purposes.

Figures 13a and b indicate that differentiation between sediment types, characterized by variations in formation factor from 2.5 to 10, is possible for induction numbers ranging from 0.37 to 3.7. This range in induction numbers corresponds to frequencies from 42 to 4200 Hz (see Equation 6).

#### System 10 m above sea floor, two-layer sea floor, deep water

Figures 14a and b present calculated magnetic fields at the sensor for antennas towed 10 m above the sea floor in infinitely deep ocean where the sea floor consists of a 6-m-thick sediment layer over an infinitely thick second layer. The resistivity of the top layer is input as 0.62, 1.25, and 2.50  $\Omega m$  with that of the bottom layer maintained at 2.50  $\Omega m$  (Fig. C-2 of Appendix C). As found for the previous model, the resistivity variations in the top 6-m-thick layer are clearly observed in the magnetic field measurements.

It is significant to observe in Figures 14c and d that the magnetic measurements for Case 1C, a low-resistivity (soft?) sediment layer of infinite thickness, are difficult to distinguish from those for Case 2B, low-resistivity (soft?) layer over the high-resistivity (stiff?) sediment layer. These data indicate that the surficial 6-m-thick layer has a dominating influence over the magnetic response at the sensor, and that the underlying layer 2 sediments will be more difficult to classify by electromagnetic methods, when the lower layer has a somewhat higher electrical resistivity.

#### System 10 m above sea floor, water depth 20 m

The influence of shallow-water depth is shown in Figures 15a and b. These figures present results for Cases 5A, B and C, Appendix C, which are the same as the Cases 1 except for water depth. Again, as in the previous two cases, the variations in the sediment resistivity from 0.6 to 1.25 to 2.50  $\Omega m$  are easily detected. A comparison between Figures 15a and 13a indicates that the fields measured in 20 m of water, as opposed to those in an infinite water depth, have

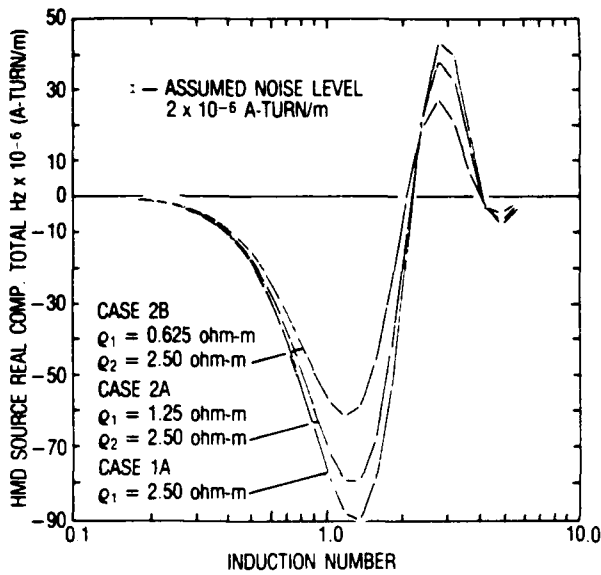


Figure 14(a). Resolution of sediment types, array 10 m above sea floor, 6 m-thick layer 1 over thick layer 2, real component of Hz generated by HMD.

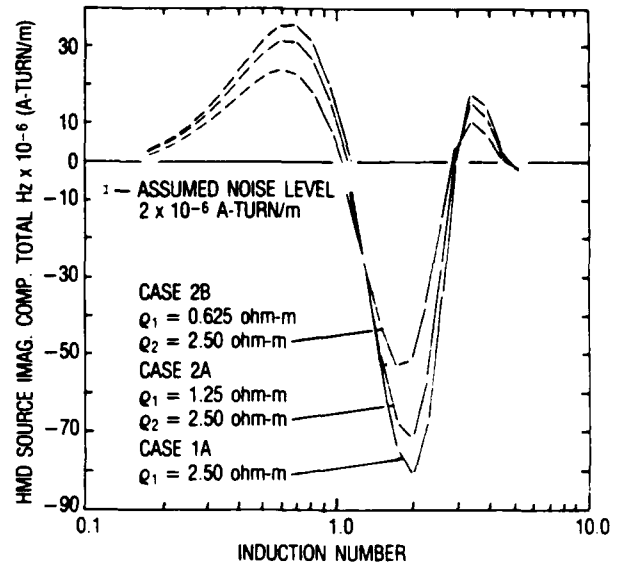


Figure 14(b). Resolution of sediment types, array 10 m above sea floor, 6-m layer 1 over thick layer 2, imaginary component of Hz generated by HMD.

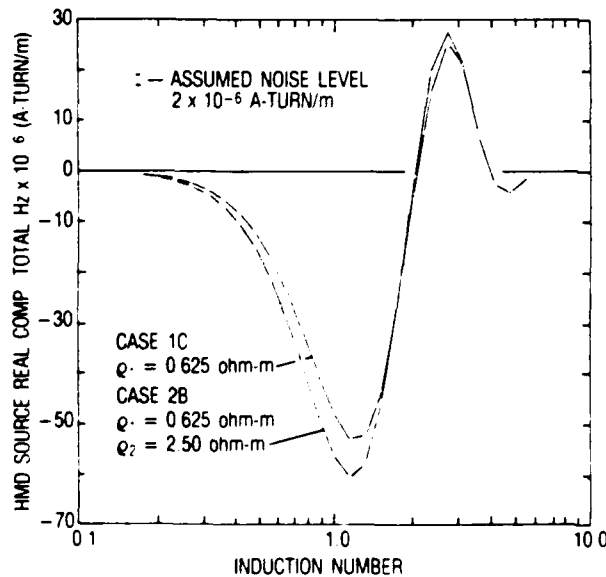


Figure 14(c). Resolution of sediment type of underlying layers, array 10 m above sea floor, 6-m layer 1 over thick layer 2, real component of Hz generated by HMD.

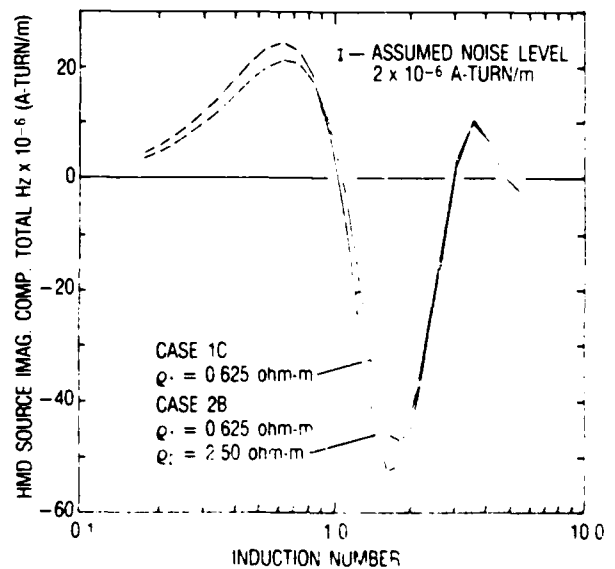


Figure 14(d). Resolution of sediment type of underlying layers, array 10 m above sea floor, 6-m layer over thick layer 2, imaginary component of Hz generated by HMD.

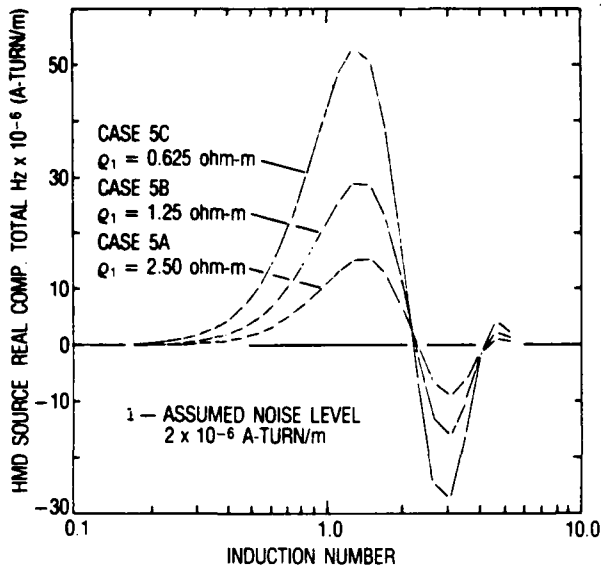


Figure 15(a). Resolution of sediment types in 20-m water depth, array 10 m above sea floor, very thick layer, real component of Hz generated by HMD.

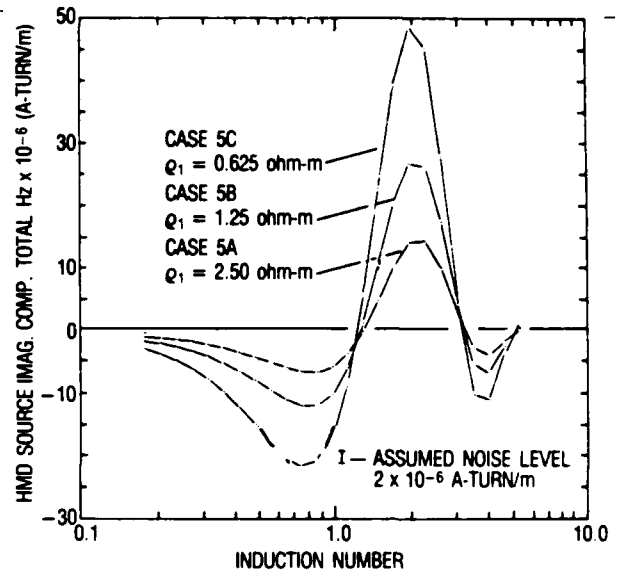


Figure 15(b). Resolution of sediment types in 20-m water depth, array 10 m above sea floor, very thick layer, imaginary component of Hz generated by HMD.

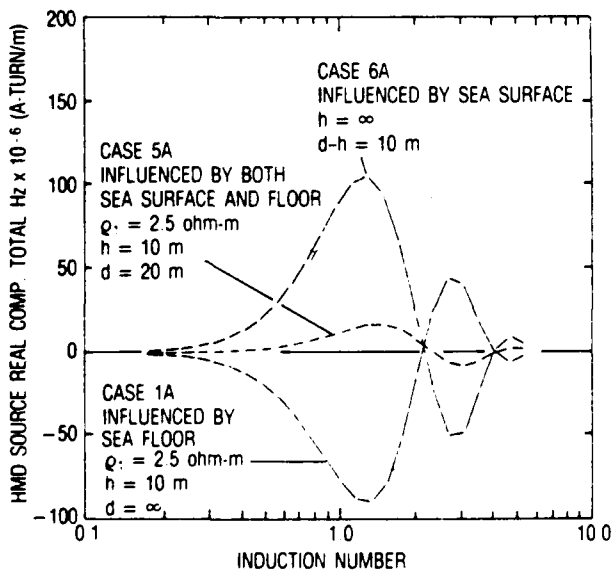


Figure 16(a). Influence of resistive boundaries, real component of Hz generated by HMD.

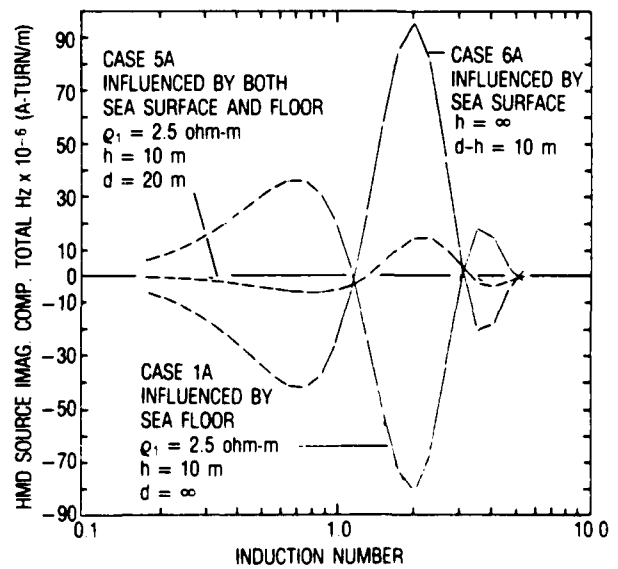


Figure 16(b). Influence resistive boundaries, imaginary component of Hz generated by HMD.

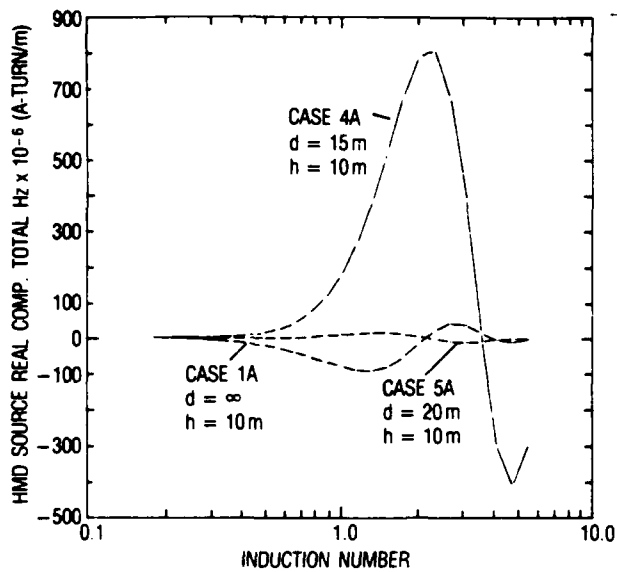


Figure 17(a). Influence of distance to sea surface, array 10 m above sea floor,  $\rho = 2.5$  ohm-m, real component of Hz generated by HMD.

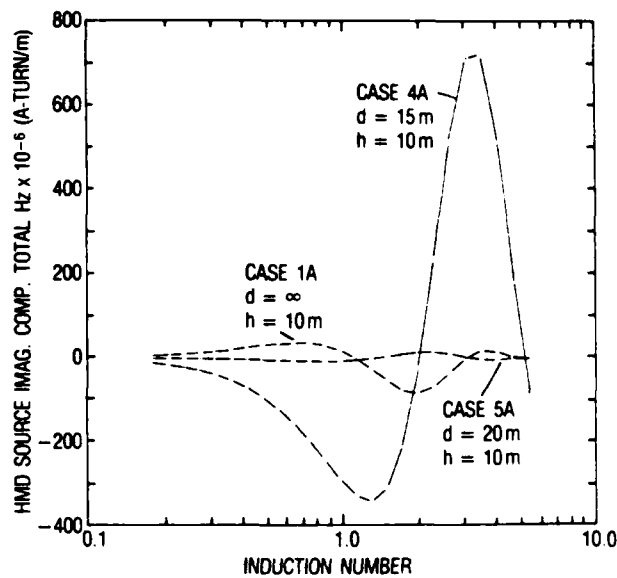


Figure 17(b). Influence of distance to sea surface, array 10 m above sea floor,  $\rho = 2.5$  ohm-m, imaginary component of Hz generated by HMD.

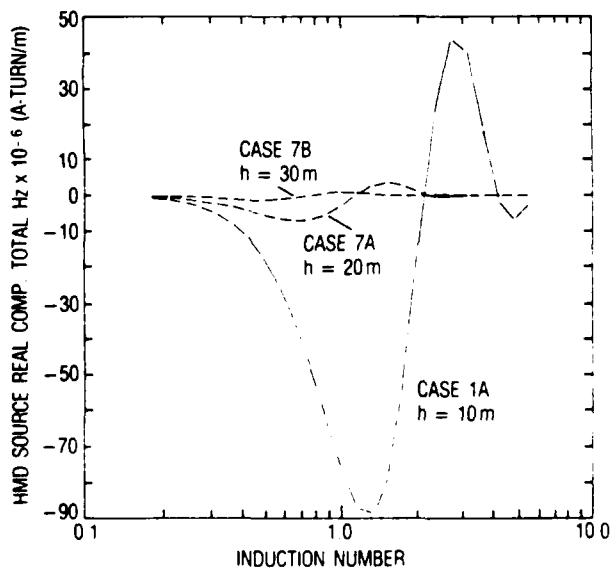


Figure 18(a). Decrease in response with increasing distance above sea floor,  $\rho = 2.5$  ohm-m, real component of Hz generated by HMD.

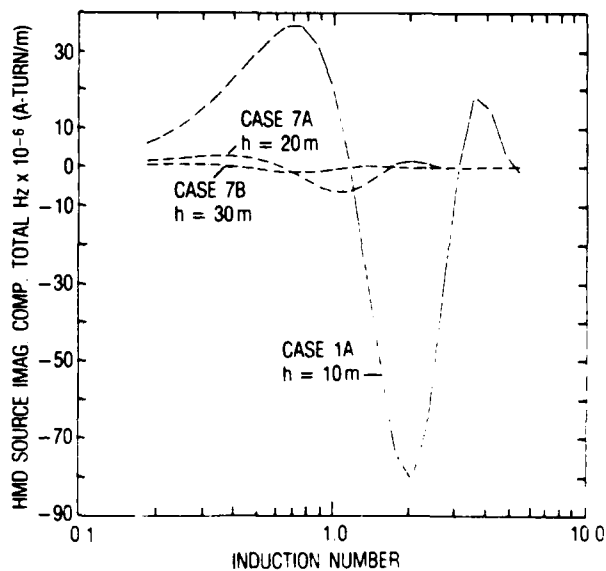


Figure 18(b). Decrease in response with increasing distance above sea floor,  $\rho = 2.5$  ohm-m, imaginary component of Hz generated by HMD.

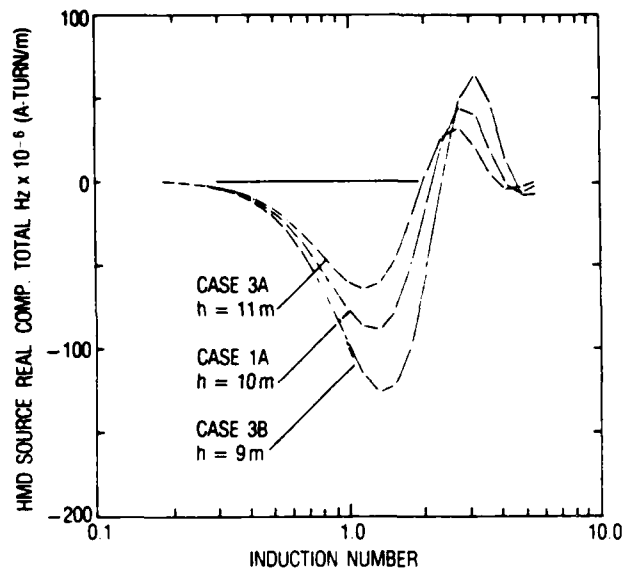


Figure 19(a). Influence of uncertainty in height of array above sea floor,  $\rho = 2.5$  ohm-m, real component of Hz generated by HMD.

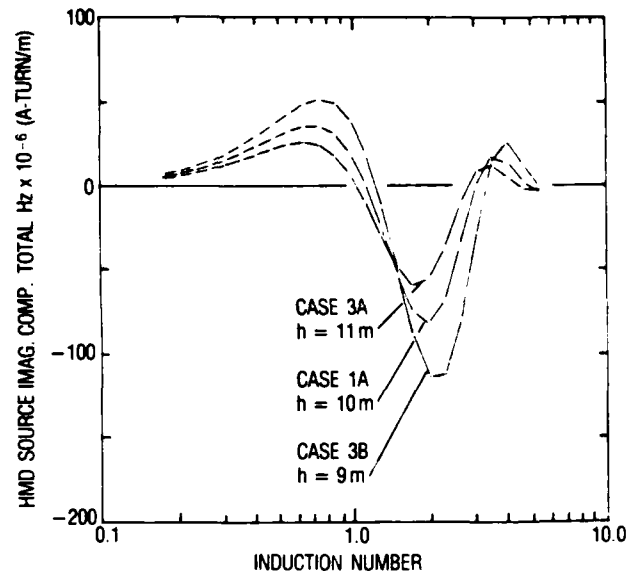


Figure 19(b). Influence of uncertainty in height of array above sea floor,  $\rho = 2.5$  ohm-m, imaginary component of Hz generated by HMD.

decreased by a factor of two, but the resolution between resistivities is similar. In addition, the magnetic response from Cases 5 and 1 are nearly  $180^\circ$  out of phase, with this difference caused by the high electrical resistivity contrast of the air-water interface.

### Distortions due to seafloor and ocean surface

Figures 16a and b show the relative magnitudes of the field distortions introduced by the sea floor and ocean surface boundaries considered in the cases treated above. Case 1A places the EM system in an infinitely deep ocean 10 m over a  $2.5 \Omega\text{m}$  sedimentary half-space, Case 5A lowers the ocean surface to just 10 m over the EM system, and Case 6A leaves the ocean surface at 10 m over the EM system but lowers the sea floor to an infinite distance away. The proximity of the ocean surface, a resistive boundary, and of the sediment surface, also a resistive boundary as compared to the water column, produces reciprocal phase differences (Fig. 16a and b). Note that within the accuracy of the simulation, the sum of the magnetic responses from Cases 1 and 6 is equal to the response calculated for Case 5.

### Influence of the distance to ocean surface

Figures 17a and b indicate the relative distortion in signal caused by towing the EM system through an ocean with various water depths. In all cases considered, the EM system is shown deployed 10 m above a  $2.5 \Omega\text{m}$  sedimentary half-space. The depth of water is varied such that the distance to the ocean surface from the EM

system is infinity (Case 1), 10 m (Case 5), and 5 m (Case 4). The results displayed in Figures 17a and b show that, by varying the towing depth of the EM system below the ocean surface from 10 to 5 m, a variation in magnetic field of nearly two orders of magnitude is induced. This large influence of the sea surface on the measurement indicates that the EM system should be deployed at considerable depth/distance from the sea surface when possible. The electromagnetic field response will depend heavily on any resistive boundaries. Therefore, it follows that EM measurements should be acquired near the boundary of interest (the seafloor/sediments) and away from a high-contrast boundary that is already defined (the ocean surface).

### Influence of height above sea floor

Figures 18a and b illustrate the variations in the magnetic field response induced by varying the height of the EM system above the sea floor. In all cases, the EM system is in an ocean of infinite depth over a  $2.5 \Omega\text{m}$  sedimentary half-space. The distance of the EM system above the sea floor is varied from 10 m (Case 1A) to 20 m (Case 7A) and to 30 m (Case 7B). By raising the EM system from 10 to 20 m above the sea floor, the magnetic response measured from the sediments decreases by an order of magnitude, with an equal change in raising the system from 20 to 30 m. This large decrease in response is caused by the large electromagnetic propagation attenuation induced by the seawater column. Note that the magnetic response for increasing

standoff distance is not only attenuated, but the response is also confined to a lower frequency range (see Eq. 4).

### Influence of elevation errors

Figures 19a and b show the variations in the vertical magnetic field at the sensor induced by  $\pm 1$ -m vertical variation in the position of the horizontal dipole EM system, i.e., standoff distances of 9, 10, and 11 m above the sea floor. The variations in magnetic field are on the order of  $35 \times 10^{-6}$  to  $65 \times 10^{-6}$  A-turns/m. In comparison, the variations in magnetic field arising due to change in sediment resistivity from 0.60 to 2.50  $\Omega$ m for a fixed standoff distance of 10 m (Fig. 13a and b) vary over a range of  $25 \times 10^{-6}$  to  $35 \times 10^{-6}$  A-turns/m—the same order of magnitude as the error caused by a  $\pm 1$  m variation/error in the EM system standoff distance. To achieve required measurement accuracy, the standoff distance from the sea floor will have to be known to better than 0.1 m. This standoff distance measurement accuracy may be provided by the combined use of an acoustic system in conjunction with the interpretation of the high-frequency components of the EM data.

### Influence of transmitter/receiver tilt.

The error in magnetic field measurement caused by tilt (or pitch) of the transmitter/receiver system in airborne systems has been studied in detail by Son (1965). His work indicated that error due to tilt could be as large as several percent. Preliminary calculations done in this study for a submerged system indicate that the tilt angle must be measured and appropriate corrections made to the field data before a reliable interpretation is possible.

## Discussion

The preliminary evaluation of EM system performance in the classification of sea-floor sediments shows that the concept is technically feasible. Implementation of the concept will not be without problems. Proper performance of the system requires that the transmitter/receiver antennas be towed within 10 m of the sea floor, that the actual standoff distance above the sea floor be known to the nearest 0.1 m and possibly slightly better, and that the pitch of the antennas be measured to the nearest 0.1°.

### Possible design

The firm design of a system would be premature at this point; however, a short summary of the requirements for an underwater electromagnetic system is provided. A frequency domain system should have a rigid support connecting the transmitter and receiver at

a fixed separation of 5 to 10 m. The source and receivers should have a bandwidth of 10–1000 Hz. Due to the small amplitude of the expected electric fields ( $\mu$ V/m), induction coil sensors should be used for magnetic field measurements. The transmitter may be short electric dipoles with lengths of 1 to 2 m or induction coils with a diameter on the order of 1 m. The ship's power supply could be used to drive the transmitter by converting the power into the desired waveform using control amplifiers. A shipboard AC power supply of 208 VAC is capable of providing a 50-A current source to either an insulated loop source or a short electric dipole. This would provide a magnetic moment of 500 to 1000 A-turns-m<sup>2</sup> or an electric dipole moment of 50 to 100 A-m. A loop with 50 to 100 turns of No. 8 AWG copper conductor with 0.045-inch polyethylene insulation would be adequate to handle these current levels with a resulting weight of less than 500 lb.

## Induced polarization (IP) methods

In both the DC and EM methods presented, the measured electrical conductivity of the sea-floor materials has been assumed to be independent of the harmonic content of the transmitted signal. In reality electrical properties do depend on frequency to some extent, but the degree of dependence is small enough that the effect can be ignored when applying the DC and EM methods to the determination of sediment layer electrical resistivities and thicknesses. On the other hand, it is possible to design measurement methods that utilize this frequency-dependent property (Keller and Frischknecht, 1966) to detect the existence of clay minerals in a sediment and possibly even determine the percentage of clay minerals in the sediment (Wynn, 1987). The method is not new (i.e., early work described by Schlumberger, 1920); however, modern development originates largely with Bleil (1953).

The electrical polarization most conductors acquire in an electric field disappears instantaneously when the field is switched off. Some materials, however, retain part of their polarization for a time of the order of a few hundred milliseconds and, although the electrochemical mechanism of the effect is not fully understood, it is associated with conductors containing disseminated metallic ore minerals or colloidal particles (clay minerals) (Griffiths and King, 1965). When the current flow is abruptly interrupted, the electric field will decay as shown in Figure 20, with a quick drop to a value  $V_1$  which is usually a small fraction of the static field,  $V_0$ . After this initial drop, the field will decay slowly with measurable size for periods of minutes to hours (Keller and Frischknecht, 1966). The depolarization or decay

curve is generally logarithmic in shape, although contributing components with different time constants can usually be identified (Sumner, 1979).

Prior to 1950, all IP measurements were of the time-domain type that used the waveforms shown in Figure 21. A simple on-off step-function current (Fig. 21a) was impressed in the earth by the grounded contacts and, in polarizable materials, a modified waveform similar to Figure 21b would be observed. Analysis of the voltage waveform, i.e., the ratio of secondary potential ( $V_s$ ) to maximum primary potential ( $V_p$ ) and the time-history of the transient voltage ( $V_t$ ), gives a measure of the IP effect (Sumner, 1979).

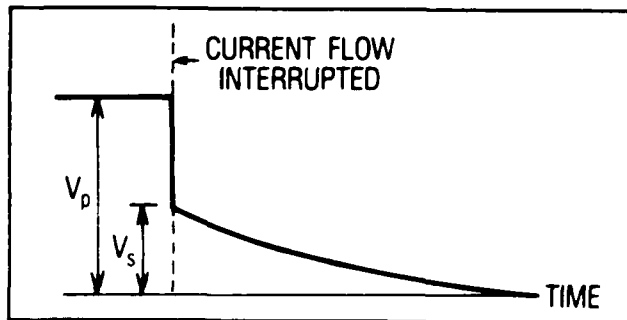


Figure 20. Transient decay of electric field strength in a rock sample (after Keller and Frischknecht, 1966).

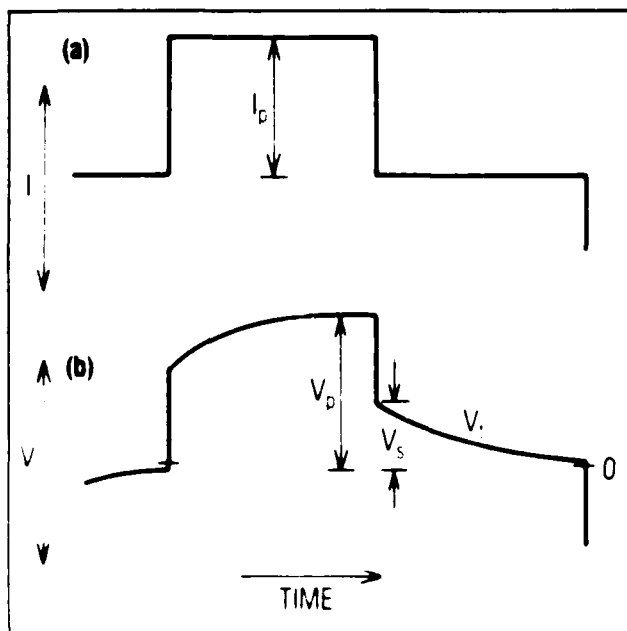


Figure 21. The time-domain transmitted and received voltage waveforms, showing the inducing primary current  $I$ , being detected as a maximum primary voltage  $V_p$ . When current is turned off, voltage drops to a secondary level  $V_s$  and the transient voltage  $V_t$  decays with time. (After Sumner, 1979)

After 1950, frequency-domain field equipment has played an increasing role in the measurement of IP data. The voltage decay ( $V_t$ ) induced by the IP phenomenon is time-dependent; therefore, the resistivity must also have a frequency dependence since the time domain data are related to the frequency domain measurements through the Fourier transform. Thus, polarized materials can be viewed as having an impedance that is frequency dependent. This impedance may be measured using frequency domain techniques; an example of the current and voltage waveform patterns for this type of IP measurement is shown in Figure 22. The difference in apparent resistivities or measured voltages at high and low frequencies is used to calculate parameters useful in estimating the degree of polarization (Sumner, 1979).

A practical way of implementing this approach requires time synchronization of the transmitter and the receiver to permit the measurement of the relative phase difference between transmitted and received signals (Fig. 23). The phase difference, determined either in time or as a phase angle, gives the polarization of the intervening earth. The resulting harmonic responses can be decomposed into in-phase and out-of-phase components over the range of observed frequencies, which may in turn be plotted in the complex plane as a series of rotating vectors. Data in this form are known as complex resistivity measurements (Fig. 24) (Sumner, 1979). Polarizable materials exhibit characteristic frequency responses, with the frequency response of the imaginary component being diagnostic of mineral type. Further, the magnitude of the maximum imaginary component is diagnostic of the percentage content of the mineral type (Wynn, 1987). Wynn has successfully used the IP method in shallow water off the Georgia coast to evaluate the technical feasibility of mapping ilmenite (titanium ore) deposits.

In addition to metallic minerals, fine-grained clays and fibrous minerals, such as serpentinite, can produce a moderately strong IP effect. In many areas, the clay minerals provide a polarization response, which may be easily measured with conventional IP instruments.

Induced polarization at low frequencies cannot be explained in terms of atomic or molecular structure. The important phenomena contributing to IP appear to be electrode reactions between electrolytes and metallic mineral grains, variation of electrolyte mobility in fine-grained materials, and related phenomena (Keller and Frischknecht, 1966). At this time, there are several proposed electrical theories, none of which has a firm foundation based on the fundamental electrochemical nature of polarizable materials. Further, electrochemistry holds the clues to the reality and meaning of mineral discrimination as gained from spectral IP data. Much more research remains to be accomplished before the IP mechanism is fully understood (Sumner, 1979).

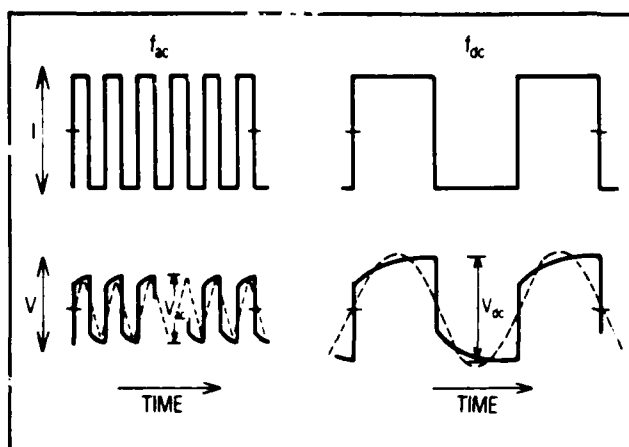


Figure 22. Frequency-method waveforms, showing a controlled constant inducing current  $I$  at frequencies  $f_{ac}$  and  $f_{dc}$  being detected as voltages  $V_{ac}$  and  $V_{dc}$  where  $V_{ac} < V_{dc}$ . The dashed line is the sinusoidal filtered voltage. (After Sumner, 1979)

At this time then, it is established that some clay minerals, specifically the montmorillonites, do exhibit a strong IP effect, and that quartz sands exhibit virtually no IP effect, leading to the hypothesis that we may be able to distinguish cohesive from cohesionless sediments by using IP (Wynn, 1987). The fundamental electrochemical nature of the clay minerals is not sufficiently well understood to support the development of electrical theories for the prediction of the IP response of a pure clay mineral assemblage, much less the usual mixture of clay minerals and other sediment components. Thus, for the near-term, a clay mineral classification and quantification scheme will have to be empirical in nature based on measured data. Further, it will probably be necessary to build that empirical data base on undisturbed sediment samples and possibly on in situ measurements. Slight drying of geologic materials is known to alter their IP response, and hydrostatic pressure release and slight sample shear deformation during coring, core extrusion, and sample preparation might also have adverse effect on the IP response. These potential problems can all be circumvented, and they do not negate the idea of using IP for sediment classification.

IP measurements require high-quality antennas, transmitter, and receiver. These components are the same as those used in a high-quality DC resistivity system. Thus, the same hardware and electronics can be used for both IP and DC resistivity (although cheaper, lesser-quality systems can suffice for DC resistivity measurements).

Overall, then, IP is a very attractive technology as an add-on to DC, EM, and acoustic technologies for near-surface sediment classification.

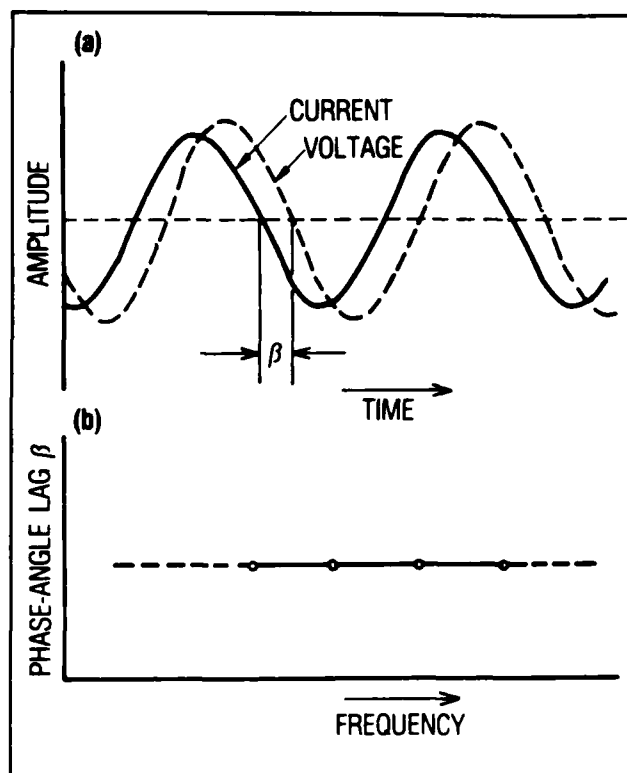


Figure 23. Phase determinations: (a) Phase lag angle  $\beta$  between input (solid) and output (dashed) sinusoidal waveforms, and (b) an ideal IP phase spectrum diagram. (After Sumner, 1979)

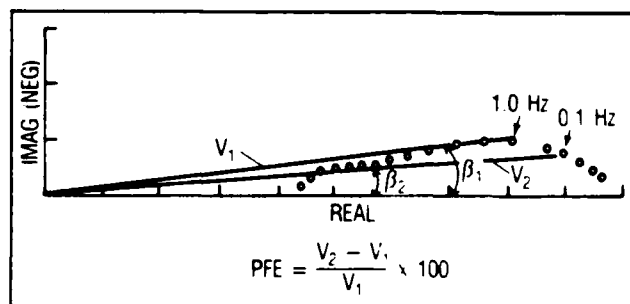


Figure 24. Representation of phase lag due to induced polarization in the complex plane. (After Sumner, 1979)

## Summary and conclusions

### Field results

- Field results show that a practical DC resistivity array of 40 m length dragged on the sea floor should give acceptable resolution of sub-seafloor layer parameters to subseafloor penetrations of 5 m.

## Analytical results

- To resolve properties of a thin surficial sediment layer (1 m thickness) the DC array must be deployed on or less than 1 m above the sea floor.

- If averaging of properties over a thicker layer of 6 m thickness is acceptable, then resolution can be achieved with a DC array standoff distance as much as 10 m.

- An EM array is predicted to resolve resistivity variations (and sediment type) in the upper 6 m of the sea-floor sediments over an EM bandwidth of several kilohertz when towed within 10 m of the sea floor.

- The EM field response is strongly influenced by the air-sea interface; therefore, the EM array must be operated/towed far away from the sea surface and close to the interface of interest, the sea floor, to enhance resolution.

- Unknown variation or error in the height of the EM array above the sea floor causes a significant error in the sediment resistivities calculated. To achieve required measurement accuracy, the distance of the EM array above the sea floor will have to be known to better than 0.1 m. This altitude accuracy is achievable through the joint use of acoustic height information and interpretation of high-frequency EM data.

- Tilt of EM system coil antennas can result in error of predictions of several percent; thus, tilt angle of the antennas must be measured and corrections made to the data to achieve a reliable interpretation. Tilt sensors are available to provide the required measurement accuracy or better.

- IP technology shows promise for the detection of clay minerals in surficial sediments and possibly even for the coarse estimation of proportion of clay.

## Recommendations

- Field data should be obtained to validate the computer predictions of DC resistivity system performance. A DC inverted Schlumberger array capable of being towed on or near the sea floor and capable of 6-m penetration (about 40 m long) should be designed and fabricated. Deckside components should be borrowed or rented. Data should be gathered over area(s) with adequate ground truth, and the quality of the data gathered and the resolution of the sediment resistivities calculated should be evaluated and compared to ground truth data. Electrode noise should be measured in these open ocean conditions and, if necessary, options developed to reduce noise levels and thus improve signal-to-noise levels and data resolution.

- The initial work on determining EM resistivity system performance should be extended to compare insulated coil transmitter performance with that of electric dipole sources, i.e., additional electric and magnetic dipole responses should be calculated. Initial

work indicates that electric dipole sources may provide adequate fields at lower cost and weight than insulated coil transmitters.

- Time domain EM techniques should be evaluated for application to the surficial sea-floor resistivity measurement problem because operating in the time domain may simplify hardware design requirements. Time domain systems measure the secondary fields after the primary fields are terminated; therefore, time domain systems are less sensitive to the relative position and orientation of the receiver. Because dimensionless tolerances are less, the transmitter and receiver may not require a rigid boom support.

- A comparison of the DC resistivity and electromagnetic responses over a suite of sedimentary models should be done. This would provide a measure of the relative sensitivity of the two techniques to variations in sea-floor sediments. The ability of the two methods to complement each other and perhaps resolve certain ambiguous cases should be considered and evaluated.

- A laboratory and field IP effort should be undertaken to determine the feasibility of detecting clay mineral existence and percent content to a degree that would provide practical input to remote sediment classification.

## References

- Alfano, L. (1962). Geoelectrical Prospecting with Underground Electrodes. *Geophysical Prospecting* 10 (3) 271-289.
- Archie, G. E. (1942). The Electrical Resistivity Log as an Aid in Determining Some Reservoir Characteristics. *Transactions, AIME* 146, 54-62.
- Barnes, B. B., R. F. Corwin, T. G. Hildenbrand, L. Jackson, R. Kessler, W. Takeyama, M. Hornick, and R. Jenkins (1973). *Geophysics Applied to Geotechnical Problems in a Marine Environment. A Case Study: Monterey Bay, California*. U.S. Department of Commerce, annual report. ARPA Order No. 1979, Amend. 3.
- Beard, R. M. (1984). *Expendable Doppler Penetrometer for Deep Ocean Sediment Strength Measurements*. Naval Civil Engineering Laboratory, Port Hueneme, California, TR-905.
- Beckman, H., and G. Demiray (1976). The Nanolog, a New Way to Log the Resistivity of the Seafloor. *Geophysical Prospecting* 22, 309-316.
- Bennett, R. H., D. N. Lambert, M. H. Hulbert, J. T. Burns, W. B. Sawyer and G. L. Freeland (1983). Electrical Resistivity/Conductivity in Seabed Sediments. In *CRC Handbook of Geophysical Exploration at Sea*, R. A. Geyer and J. R. Moore (eds.), CRC Press, Boca Raton, Florida, pp. 333-375.

- Beyer, J. H. (1971). Unpublished report retained by R. F. Corwin.
- Bischoff, J. (1978). *Die Anwendung Geoelektrischer Widerstandsmethoden in Marinen Bereich*. Ph.D. thesis, Tech. University of Berlin (in German).
- Bleil, D. F. (1953). Induced Polarization: A Method of Geophysical Prospecting. *Geophysics* 18(3) 636.
- Bogolovski, V. A. and A. A. Ogilvy (1974). Detailed Electrometric and Thermometric Observations in Offshore Areas. *Geophysical Prospecting* 22, 381-392.
- Boyce, R. E. (1967). *Electrical Resistivity of Modern Marine Sediments from the Bering Sea*. M. S. thesis, San Diego State College, California.
- Chave, A. D. (1983). Numerical Integration of Related Hankel Transforms by Quadrature and Fraction Expansion. *Geophysics* 48, 1671-1687.
- Coggon, J. H. and H. F. Morrison (1970). Electromagnetic Investigation of the Sea Floor. *Geophysics* 35, 467-489.
- Constable, S. C., C. S. Cox, and A. D. Chave (1986). Offshore Electromagnetic Surveying Techniques. *Expanded Abstracts, Fifty-Sixth Annual International Meeting of the Society of Exploration Geophysicists*, November 2-6, Houston, Texas, pp. 81-85.
- Corwin, R. F. (1976). Offshore Use of the Self-Potential Method. *Geophysical Prospecting* 24(1), 79-90.
- Corwin, R. F. (1983). Marine Permafrost Detection Using Galvanic Electrical Resistivity Methods. *Proceedings, 1983 Offshore Technology Conference*, Houston, Texas, OTC 4480, pp. 329-336.
- Corwin, R. F. (1985). Electrical Resistivity Techniques for Offshore Arctic Geotechnical Engineering Applications, Civil Engineering in the Arctic Offshore. *Proceedings, Arctic '85*, American Society of Civil Engineers, pp. 137-143.
- Corwin, R. F. (1986). *Investigation of the Direct-Current Electrical Resistivity Method for Sea-Floor Property Classification*. Report prepared by Harding-Lawson Assoc., Novato, California, for the Naval Ocean Research and Development Activity, NSTL, Mississippi, under Contract No. N00014-86-M-6035, 5 August, p. 39.
- Corwin, R. F. and U. Conti (1973). A Rugged Silver-Silver Chloride Electrode for Field Use. *Review of Scientific Instruments* 44, 708-711.
- Corwin, R. F. and U. Conti (1973a). Sea-Floor Electrical Resistivity Measurement, Using a Diver-Operated System. *Proceedings, Offshore Technology Conference*, 1, 1-637 - 1-644.
- Francis, T. J. G. (1977). *Electrical Prospecting on the Continental Shelf*. Institute of Geological Sciences, London, Report 77/4.
- Fraser, D. C. (1978). Resistivity Mapping with an Airborne Multicoil Electromagnetic System. *Geophysics* 43, 144-172.
- Fraser, D. C. (1979). The Multicoil II Airborne Electromagnetic System. *Geophysics* 44, 1367-1394.
- Fraser, D. C. (1981). Magnetic Mapping with a Multicoil Airborne Electromagnetic System. *Geophysics* 46, 1579-1593.
- Fullagar, P. K. and D. W. Oldenburg (1984). Inversion of Horizontal Loop Electromagnetic Frequency Soundings. *Geophysics* 49, 150-164.
- Giannini, J. and D. Thayer (1982). Extremely Low Frequency (ELF) Quasi-Static Propagation Measurements for a Calibrated Electric Field Source in the Ocean. *IEEE Transactions on Antennas and Propagation*, AP-30, (5), September, pp. 825-831.
- Glenn, W. E., Jisoo Ryu, S. H. Ward, W. J. Peeples and R. J. Phillips (1973). The Inversion of Vertical Magnetic Dipole Sounding Data. *Geophysics* 38(6) 1109-1129.
- Griffiths, D. H. and R. F. King (1965). *Applied Geophysics for Engineers and Geologists*. Pergamon Press, New York.
- Hutt, J. R., and J. W. Berg, Jr. (1968). Thermal and Electrical Conductivities of Sandstone Rocks and Ocean Sediments. *Geophysics* 33(3), 489-500.
- Keller, G. V. and F. C. Frischknecht (1966). *Electrical Methods in Geophysical Prospecting*. Pergamon Press, New York.
- Kermabon, A., C. Gehin, and P. Blavier (1969). A Deep-Sea Electrical Resistivity Probe for Measuring Porosity and Density of Unconsolidated Sediments. *Geophysics* 34(4), 554-571.
- Kong, J. A. (1972). Electromagnetic Fields due to Dipole Antennas over Stratified Anisotropic Media. *Geophysics* 37, 985-996.
- Lambert, D. N. (1987). *An Evaluation of a Computerized Acoustic Sediment Classification System*. Naval Ocean Research and Development Activity, NSTL, Mississippi, NORDA Report 169 (in press).
- Roy, K. K. and H. M. Elliot (1981). Some Observations Regarding Depth of Exploration in DC Electrical Methods. *Geoexploration* 19, 1-13.
- Schlumberger, C. (1920). *Etude sur la Prospection Electrique du Sous-Sol*. Gauthier-Villars et Cie., Paris.
- Schlumberger, C., M. Schlumberger, and E. G. Leonardon (1934). Electrical Exploration of Water-Covered Areas. *Transactions, American Institute of Mining and Metallurgical Engineers* 110, 122-134.
- Son, K. H. (1985). *Interpretation of Electromagnetic Dipole-Dipole Frequency Sounding Data over a Vertically Stratified Earth*. Ph.D. Thesis, North Carolina State University.

Sumner, J. S. (1979). The Induced-Polarization Exploration Method. In *Geophysics and Geochemistry in the Search for Metallic Ores*, P. J. Hood (ed.), Geological Survey of Canada, Economic Geology Report 31, pp. 123-133.

Tang, C. M. (1979). Electromagnetic Fields due to Dipole Antennas Embedded in Stratified Anisotropic Media. *IEEE Transactions on Antennas and Propagation* AP-27 (5), 665-670.

Valent, P. J. (1986). *Shallow-Water Recoverable Penetrometer System*. Proposal for assembly to Naval Oceanographic Office from Naval Ocean Research and Development Activity, NSTL, Mississippi, 24 November.

Wait, J. R. (1954). Mutual Coupling of Loops Lying on the Ground. *Geophysics* 19(2), 290-296.

Weaver, J. T. (1967). The Quasi-Static Field of an Electric Dipole Embedded in a Two-Layer Conducting Half-Space. *Canadian Journal of Physics* 45, 1981-2002.

Webb, S. C., S. C. Constable, C. S. Cox, and T. K. Deaton, 1985. A Seafloor Electric Field Instrument, *J. Geomagnetism and Geoelectr.*, Vol. 37, pp. 1115-1129.

Won, I. J. and K. Smits (1985). *Airborne Electromagnetic Bathymetry*. Naval Ocean Research and Development Activity, NSTL, Mississippi, NORDA Report 94.

Wynn, J. (1987). Personal Communication. Office of Mineral Resources, U. S. Geological Survey, Reston, Virginia, 8 January.

**Appendix A. Calculated resistivity resolutions for DC  
Schlumberger array**

---

RhoA  
(ohm-m)

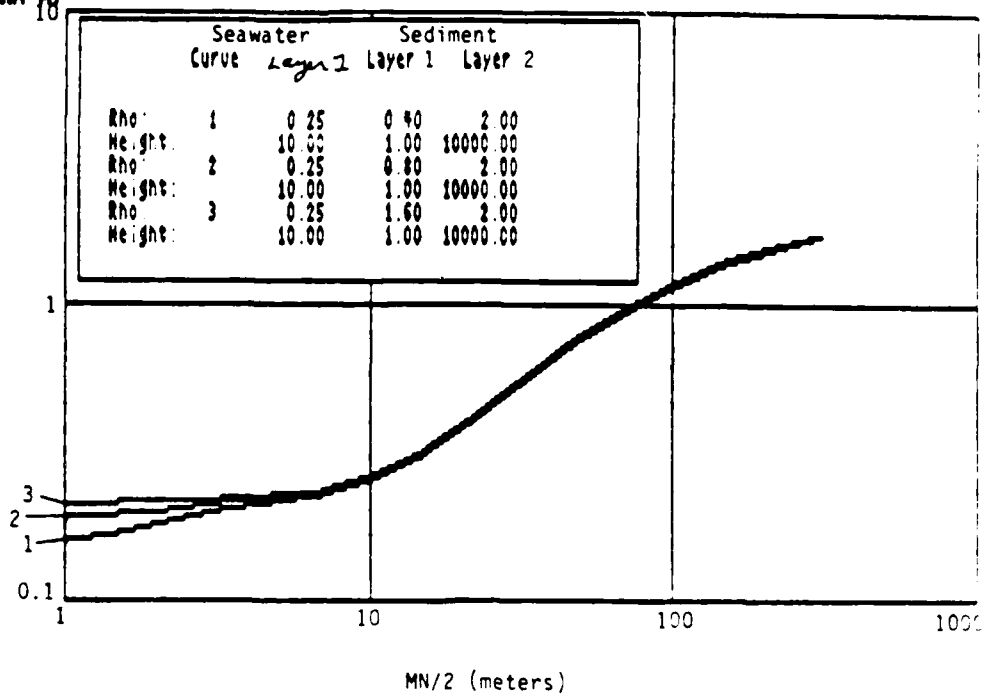


Figure A-1. Case 1, DC Resistivity Resolution, 10m Water Depth, Array on Sea Floor, 1m Thick Layer 1

RhoA  
(ohm-m)

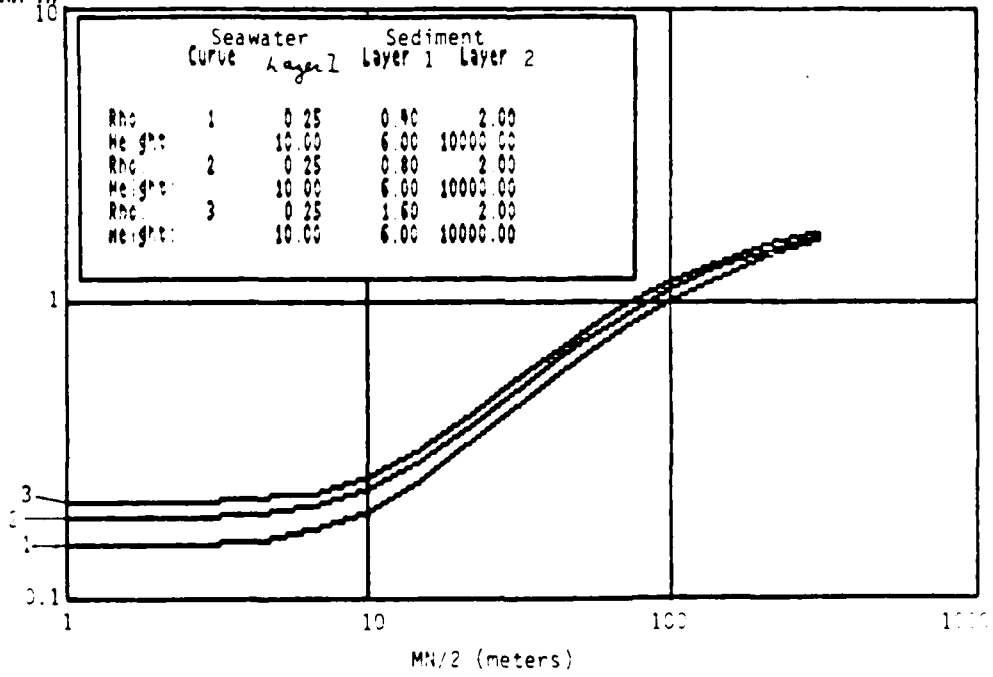


Figure A-2. Case 2, DC Resistivity Resolution, 10m Water Depth, Array on Sea Floor, 6m Thick Layer 1

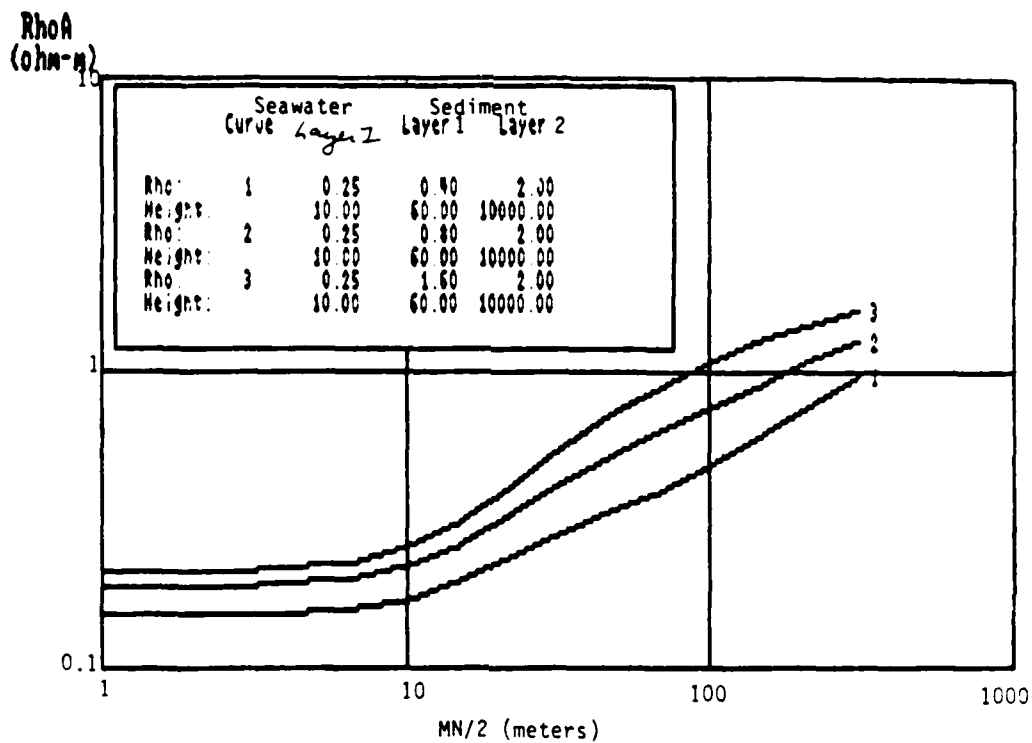


Figure A-3. Case 3, DC Resistivity Resolution, 10m Water Depth, Array on Sea Floor, 60m Thick Layer 1

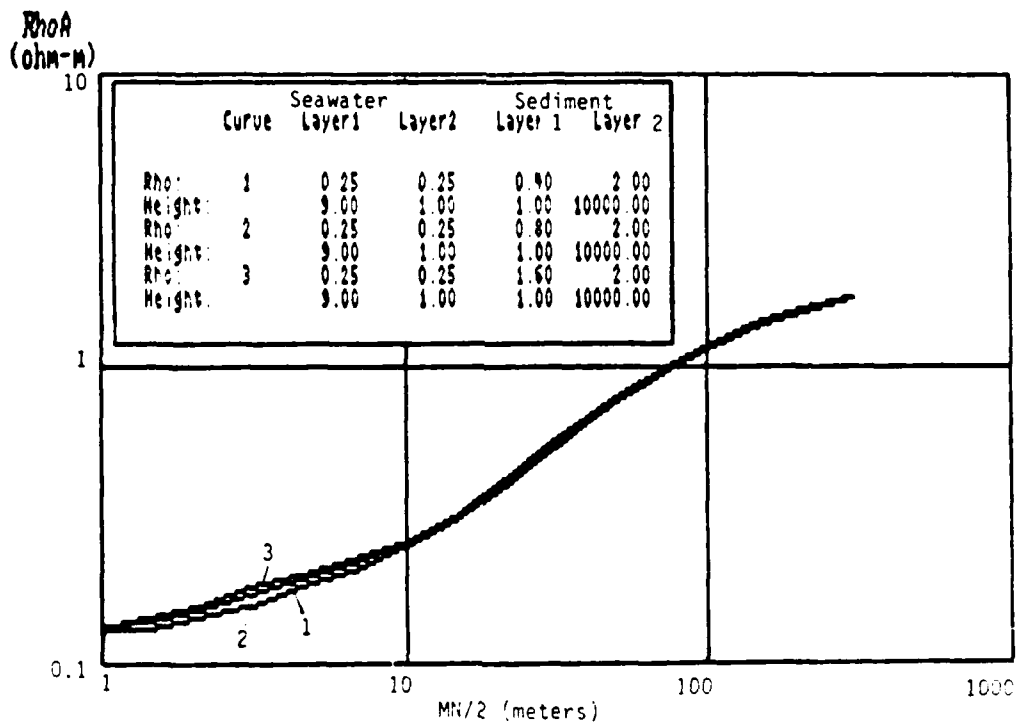


Figure A-4. Case 4, DC Resistivity Resolution, 10m Water Depth, Array 1m Above Sea Floor, 1m Thick Layer 1

RhoA  
(ohm-m)

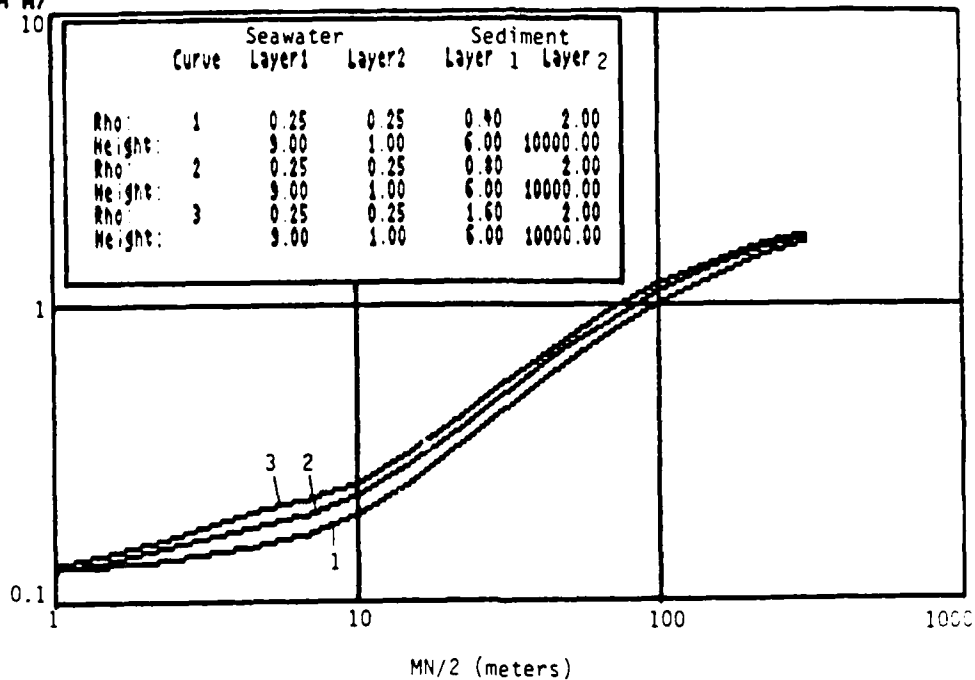


Figure A-5. Case 5, DC Resistivity Resolution, 10m Water Depth, Array 1m Above Sea Floor, 6m Thick Layer 1

RhoA  
(ohm-m)

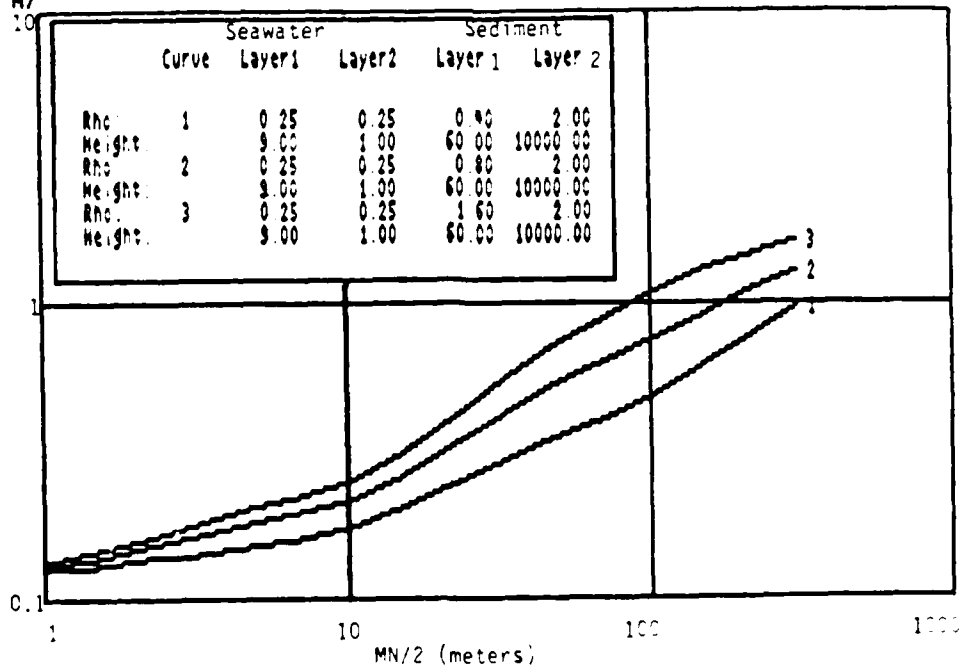


Figure A-6. Case 6, DC Resistivity Resolution, 10m Water Depth, Array 1m Above Sea Floor, 60m Thick Layer 1

RhoA  
(ohm-m)  
10

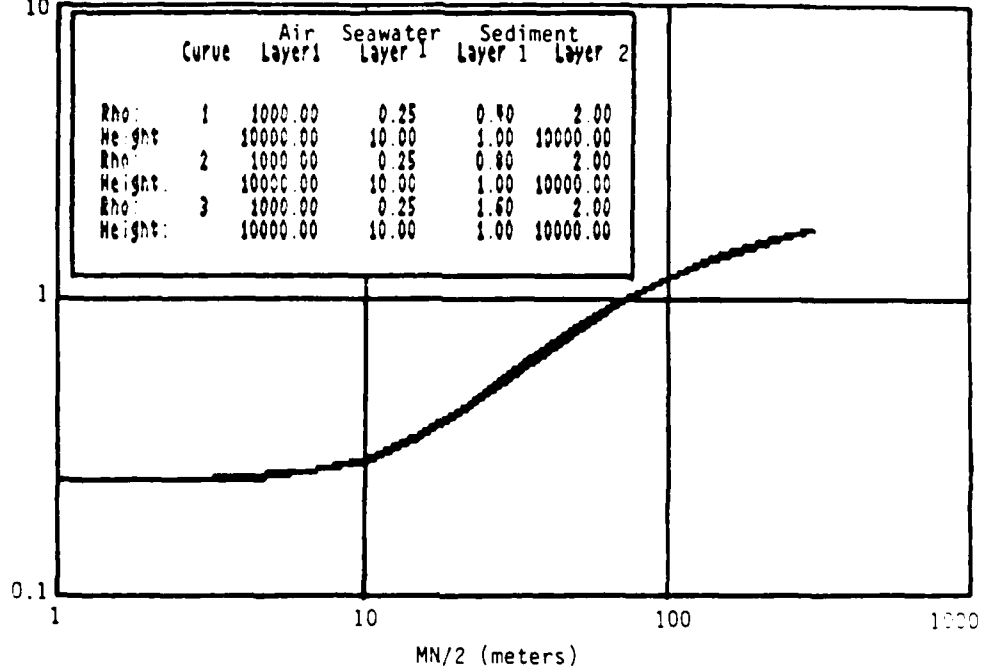


Figure A-7. Case 7, DC Resistivity Resolution, Array at Sea Surface in 10m Water Depth, 1m Thick Layer 1

RhoA  
(ohm-m)  
10

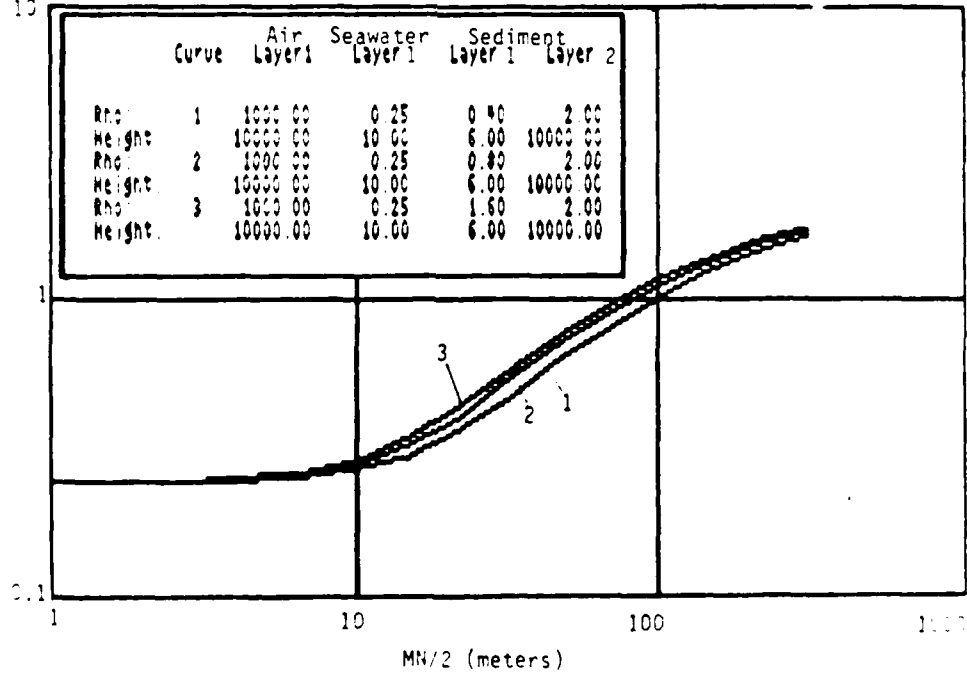


Figure A-8. Case 8, DC Resistivity Resolution, Array at Sea Surface in 10m Water Depth, 6m Thick Layer 1

RhoA  
(ohm-m)

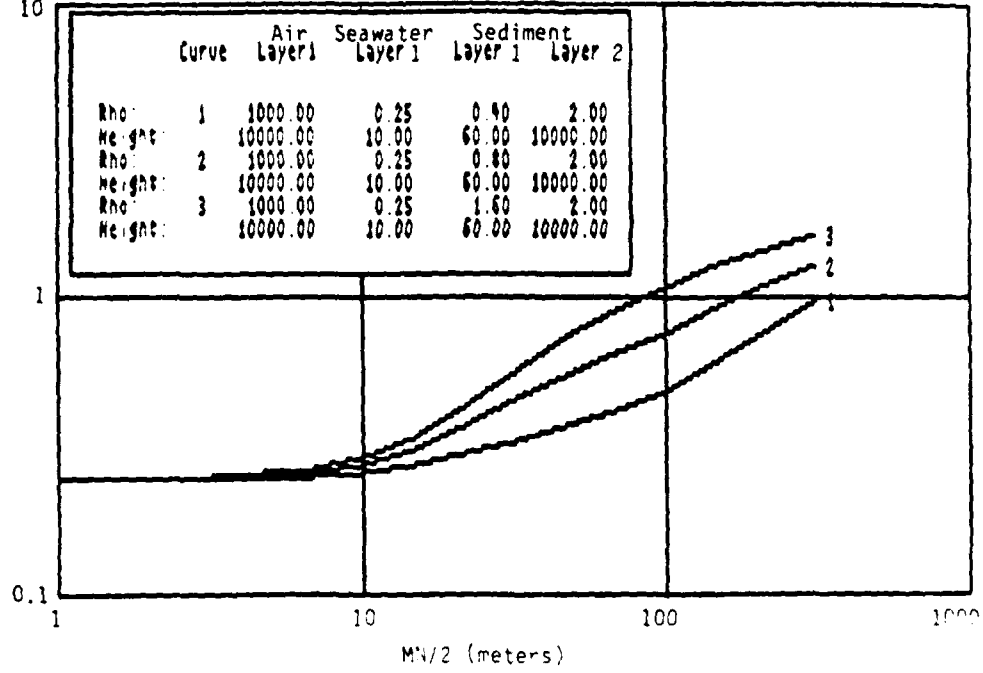


Figure A-9. Case 9, DC Resistivity Resolution, Array at Sea Surface in 10m Water Depth, 60m Thick Layer 1

RhoA  
(ohm-m)

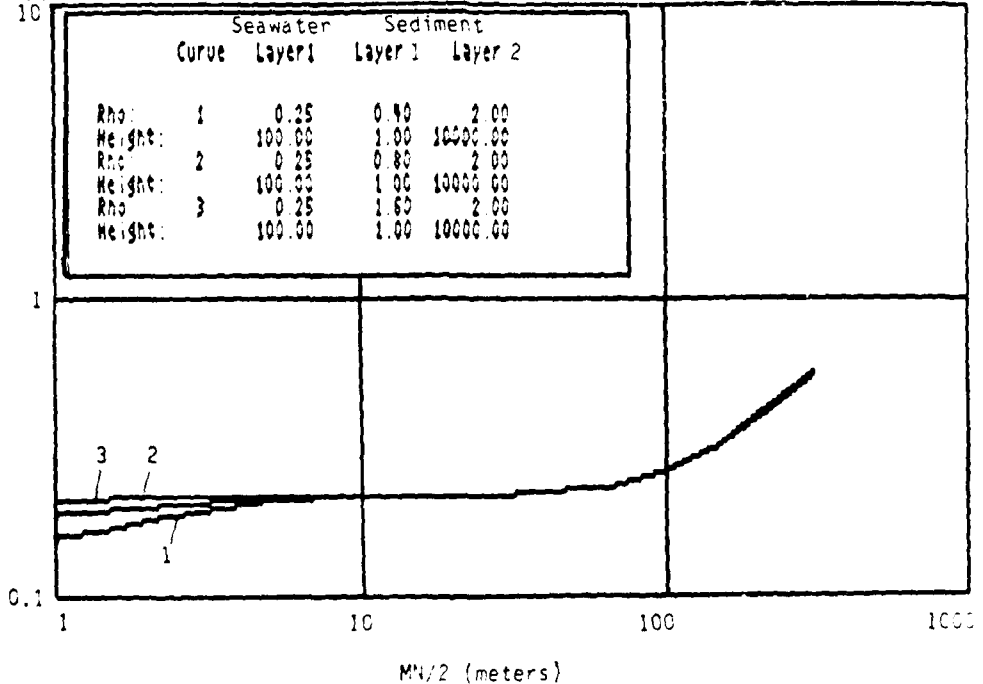


Figure A-10. Case 10, DC Resistivity Resolution, Array on Sea Floor in 100m Water Depth, 1m Thick Layer 1

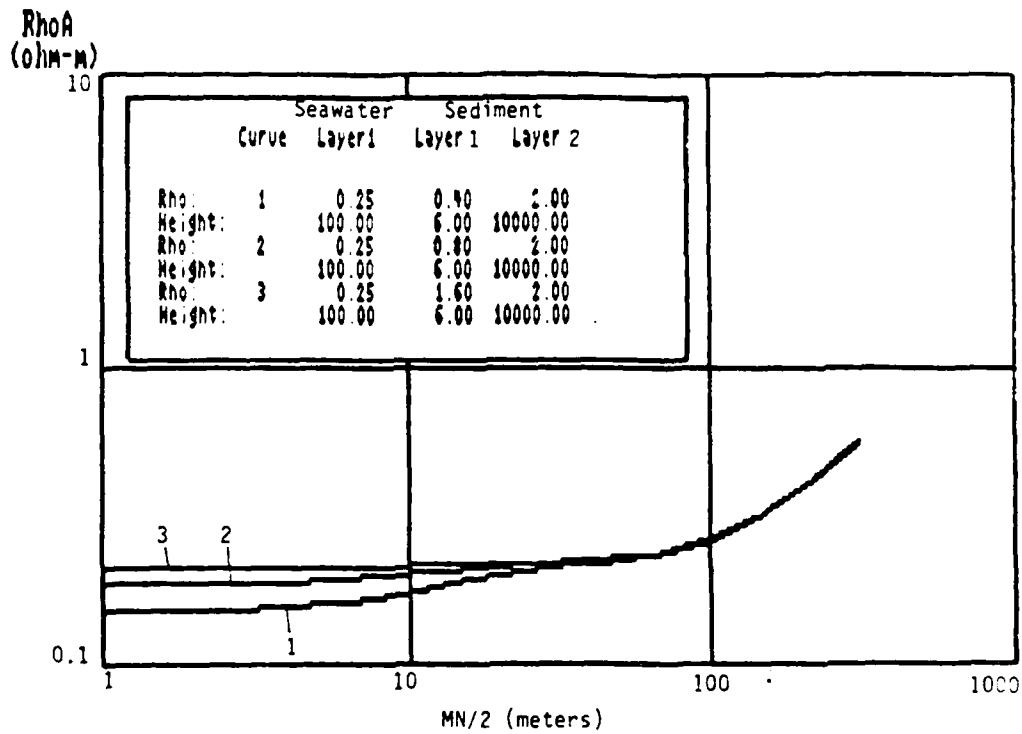


Figure A-11. Case 11, DC Resistivity Resolution, Array on Sea Floor in 100m Water Depth, 6m Thick Layer 1

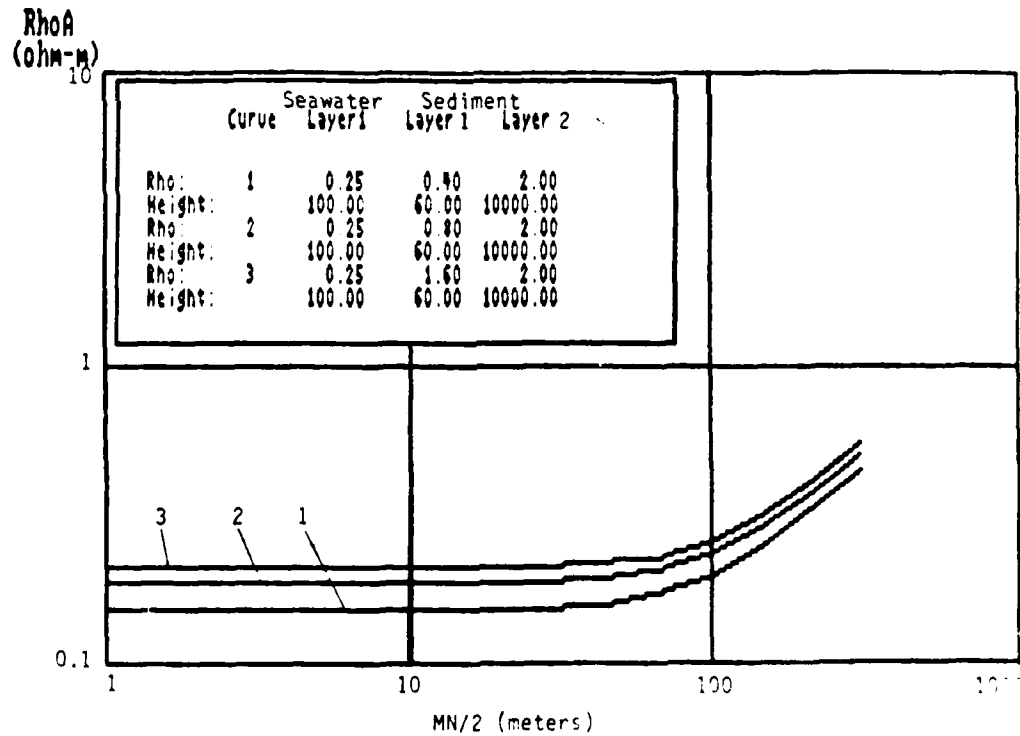


Figure A-12. Case 12, DC Resistivity Resolution, Array on Sea Floor in 100m Water Depth, 60m Thick Layer 1

RhoA  
(ohm-m)

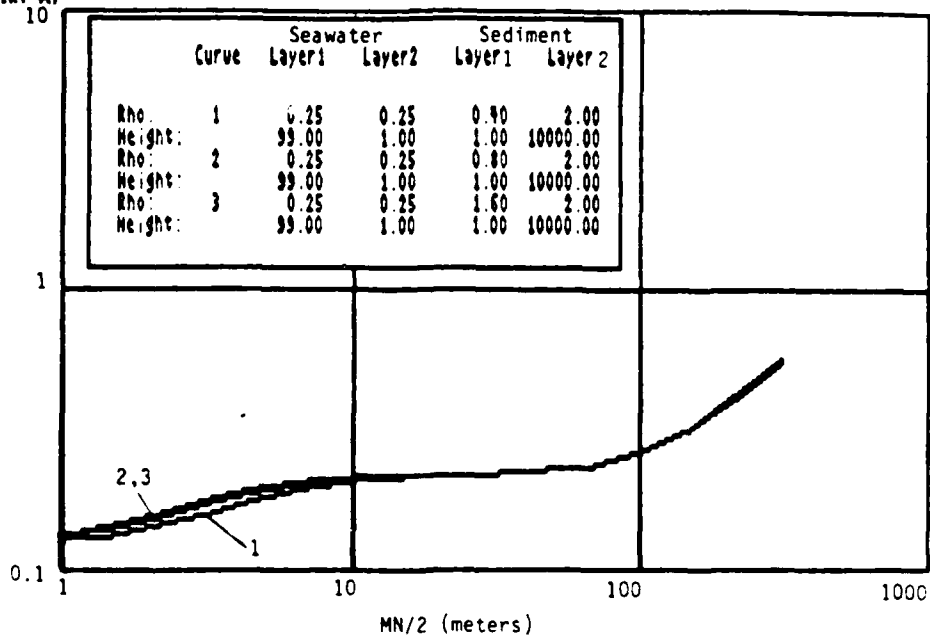


Figure A-13. Case 13, DC Resistivity Resolution, 100m Water Depth, Array 1m Above Sea Floor, 1m Thick Layer 1

RhoA  
(ohm-m)

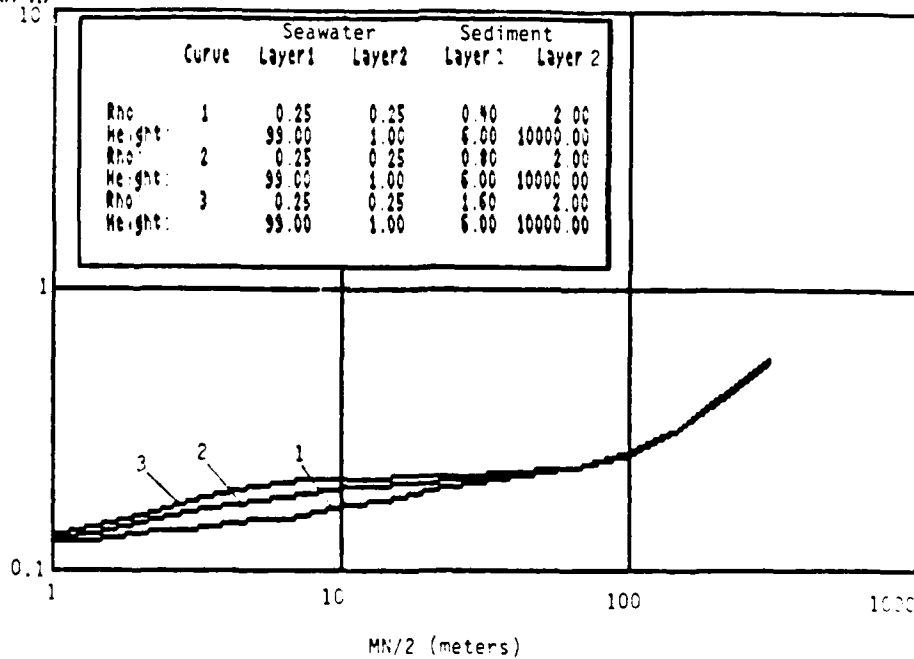


Figure A-14. Case 14, DC Resistivity Resolution, 100m Water Depth, Array 1m Above Sea Floor, 6m Thick Layer 1

RhoA  
(ohm-m)

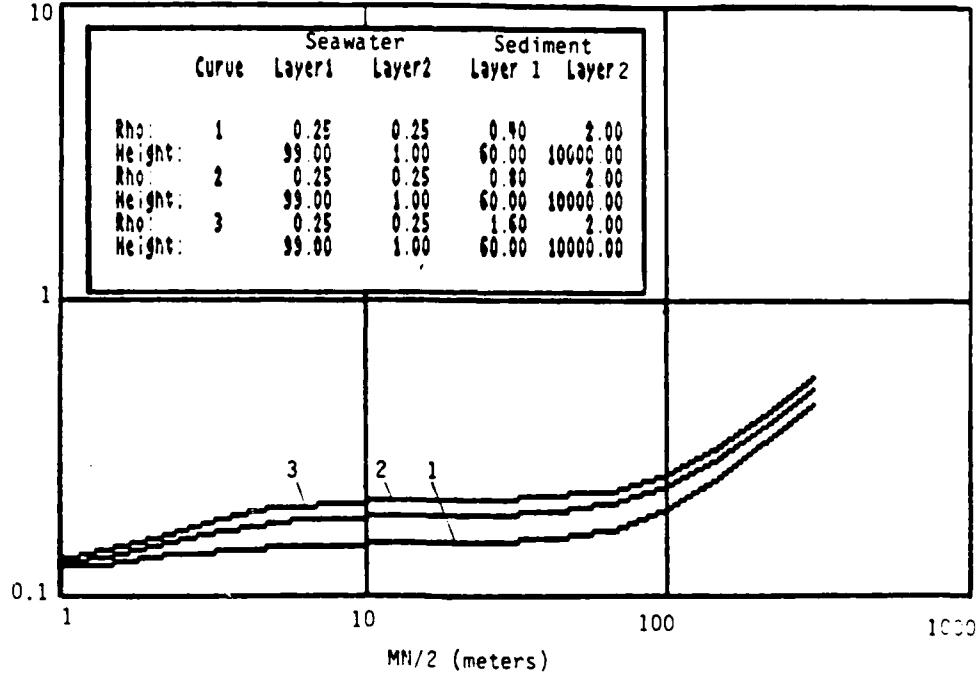


Figure A-15. Case 15, DC Resistivity Resolution, 100m Water Depth, Array 1m Above Sea Floor, 6m Thick Layer 1

RhoA  
(ohm-m)

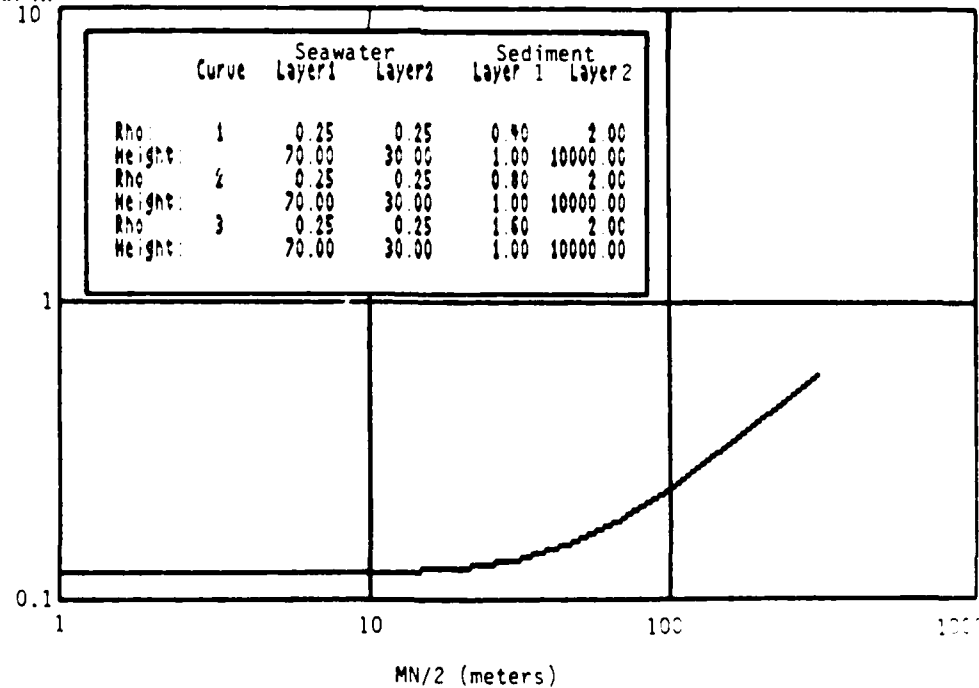


Figure A-16. Case 16, DC Resistivity Resolution, 100m Water Depth, Array 30m Above Sea Floor, 1m Thick Layer 1

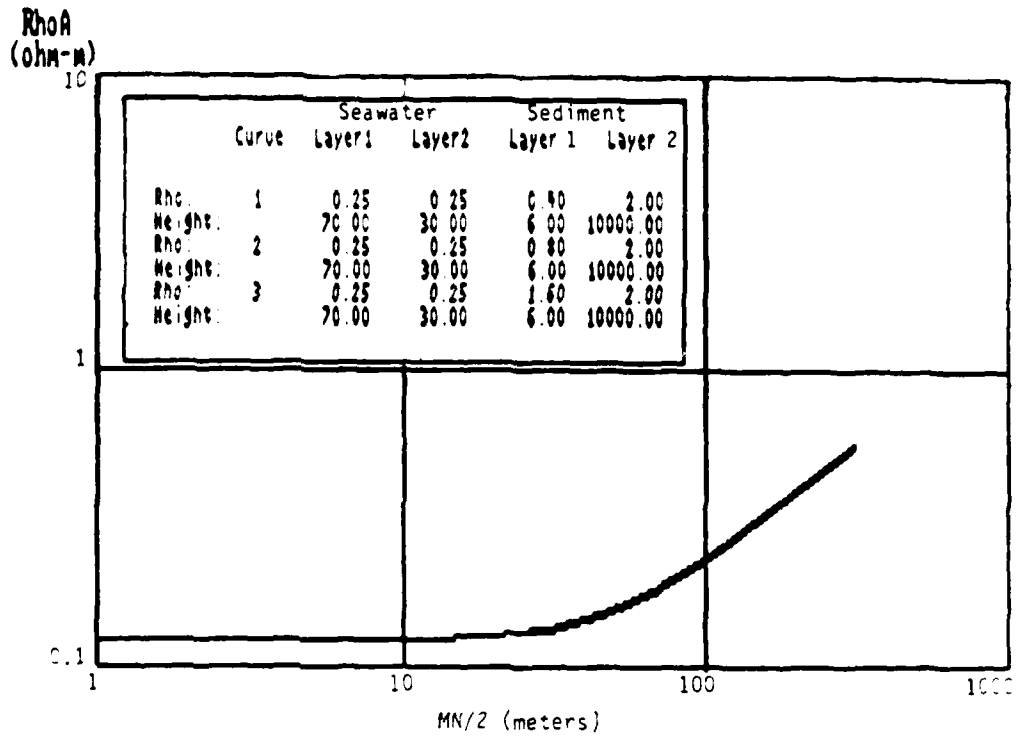


Figure A-17. Case 17, DC Resistivity Resolution, 100m Water Depth, Array 30m Above Sea Floor, 6m Thick Layer 1

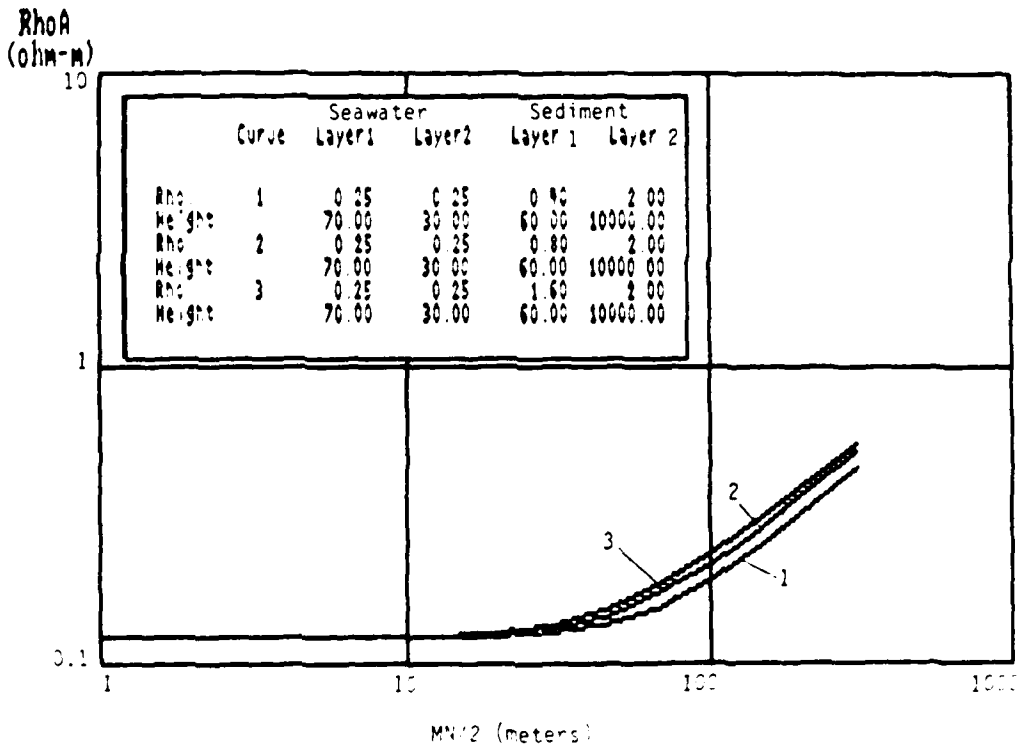


Figure A-18. Case 18, DC Resistivity Resolution, 100m Water Depth, Array 30m Above Sea Floor, 60m Thick Layer 1

RhoA  
(ohm-m)

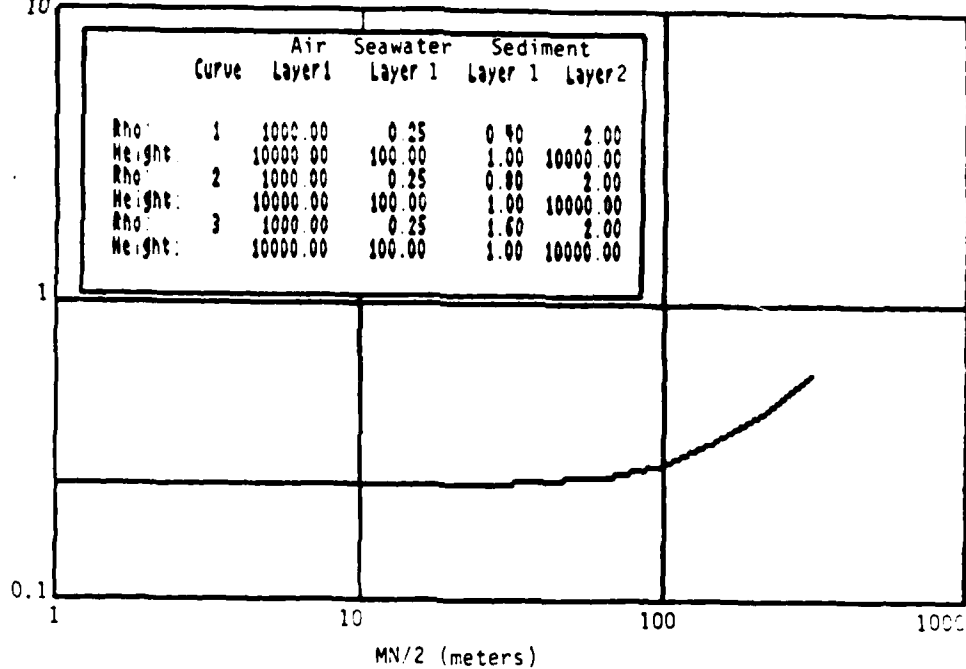


Figure A-19. Case 19, DC Resistivity Resolution, Array at Sea Surface in 100m Water Depth, 1m Thick Layer 1

RhoA  
(ohm-m)

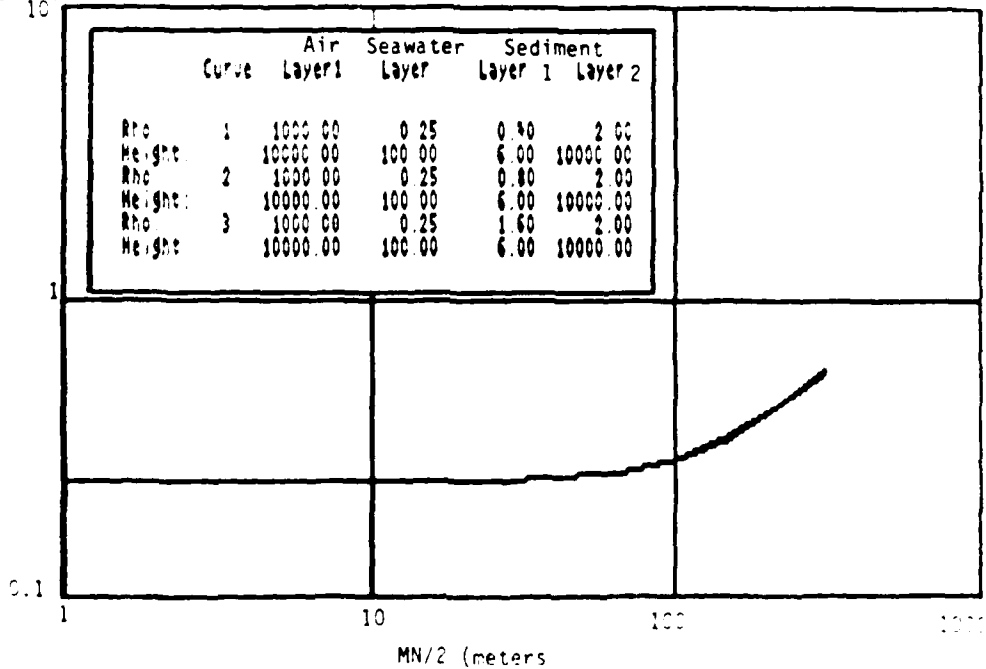


Figure A-20. Case 20, DC Resistivity Resolution, Array at Sea Surface in 100m Water Depth, 6m Thick Layer 1

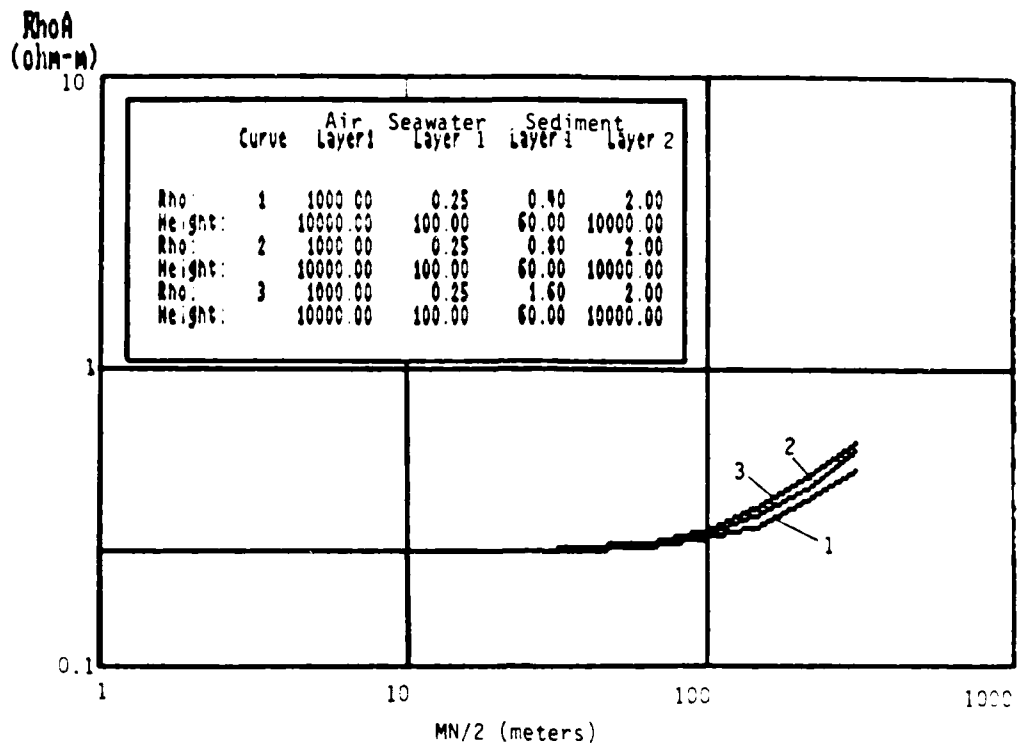


Figure A-21. Case 21, DC Resistivity Resolution, Array at Sea Surface  
in 100m Water Depth, 60m Thick Layer 1

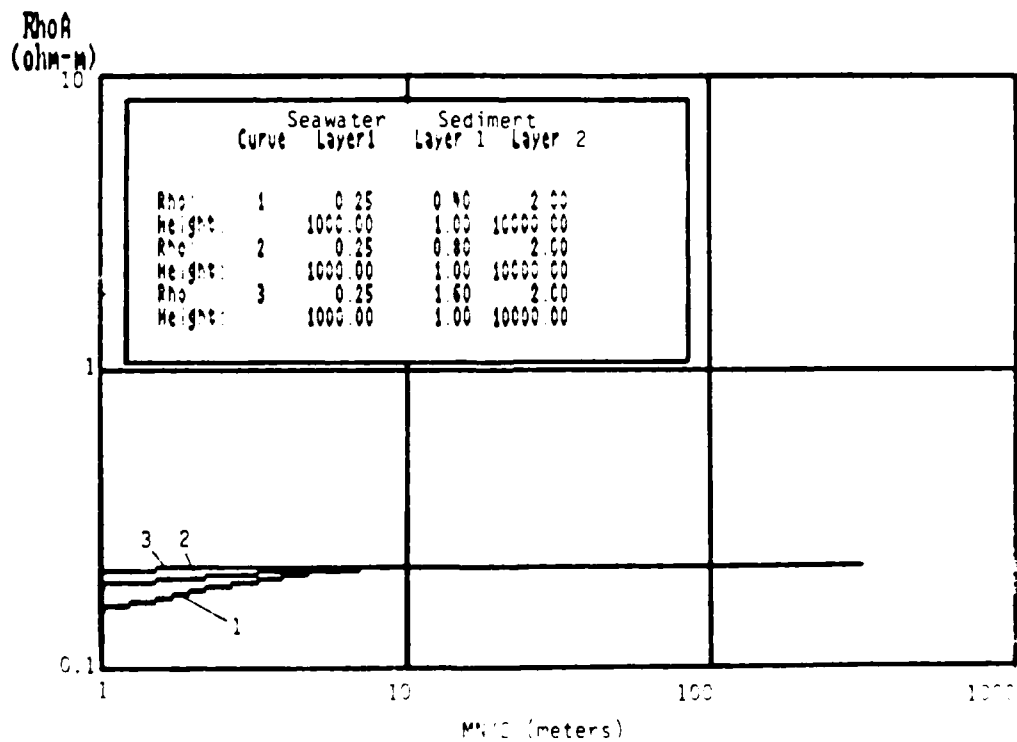


Figure A-22. Case 22, DC Resistivity Resolution, Array on Sea Floor  
in 1000m Water Depth, 1m Thick Layer 1

RhoA  
(ohm-m)  
10

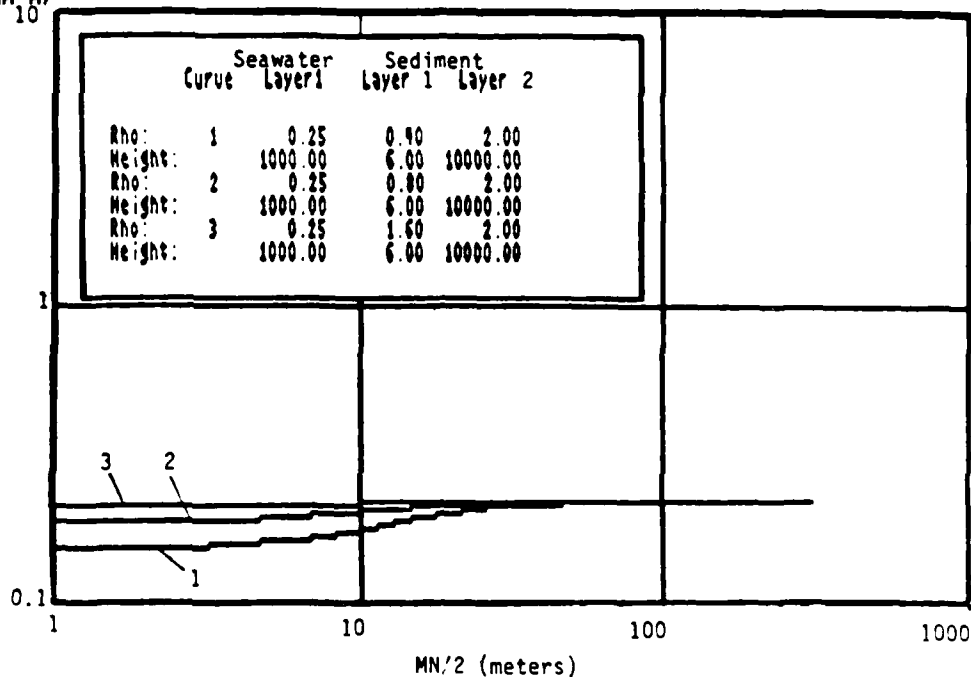


Figure A-23. Case 23, DC Resistivity Resolution, Array on Sea Floor in 1000m Water Depth, 6m Thick Layer 1

RhoA  
(ohm-m)  
10

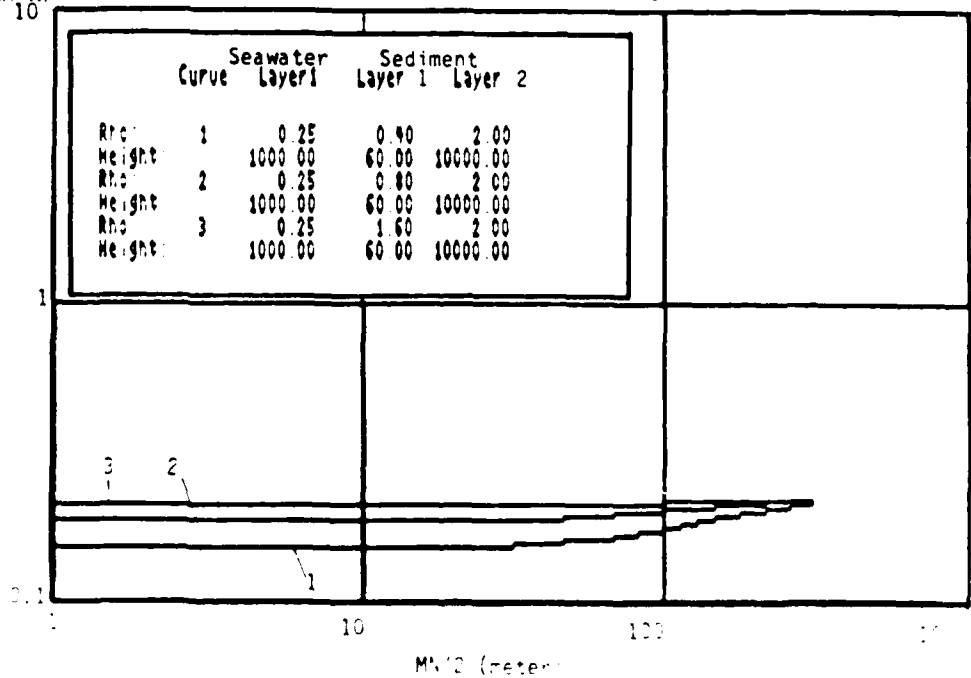


Figure A-24. Case 24, DC Resistivity Resolution, Array on Sea Floor in 1000m Water Depth, 60m Thick Layer 1

RhoA  
(ohm-m)  
10

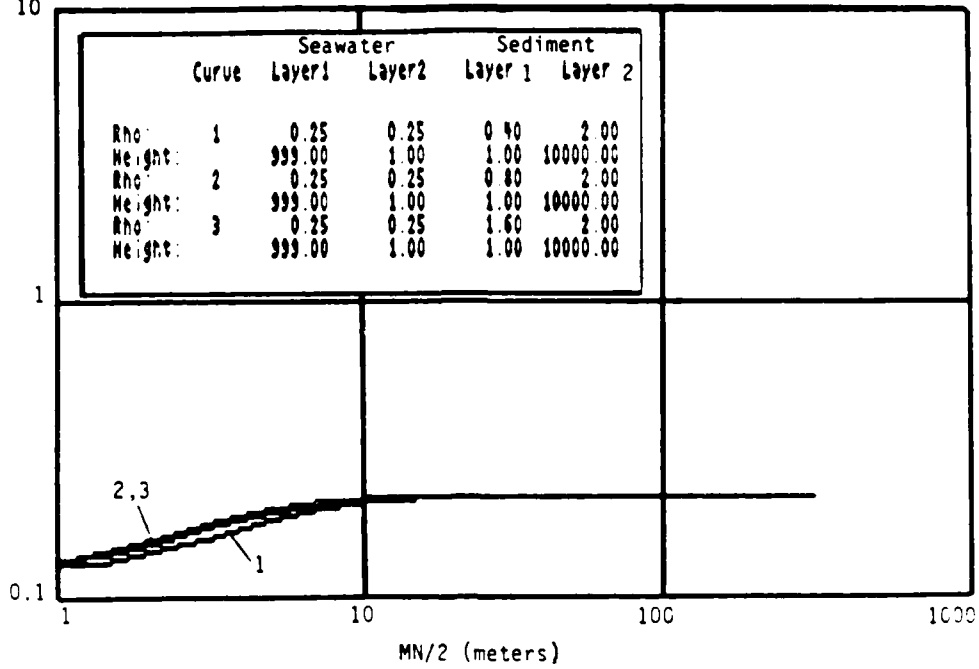


Figure A-25. Case 25, DC Resistivity Resolution, 1000m Water Depth, Array 1m Above Sea Floor, 1m Thick Layer 1

RhoA  
(ohm-m)  
10

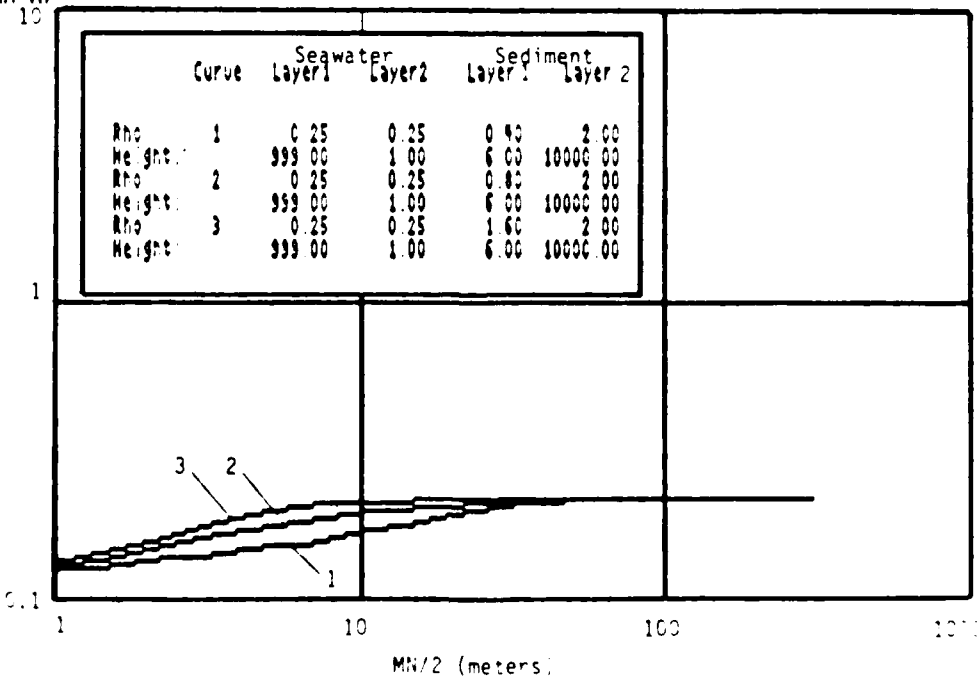


Figure A-26. Case 26, DC Resistivity Resolution, 1000m Water Depth, Array 1m Above Sea Floor, 6m Thick Layer 1

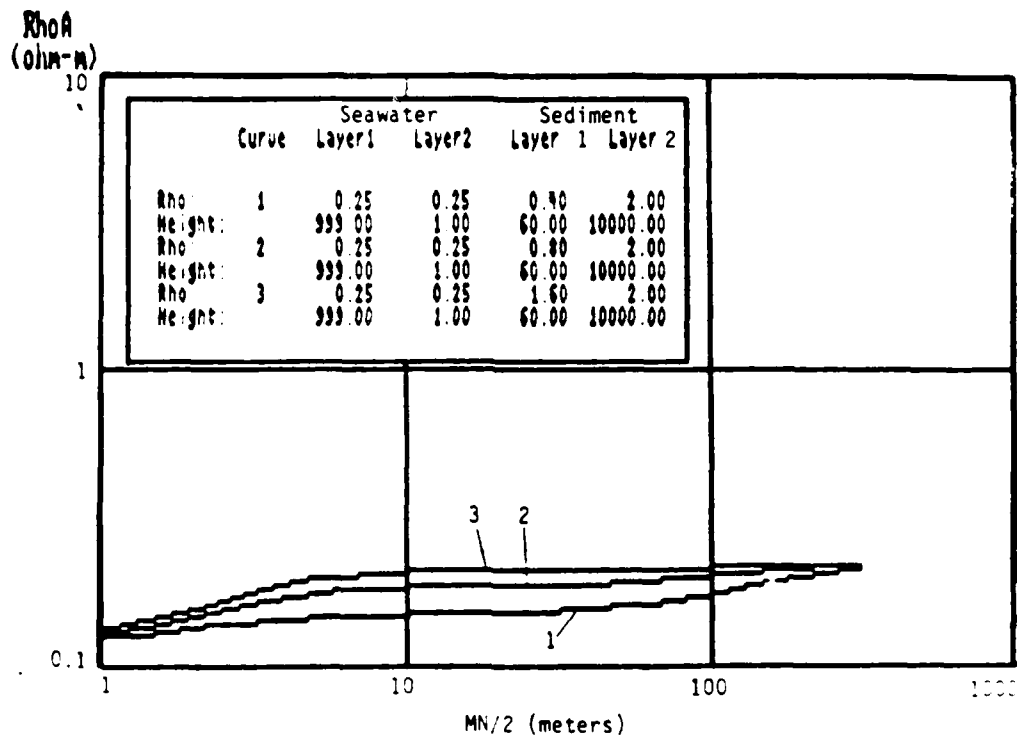


Figure A-27. Case 27, DC Resistivity Resolution, 1000m Water Depth, Array 1m Above Sea Floor, 60m Thick Layer 1

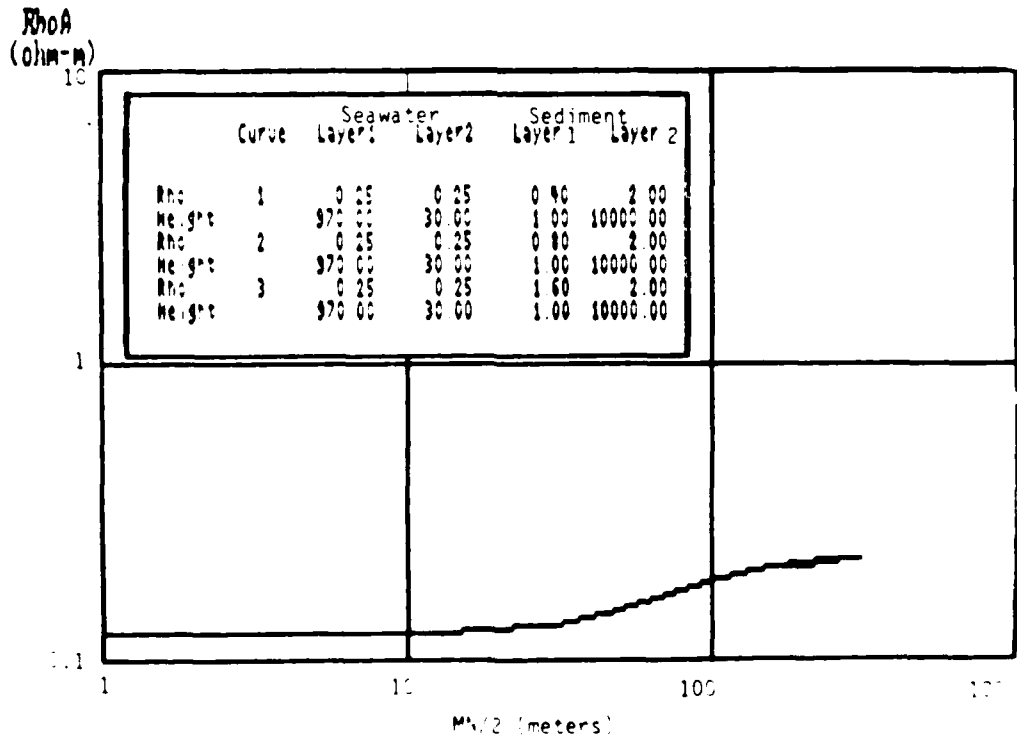


Figure A-28. Case 28, DC Resistivity Resolution, 1000m Water Depth, Array 30m Above Sea Floor, 1m Thick Layer 1

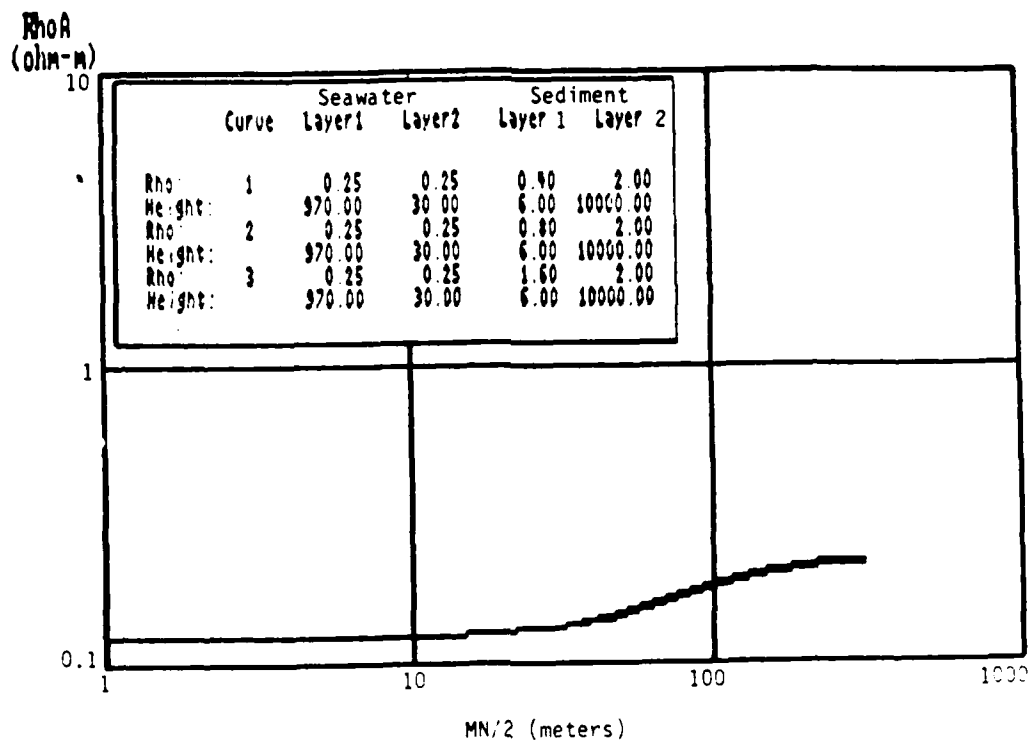


Figure A-29. Case 29, DC Resistivity Resolution, 1000m Water Depth, Array 30m Above Sea Floor, 6m Thick Layer 1

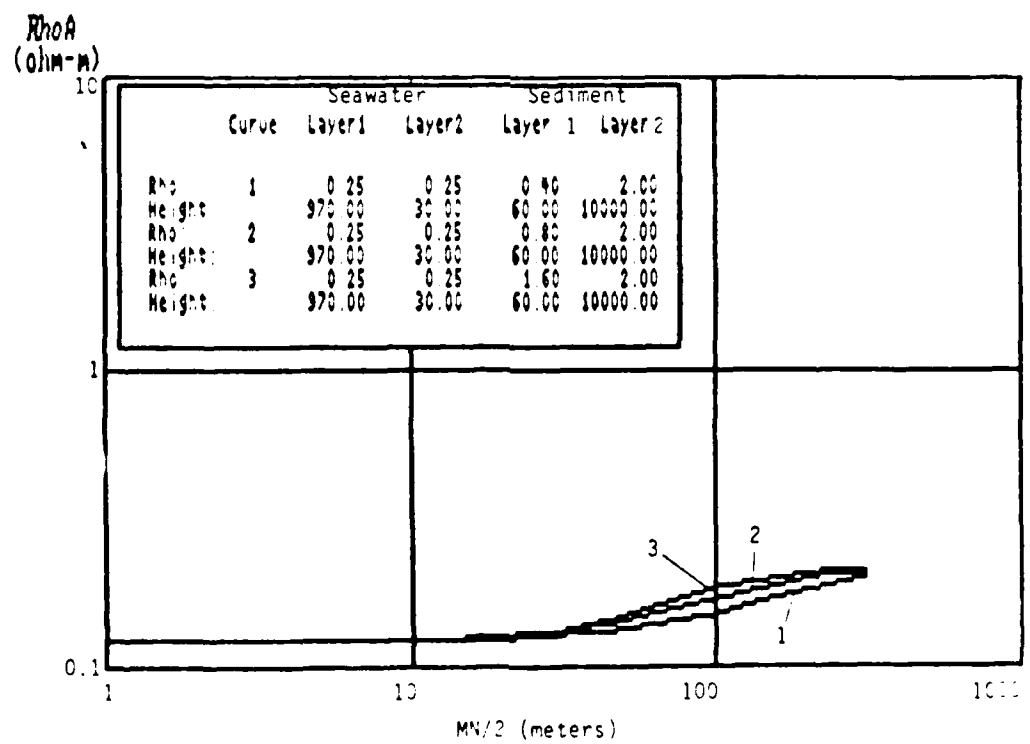


Figure A-30. Case 30, DC Resistivity Resolution, 1000m Water Depth, Array 30m Above Sea Floor, 60m Thick Layer 1

RhoA  
(ohm-m)

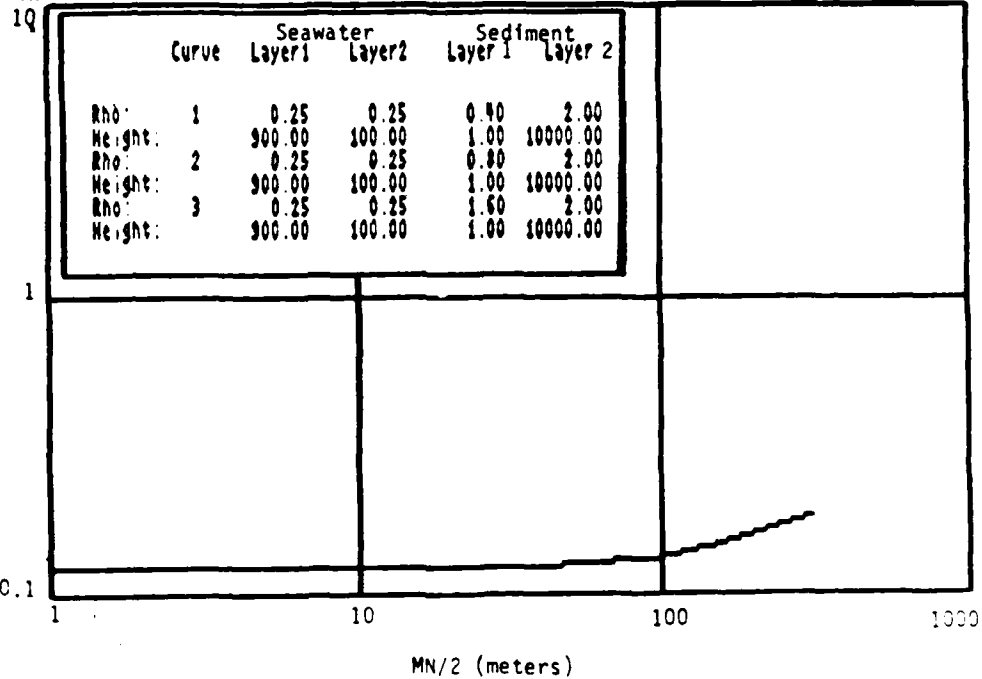


Figure A-31. Case 31, DC Resistivity Resolution, 1000m Water Depth, Array 100m Above Sea Floor, 1m Thick Layer 1

RhoA  
(ohm-m)

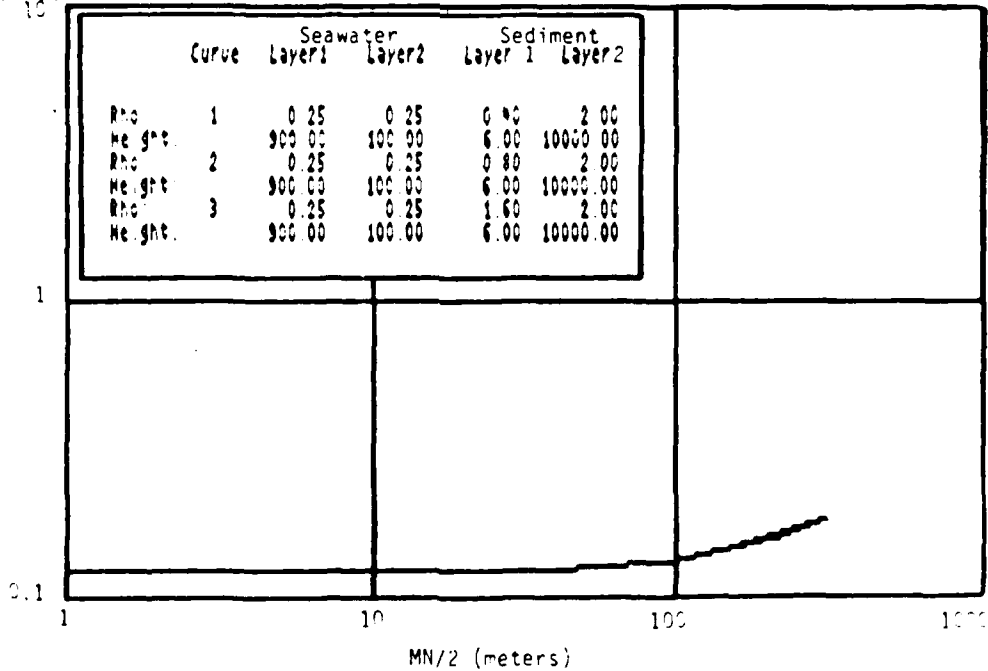


Figure A-32. Case 32, DC Resistivity Resolution, 1000m Water Depth, Array 100m Above Sea Floor, 6m Thick Layer 1

Rho A  
(ohm-m)

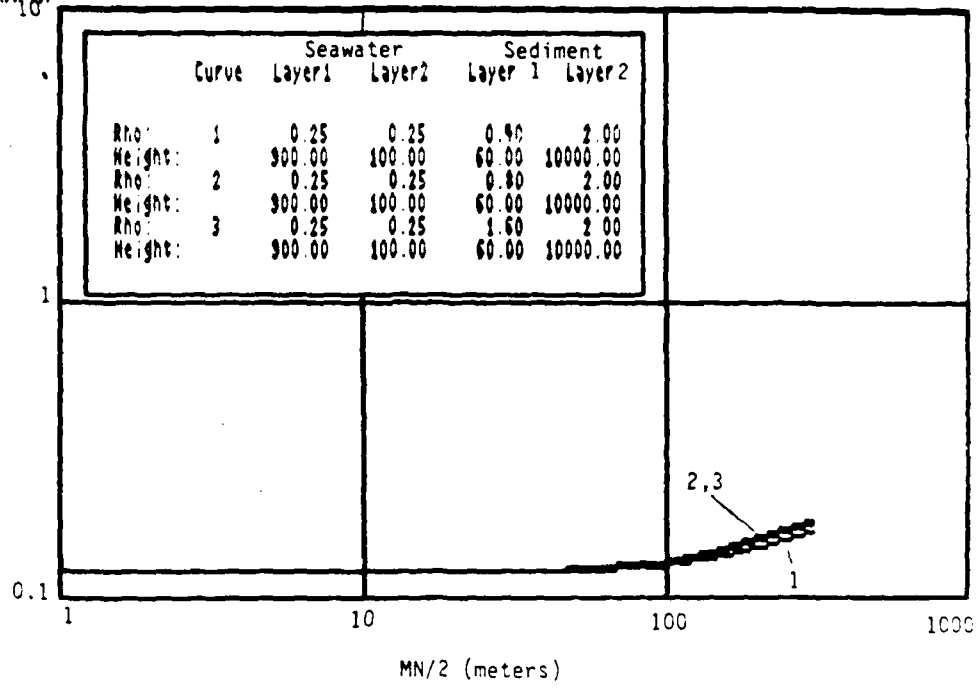


Figure A-33. Case 33, DC Resistivity Resolution, 1000m Water Depth,  
Array 100m Above Sea Floor, 60m Thick Layer 1

**Appendix B. Analytical model for transverse electric (TE)  
and transverse magnetic (TM) fields**

---

The electromagnetic modeling work conducted as part of this feasibility study was done using software developed at NORDA. This modeling package was based on the formulation by J. A. Kong (1972) and generalized for buried dipoles by C-M Tang (1979). The algorithm assumes that the earth is composed of a series of uniaxial anisotropic layers. The details of the computational scheme are the same as those presented by Tang (1979) with the exception of the derivation of the primary field terms. There exists a discrepancy in the calculation of these terms between this development and the earlier derivation by Tang (1979) for the case of anisotropic media.

In summary, the electromagnetic fields due to dipole antennas buried in a stratified anisotropic media may be obtained using a Transverse Electric (TE) and Transverse Magnetic (TM) mode formulation. The technique provides a closed form solution in terms of a set of integral equations which may be numerically evaluated using various schemes, Chave (1983).

The geometry of the problem is indicated in Figure B-1. The fields are calculated in a cylindrical coordinate system  $(r, \phi, z)$  with the  $z$  axis directed up. A time dependence of  $\exp(-i\omega t)$  was used. The sources or various electromagnetic antennas were located in layer (0) with  $m$  layers above and  $n$  layers below the source layer. Each of these layers is represented by a uniaxial anisotropic material, with the conductivity  $\bar{\sigma}$ , permittivity  $\bar{\epsilon}$  and permeability  $\bar{\mu}$  defined by the following tensors:

$$\bar{\mu} = \begin{bmatrix} \mu & 0 & 0 \\ 0 & \mu & 0 \\ 0 & 0 & \mu_z \end{bmatrix}$$

$$\bar{\epsilon} = \begin{bmatrix} \epsilon & 0 & 0 \\ 0 & \epsilon' & 0 \\ 0 & 0 & \epsilon'_z \end{bmatrix}$$

$$\epsilon' = \epsilon + \frac{ig}{\omega}$$

The electric (E) and magnetic (H) fields may be decomposed into two orthogonal components, TE and TM modes. The field components from each of these modes may have vector components, one of which propagates parallel to the direction of the layers (transverse components ( $E_t, H_t$ )) and the other normal to the layer interface (vertical component ( $E_z, H_z$ )). The z components of the fields  $\bar{E}$  and  $\bar{H}$  are composed of only TM and TE modes, respectively. These components may be defined as a Sommerfeld integral as follows:

$$E_z^{TM}(r) = \int_{-\infty}^{\infty} E_z(\lambda) d\lambda$$

$$H_z^{TE}(r) = \int_{-\infty}^{\infty} H_z(\lambda) d\lambda$$

when the z components of the fields are known, the transverse components may be calculated using the following relations:

$$\vec{E}_i^{TM(\lambda)} = \frac{1}{\lambda^2} \nabla_i \frac{\partial}{\partial z} E_z(\lambda)$$

$$H_i^{TM(\lambda)} = \left( \frac{-i\omega\epsilon'}{\lambda^2} \right) \nabla_i \times (E_z(\lambda) \hat{z})$$

$$E_i^{TE(\lambda)} = \left( \frac{i\omega\mu}{\lambda^2} \right) \nabla_i \times (H_z(\lambda) \hat{z})$$

$$H_i^{TE(\lambda)} = \frac{1}{\lambda^2} \nabla_i \frac{\partial}{\partial z} H_z(\lambda)$$

where

$$\nabla_i = \hat{r} \frac{\partial}{\partial r} + \hat{\phi} \frac{1}{r} \frac{\partial}{\partial \phi}$$

The governing equations for the electromagnetic fields in a region outside of any source are provided by Maxwell's source free equations which are as follows:

$$\nabla \times \vec{E} = i\omega\vec{H} \quad \nabla \times \vec{H} = -i\omega\vec{E}$$

These equations with the previously defined permeability and permittivity tensors may be transformed into two sets of uncoupled differential equations. These equations may then be solved for the TE and TM solutions.

In the case of the TM mode, Maxwell's equations provide a differential equation for the  $E_z$  field component. This has the following form:

$$\nabla_i^2 E_z + \frac{1}{a} \frac{\partial^2 E_z}{\partial z^2} z + \frac{k^2}{a} E_z = 0$$

where

$$\nabla_t^2 = \frac{1}{r} \frac{\partial}{\partial r} \left( \frac{r \partial}{\partial r} \right) + \frac{1}{r^2} \frac{\partial^2}{\partial \phi^2}$$

$$k^2 = \omega^2 \mu \epsilon' \text{ and } a = \frac{\epsilon'}{\epsilon'_z}$$

which may be transformed as follows,

$$\nabla_t^2 E_z + \lambda^2 E_z = 0$$

where

$$\lambda^2 = \frac{\gamma^{(e)2} + k^2}{a}, \quad \gamma^{(e)} = [\lambda^2 a - k^2]^{1/2}$$

The solution for  $E_z$  provides the TM mode response for the general electromagnetic induction problem.

The TE mode may be obtained by again transforming the source free Maxwell's equations into a differential equation which this time is a function of only  $H_z$ . This frequency domain relationship has the following form:

$$\nabla_t^2 H_z + \frac{1}{b} \frac{\partial^2 H_z}{\partial z^2} + \frac{k^2}{b} H_z = 0$$

where

$$\nabla_t^2 = \frac{1}{r} \frac{\partial}{\partial r} \left( r \frac{\partial}{\partial r} \right) + \frac{\partial^2}{\partial \phi^2}$$

$$k^2 = \omega^2 \mu \epsilon' \text{ and } b = \frac{\mu}{\mu_2}$$

which may be transformed as before into the following form:

$$\nabla_t^2 H_z + \lambda^2 H_z = 0$$

where

$$\lambda^2 = \frac{\gamma^{(m)2} + k^2}{b} \quad \gamma^{(m)} = [\lambda^2 b - k^2]^{1/2}$$

The electromagnetic response from a vertical magnetic dipole or small horizontal loop of wire with a time varying current will be composed of only a TE mode component, when the source is embedded in a layered environment. An example of this situation is shown in Figure B-2. For this case, a vertical magnetic dipole is submerged in the ocean with a sea floor composed of horizontal sedimentary layers.

The response generated by this source-model configuration is composed of a vertical magnetic field  $H_z$ , a radial (horizontal) magnetic field  $H_r$ , and a circular (horizontal) electric field  $E_\phi$ . Each vector field is composed of a primary and secondary component.

$$H_z = H_z^S + H_z^P \quad H_r = H_r^S + H_r^P \quad E_\phi = E_\phi^S + E_\phi^P$$

where the primary fields are defined as follows:

PRIMARY FIELDS:

$$H_z^P = I \frac{AN}{4\pi} \frac{e^{ikR}}{R^5} [(3z'^2 - R^2 + k^2R^2(R^2 - z'^2) + ikR(R^2 - 3z'^2)]$$

$$H_r^P = I \frac{AN}{4\pi} \frac{r'z'e^{ikR}}{R^5} [(3 - k^2R^2 - ik3R)]$$

$$E_\phi^P = \frac{i\omega\mu}{4\pi} \frac{IAN}{R^3} \frac{re^{ikR}}{R^3} [1 - ikR]$$

$$R = (r^2 + z'^2)^{1/2}, \quad z' = z-h$$

$$k = [\omega^2\mu\epsilon + i\omega\mu\sigma]^{1/2}$$

$$\omega = 2\pi f$$

$$\mu = \text{PERMEABILITY (Henry/m)}$$

$$\epsilon = \text{PERMITTIVITY (Farad/m)}$$

$$\sigma = \text{CONDUCTIVITY (S/m)}$$

$$f = \text{FREQUENCY (Hz)}$$

The primary components are simply those field components which would be measured if the source layer were infinitely thick. The secondary field component is generated by variations in physical parameters at each layer interface.

The total field response for an arbitrary number of layers may be formulated as a set of integral equations. The TE mode response is given by the following relations:

$$H_z = \frac{IA\eta}{4\pi} \int_0^{\infty} \frac{\lambda^3}{\gamma_0^{(m)}} \left\{ e^{\pm \gamma_0^{(m)}(n-z)} + C_0^{(1)}(\lambda)e^{\gamma_0^{(m)}z} + D_0^{(1)}(\lambda)e^{-\gamma_0^{(m)}z} \right\} J_0(\lambda r) d\lambda$$

$$H_r = \frac{IA\eta}{4\pi} \int_0^{\infty} \lambda^2 \left\{ \pm e^{\pm \gamma_0^{(m)}(n-z)} - C_0^{(1)}(\lambda)e^{\gamma_0^{(m)}z} + D_0^{(1)}(\lambda)e^{-\gamma_0^{(m)}z} \right\} J_1(\lambda r) d\lambda$$

$$E_\phi = \frac{i\omega\mu_0 IA\eta}{4\pi} \int_0^{\infty} \frac{\lambda^2}{\gamma_0^{(m)}} \left\{ e^{\pm \gamma_0^{(m)}(n-z)} + C_0^{(1)}(\lambda)e^{\gamma_0^{(m)}z} + D_0^{(1)}(\lambda)e^{-\gamma_0^{(m)}z} \right\} J_1(\lambda r) d\lambda$$

where

$$\gamma_0^{(m)} = \left[ \lambda^2 \frac{\mu_0}{\mu_{0z}} - k_0^2 \right]^{1/2} \quad z = \text{OBSERVATION DEPTH}$$

$J_j(\lambda r)$ ,  $j = 0, 1$  BESSEL FUNCTIONS OF ZERO AND FIRST ORDER

$C_0^{(1)}(\lambda)$  AND  $D_0^{(1)}(\lambda)$  COEFFICIENTS DUE TO PHYSICAL PROPERTY VARIATIONS

The first term under the integral is the primary field component and the second and third terms represent the secondary fields. These secondary

components may easily be calculated by generating the  $C_0$  and  $D_0$  coefficients and then numerically integrating the resulting kernel. The coefficients are defined as follows:

$$C_0^{(1)}(\lambda) = \zeta_1^{(m)} e^{-2\gamma_0^{(m)} d_0} \left[ D_0^{(1)}(\lambda) + e^{\gamma_0^{(m)} \lambda} \right]$$

$$D_0^{(1)}(\lambda) = e^{2\gamma_0^{(m)} d_1} \frac{\left[ \zeta_1^{(m)} e^{-2\gamma_0^{(m)} d_0} e^{\gamma_0^{(m)} h} + e^{-\gamma_0^{(m)} h} \right]}{\left[ 1 - \zeta_1^{(m)} \zeta_{-1}^{(m)} e^{2\gamma_0^{(m)} (d_1 - d_0)} \right]} \zeta_{-1}^{(m)}$$

where

$$\zeta_1^{(m)} = \frac{\left( \dot{\mu}_{1,0} + e^{2\gamma_1^{(m)} d_0} Q^{TE} \right)}{\left( 1 + \dot{\mu}_{1,0} e^{2\gamma_1^{(m)} d_0} Q^{TE} \right)}$$

$$\zeta_{-1}^{(m)} = \frac{\left( \dot{\mu}_{1,0} + e^{-2\gamma_{-1}^{(m)} d_1} R^{TE} \right)}{\left( 1 + \dot{\mu}_{1,0} e^{-2\gamma_{-1}^{(m)} d_1} R^{TE} \right)}$$

$d_1$  = DEPTH TO BASE OF SOURCE LAYER  
 $d_0$  = DEPTH TO TOP OF SOURCE LAYER  
 $h$  = DEPTH TO SOURCE

$$\dot{\mu}_{pq} = \frac{\frac{\mu_p}{\mu_q} - \frac{\gamma_p^{(m)}}{\gamma_q^{(m)}}}{\frac{\mu_p}{\mu_q} + \frac{\gamma_p^{(m)}}{\gamma_q^{(m)}}}$$

These coefficients are related to the physical properties of not only the source layer but to the relative property variations between the other

layers as well. This relationship to the other layers is indicated explicitly through the  $Q^{TE}$  and  $R^{TE}$  terms. These terms may be calculated via the following recursive relations for  $R^{TE}$ :

$$R^{TE} = \frac{D_{-1}}{C_{-1}}$$

$$\frac{D_{i+1}}{C_{i+1}} = \frac{e^{2\gamma_{i+1}^{(m)} d_i}}{\dot{\mu}_{i, i+1}} \left( 1 + \frac{(\dot{\mu}_{i, i+1})^2 - 1}{1 + \dot{\mu}_{i, i+1} e^{-2\gamma_i^{(m)} d_i} \frac{D_i}{C_i}} \right)$$

$$\frac{D_i}{C_i} = 0 \quad i = -n, -n+1, -n+2 \dots -2$$

and for  $Q^{TE}$ :

$$Q^{TE} = \frac{C_1}{D_1}$$

$$\frac{C_j}{D_j} = \frac{e^{-2\gamma_j^{(m)} d_j}}{\dot{\mu}_{j, j+1}} \left( 1 + \frac{(\dot{\mu}_{j+1, j})^2 - 1}{1 + \dot{\mu}_{j+1, j} e^{2\gamma_{j+1}^{(m)} d_j} \frac{C_{j+1}}{D_{j+1}}} \right)$$

$$\frac{C_m}{D_m} = 0 \quad j = m-1, m-2, m-3, \dots 1$$

When the  $R^{TE}$  and  $Q^{TE}$  terms have been generated the calculation of the kernel function is a straightforward procedure. The remaining integral equation is

then evaluated using an adaptive quadrature scheme in conjunction with a continued fraction algorithm which easily evaluates the slowly convergent integrals, Chave (1983).

The above equations may be transformed into the TM mode solution for the  $E_z$ ,  $H_\phi$ ,  $E_r$  field components. This is easily done by making the following substitutions:

$$\mu_j \Rightarrow \epsilon'_j = \epsilon_j + \frac{lo_j}{w}$$

$$\gamma_j^{(m)} \Rightarrow \gamma_j^{(e)} = \left[ \lambda^2 \frac{\epsilon'_j}{\epsilon'_{zj}} - k_j^2 \right]^{1/2}$$

The resulting TM field response is generated by a buried vertical electric dipole in a layered media.

The last case to be considered would be related to the response generated by horizontal electric or magnetic dipoles. The resulting secondary fields generated in a layered environment by these sources have the following components:

$$H_z, H_r, H_\phi, E_z, E_r, E_\phi$$

The evaluation of these fields proceeds in a manner similar to the previous case (TE mode) except that these fields have a much more complex kernel function which has a contribution from both TE and TM modes.

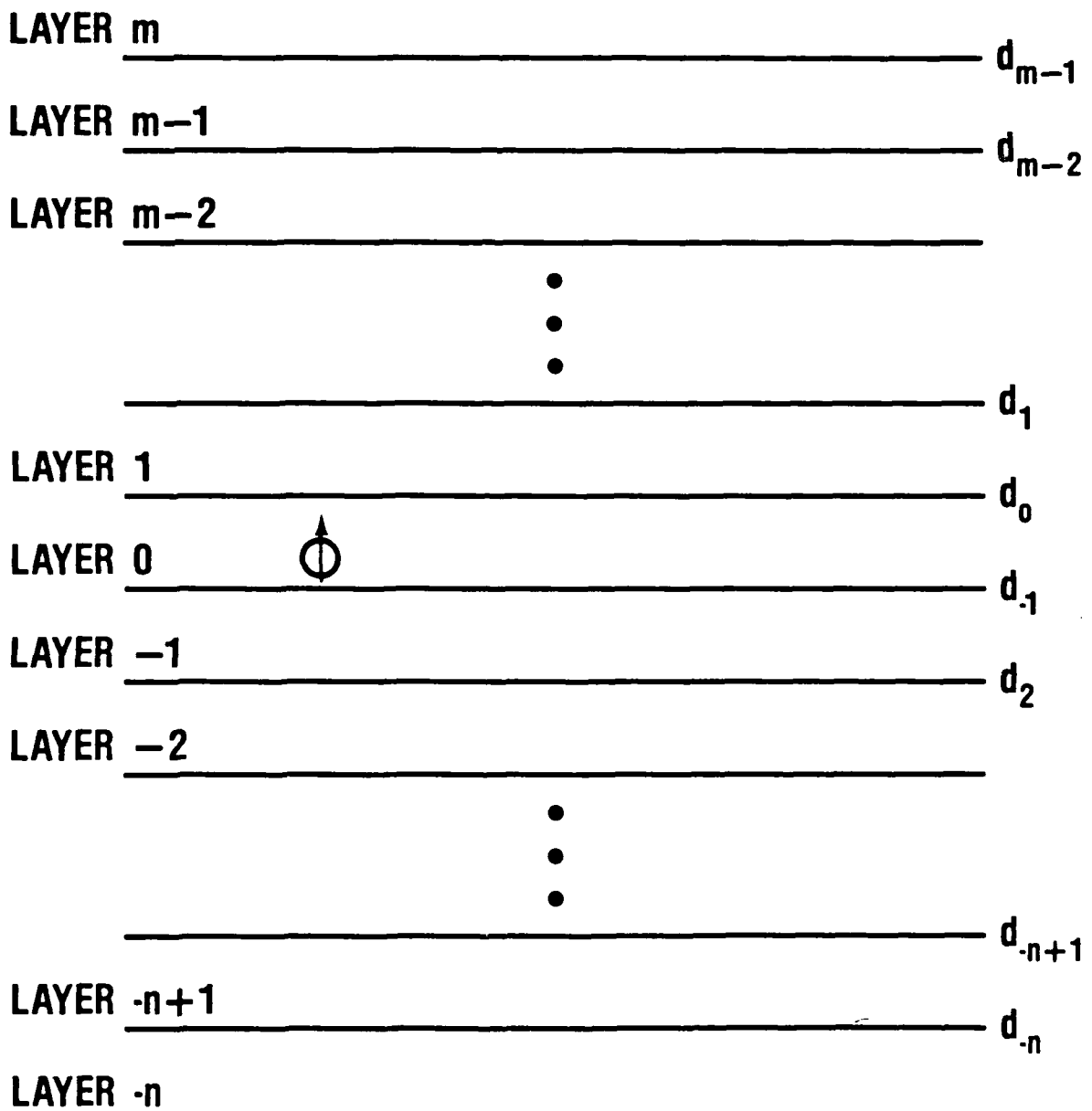


FIGURE B-1 MODEL GEOMETRY

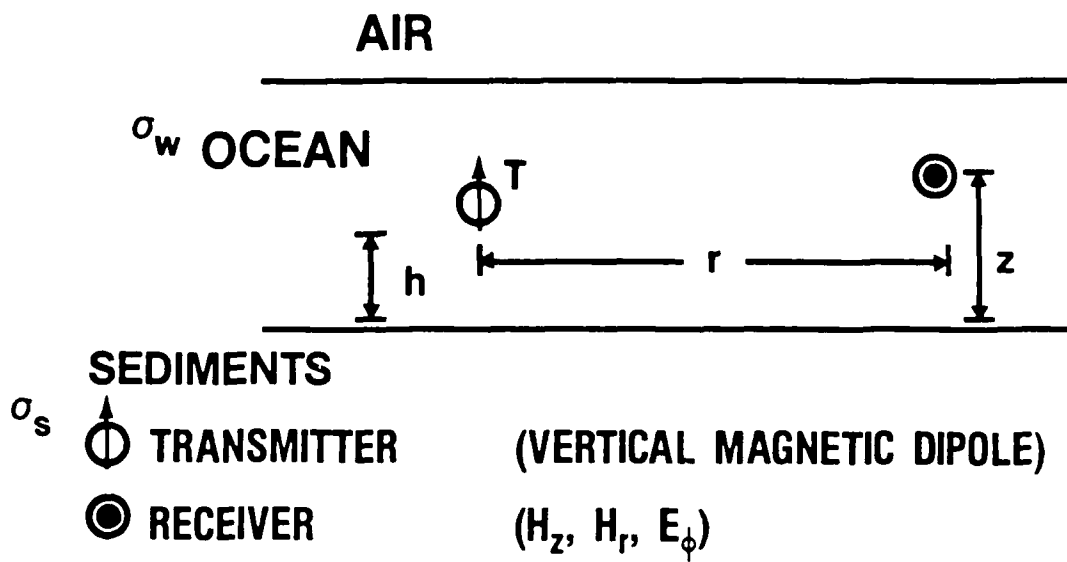
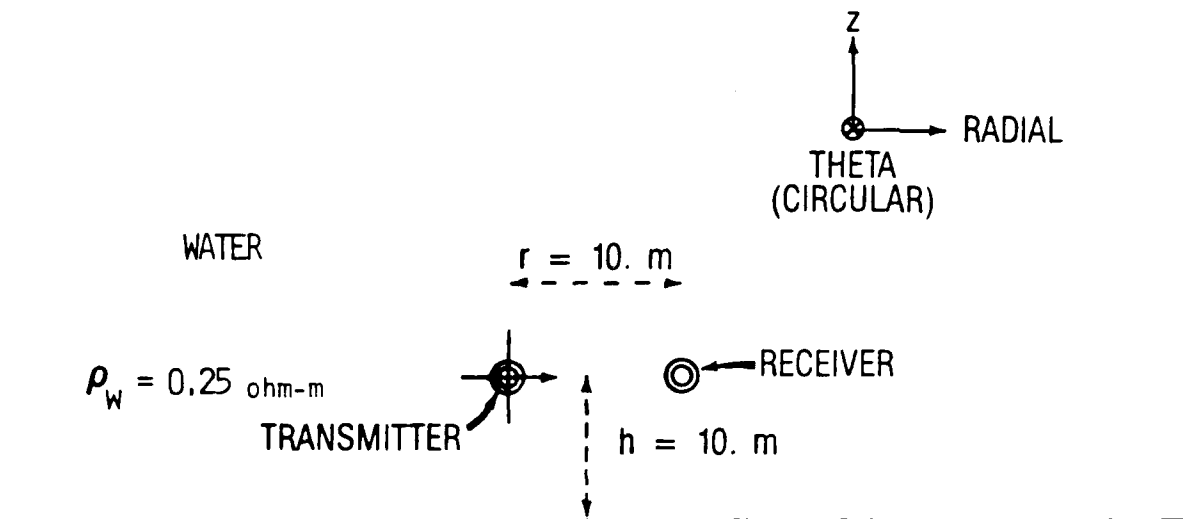


FIGURE B-2 VERTICAL MAGNETIC DIPOLE SUBMERGED IN THE OCEAN

**Appendix C. Sketches of seven cases examined in EM  
analytical studies**

---



SEDIMENT

$\rho_1 = 2.5, 1.25, \text{ AND } 0.625 \text{ ohm-m}$

Figure C-1. Cases 1A, B, and C; Resistivity Study

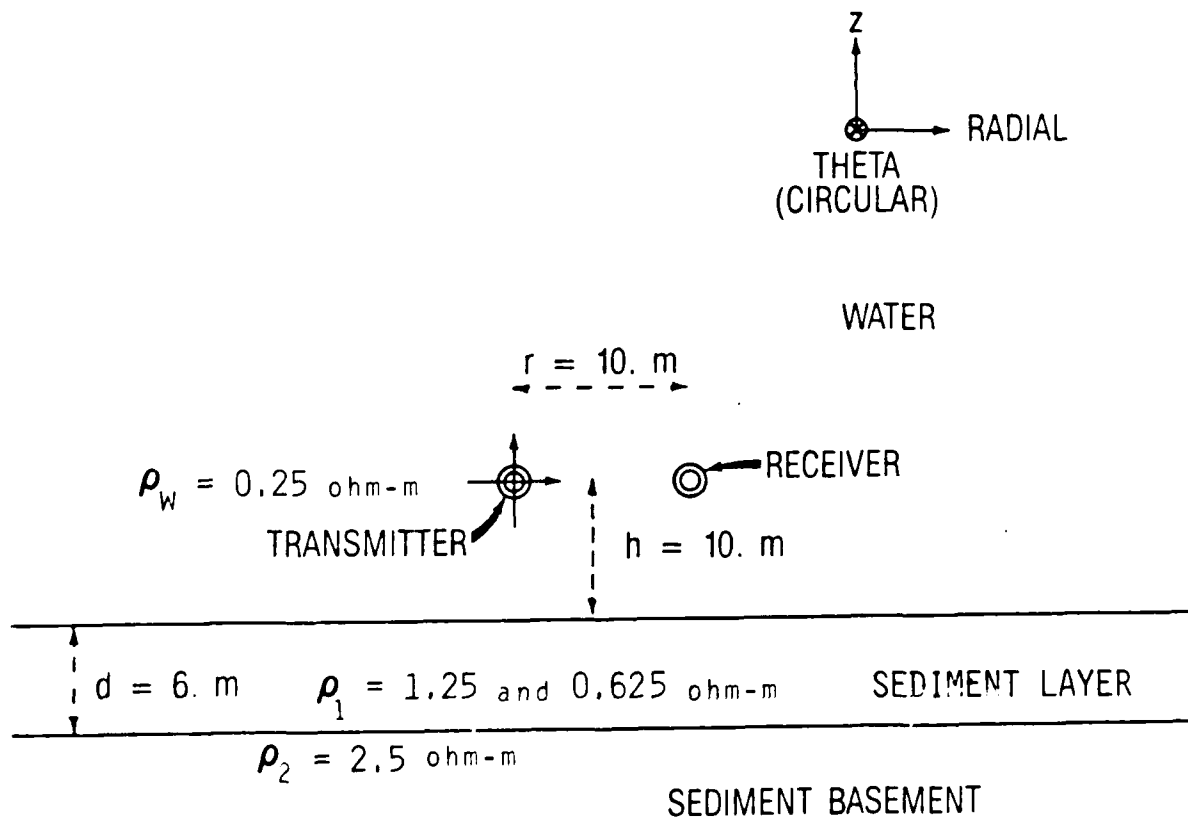
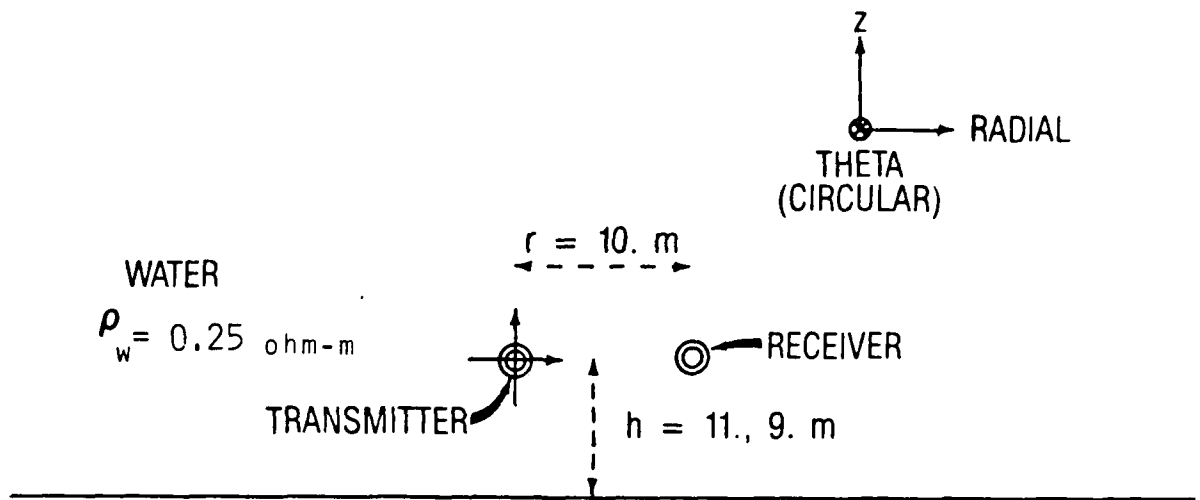


Figure C-2. Cases 2A and B, Resistivity Study



SEDIMENT

$\rho_1 = 2.5 \text{ ohm-m}$

Figure C-3. Cases 3A and B, Resistivity Study

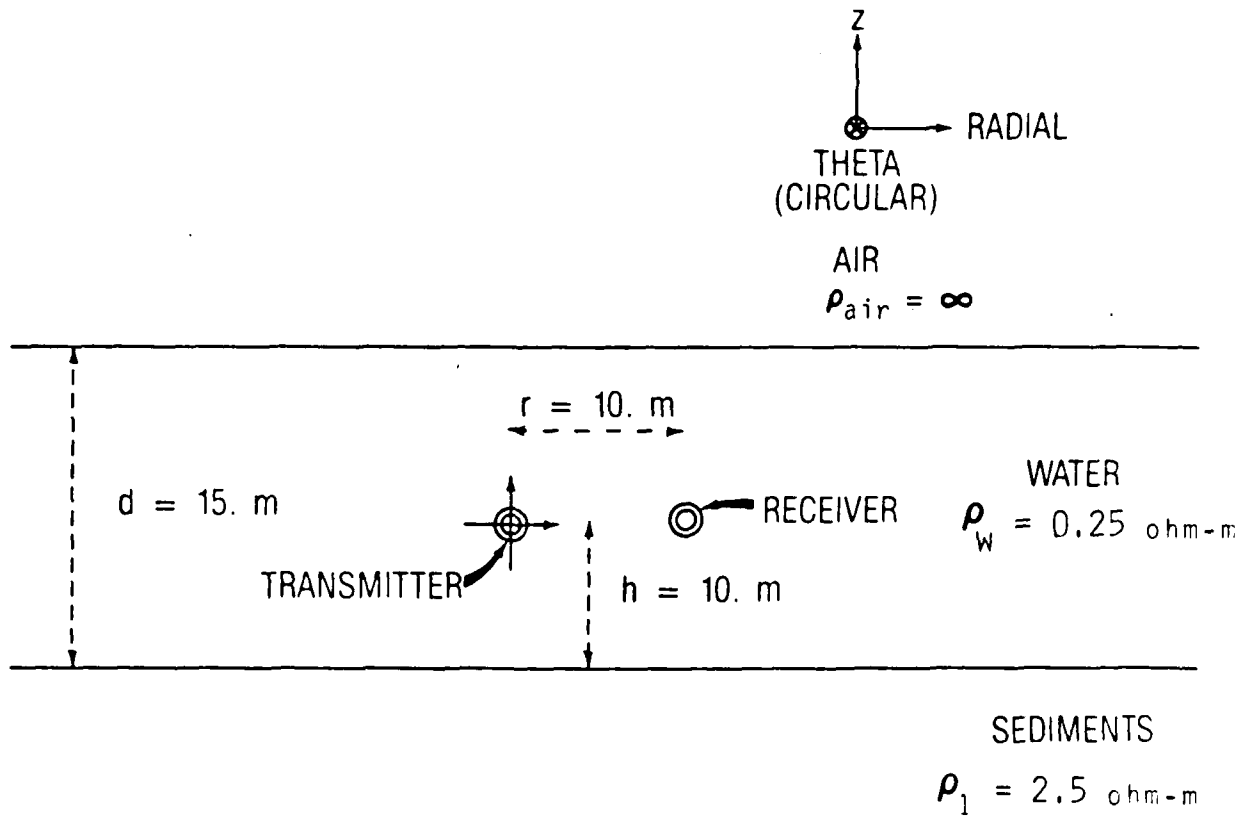


Figure C-4. Case 4A, Resistivity Study

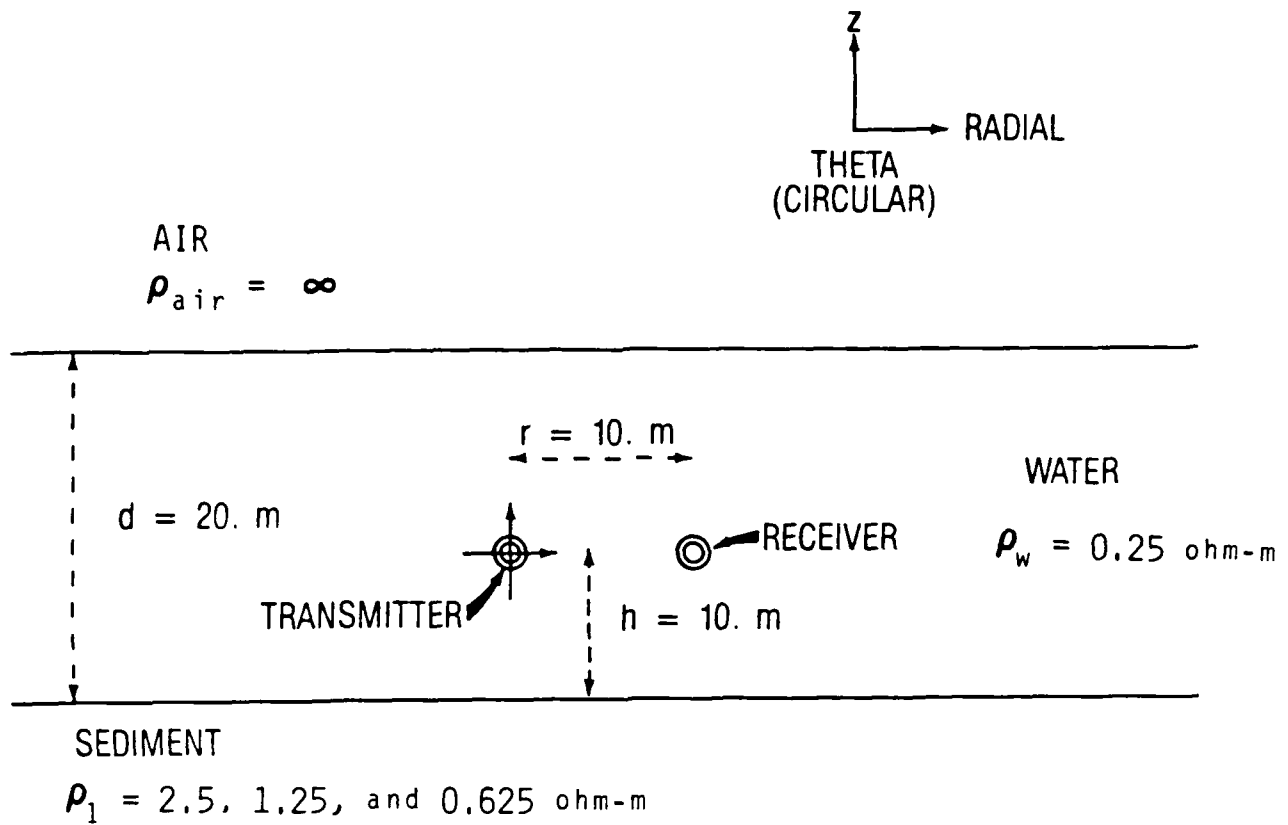


Figure C-5. Cases 5A, B, and C, Resistivity Study

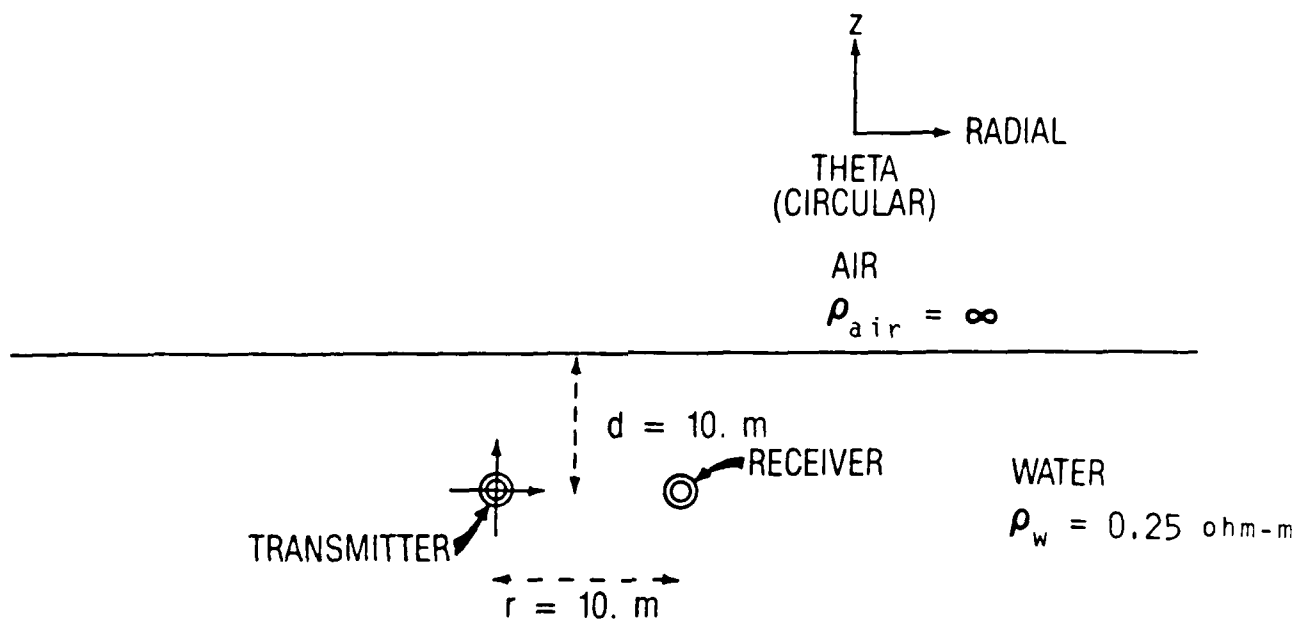


Figure C-6. Case 6A, Resistivity Study

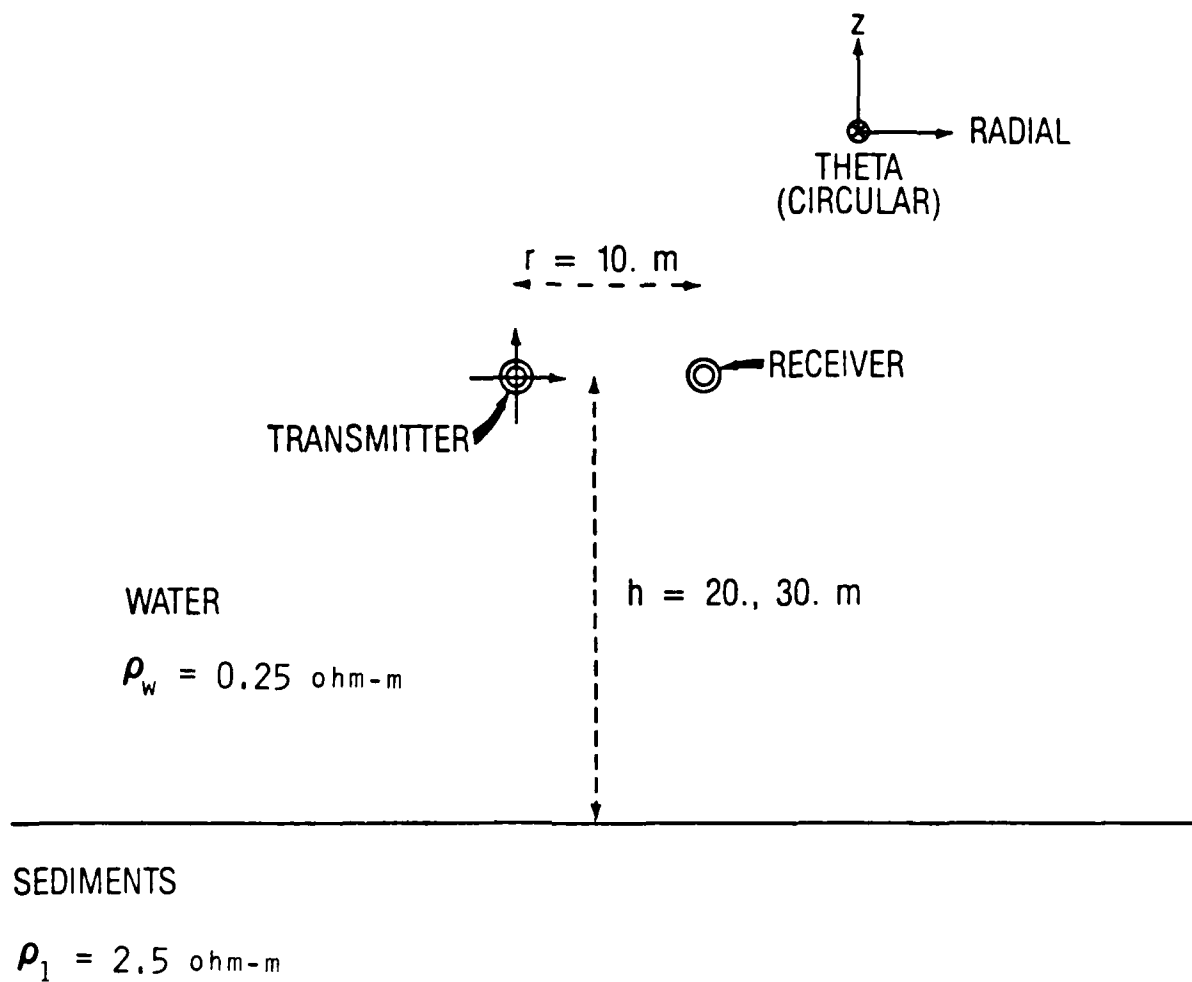


Figure C-7. Cases 7A and B, Resistivity Study

UNCLASSIFIED

SECURITY CLASSIFICATION OF THIS PAGE

ADA187477

REPORT DOCUMENTATION PAGE				
1a REPORT SECURITY CLASSIFICATION <b>Unclassified</b>		1b RESTRICTIVE MARKINGS <b>None</b>		
2a SECURITY CLASSIFICATION AUTHORITY		3 DISTRIBUTION/AVAILABILITY OF REPORT <b>Approved for public release; distribution is unlimited.</b>		
2b DECLASSIFICATION/DOWNGRADING SCHEDULE				
4 PERFORMING ORGANIZATION REPORT NUMBER(S) <b>NORDA Report 211</b>		5 MONITORING ORGANIZATION REPORT NUMBER(S) <b>NORDA Report 211</b>		
6 NAME OF PERFORMING ORGANIZATION <b>Naval Ocean Research and Development Activity</b>		7a NAME OF MONITORING ORGANIZATION <b>Naval Ocean Research and Development Activity</b>		
6c ADDRESS (City, State, and ZIP Code) <b>Ocean Science Directorate NSTL, Mississippi 39529-5004</b>		7b ADDRESS (City, State, and ZIP Code) <b>Ocean Science Directorate NSTL, Mississippi 39529-5004</b>		
8a NAME OF FUNDING/SPONSORING ORGANIZATION <b>Naval Ocean Research and Development Activity</b>	8b OFFICE SYMBOL <i>(if applicable)</i>	9 PROCUREMENT INSTRUMENT IDENTIFICATION NUMBER		
8c ADDRESS (City, State, and ZIP Code) <b>Ocean Science Directorate NSTL, Mississippi 39529-5004</b>		10 SOURCE OF FUNDING NOS		
		PROGRAM ELEMENT NO <b>62435N</b>	PROJECT NO <b>03585</b>	TASK NO <b>MOG</b>
				WORK UNIT NO <b>13527E/13637G</b>
11 TITLE (include Security Classification) <b>Rapid Underway Sediment Classification by Electrical Methods</b>				
12 PERSONAL AUTHOR(S) <b>Philip J. Valent, Edward C. Mozley, and Robert F. Corwin*</b>				
13a TYPE OF REPORT <b>Final</b>	13b TIME COVERED From _____ To _____	14 DATE OF REPORT (Yr., Mo., Day) <b>August 1987</b>	15 PAGE COUNT <b>76</b>	
16 SUPPLEMENTARY NOTES <b>*Consulting Geotechnical Engineer, El Cerrito, California</b>				
17 COSATI CODES		18 SUBJECT TERMS (Continue on reverse if necessary and identify by block number)		
FIELD	GROUP	SUB GR		
19 ABSTRACT (Continue on reverse if necessary and identify by block number)				
<p>The initial results of a technical feasibility study for using direct current (DC) electric resistivity, electromagnetic (EM), and induced polarization (IP) methods to classify surficial sea-floor sediments are reported herein. Analytical work performed in this study and a review of related work show that both the DC and EM resistivity techniques can provide electrical measurements of sufficient resolution to classify sediments according to type (mud, clay, silt, sand, gravel, etc.). Both DC and EM antennas must be close to the sea-floor surface (within 10 m) so that surficial sediment resistivities can be sufficiently resolved to permit sediment classification. To resolve the resistivity of a 1-m-thick surficial sea-floor sediment layer, the DC antennas must be deployed less than 1 m above the sea floor. Both DC and EM methods can adequately resolve the resistivity of a 6-m-thick surficial layer at a standoff distance of 10 m. Noise tests with an inverted Schlumberger array towed in the water column and on the sea floor show noise levels to be within acceptable limits. The level of development of the IP method for clay mineral detection is reported; this method shows considerable promise as a contributor to a remote underway sediment classification system.</p>				
20 DISTRIBUTION AVAILABILITY OF ABSTRACT UNCLASSIFIED/UNLIMITED    SAME AS RPT    DTIC USERS		21 ABSTRACT SECURITY CLASSIFICATION <b>Unclassified</b>		
22a NAME OF RESPONSIBLE INDIVIDUAL <b>Philip J. Valent</b>		22b TELEPHONE NUMBER (include Area Code) <b>(601) 688-4906</b>	22c OFFICE SYMBOL <b>Code 363</b>	

END

FEB.

1988

DTIC